


Rationally targeted anti-VISTA antibody that blockades the C-C' loop region can reverse VISTA immune suppression and remodel the immune microenvironment to potently inhibit tumor growth in an Fc independent manner

Dipti Thakkar,¹ Shalini Paliwal,¹ Bhushan Dharmadhikari,¹ Siyu Guan,¹ Lillian Liu,¹ Shreya Kar,¹ Nikhil K Tulsian,² Joshua J Gruber,³ Leah DiMascio,⁴ Konrad H Paszkiewicz,¹ Piers J Ingram,⁴ Jerome D Boyd-Kirkup ⁴

To cite: Thakkar D, Paliwal S, Dharmadhikari B, *et al.* Rationally targeted anti-VISTA antibody that blockades the C-C' loop region can reverse VISTA immune suppression and remodel the immune microenvironment to potently inhibit tumor growth in an Fc independent manner. *Journal for ImmunoTherapy of Cancer* 2022;**10**:e003382. doi:10.1136/jitc-2021-003382

► Additional supplemental material is published online only. To view, please visit the journal online (<http://dx.doi.org/10.1136/jitc-2021-003382>).

Accepted 16 November 2021



© Author(s) (or their employer(s)) 2022. Re-use permitted under CC BY-NC. No commercial re-use. See rights and permissions. Published by BMJ.

For numbered affiliations see end of article.

Correspondence to

Dr Jerome D Boyd-Kirkup;
j.boydkirkup@hummingbirdbio.com

ABSTRACT

Background Despite significant progress in cancer immunotherapy in recent years, resistance to existing immune checkpoint therapies (ICT) is common. V-domain Ig suppressor of T cell activation (VISTA), a predominantly myeloid immune checkpoint regulator, represents a promising therapeutic target due to its role in suppressing proinflammatory antitumor responses in myeloid-enriched tumor microenvironments. However, uncertainty around the cognate VISTA ligand has made the development of effective anti-VISTA antibodies challenging. The expression of VISTA on normal immune cell subtypes argues for a neutralizing non-depleting antibody, however, previous reported anti-VISTA antibodies use IgG1 Fc isotypes that deplete VISTA+ cells by antibody dependent cellular cytotoxicity/complement dependent cytotoxicity and these antibodies have shown fast serum clearance and immune toxicities.

Method Here we used a rational antibody discovery approach to develop the first Fc-independent anti-VISTA antibody, HMBD-002, that binds a computationally predicted functional epitope within the C-C-loop, distinct from other known anti-VISTA antibodies. This epitope is species-conserved allowing robust in vitro and in vivo testing of HMBD-002 in human and murine models of immune activation and cancer including humanized mouse models.

Results We demonstrate here that blockade by HMBD-002 inhibits VISTA binding to potential partners, including V-Set and Immunoglobulin domain containing 3, to reduce myeloid-derived suppression of T cell activity and prevent neutrophil migration. Analysis of immune cell milieu suggests that HMBD-002 treatment stimulates a proinflammatory phenotype characterized by a Th1/Th17 response, recapitulating a phenotype previously noted in VISTA knockout models. This mechanism of action is further supported by immune-competent syngenic and humanized mouse models of colorectal, breast and lung

cancer where neutralizing VISTA, without depleting VISTA expressing cells, significantly inhibited tumor growth while decreasing infiltration of suppressive myeloid cells and increasing T cell activity. Finally, we did not observe either the fast serum clearance or immune toxicities that have been reported for IgG1 antibodies.

Conclusion In conclusion, we have shown that VISTA-induced immune suppression can be reversed by blockade of the functional C-C' loop region of VISTA with a first-in-class rationally targeted and non-depleting IgG4 isotype anti-VISTA antibody, HMBD-002. This antibody represents a highly promising novel therapy in the VISTA-suppressed ICT non-responder population.

BACKGROUND

Cancer treatment has evolved significantly with the discovery of drugs targeting immune checkpoint regulators (immune checkpoint therapy, ICT) and their subsequent inclusion in the standard of care for patients with cancer. However, long-term survival benefit is only observed in a fraction of patients, due to primary, adaptive, and acquired resistance mechanisms.¹ Novel agents are, therefore, required to improve treatment outcomes in non-responsive or resistant patients. V-domain Ig suppressor of T cell activation (VISTA) is a type I transmembrane immunomodulatory glycoprotein of the B7 protein family, with 24% sequence identity to programmed death-ligand 1 (PD-L1).² VISTA is predominantly expressed on the myeloid cell population, particularly myeloid-derived suppressor cells (MDSCs), neutrophils, monocytes, macrophages, and dendritic cells,²⁻⁵ however,

it can also be expressed on CD4⁺ T regulatory cells⁶ and CD4⁺ naïve T lymphocytes.⁷ VISTA has been identified as a negative checkpoint regulator of T cell function^{3,7} and is known to suppress autoimmune responses in a variety of human and mouse models of autoimmunity.^{2,8,9} More recently, VISTA was identified as the earliest checkpoint regulator of peripheral T cell tolerance, particularly in the maintenance of naïve T cell quiescence.⁴

In preclinical cancer models, the presence of VISTA has been shown to promote tumorigenesis, block T cell function, and modulate the activity of macrophages and immunosuppressive MDSCs, a function that is consistent with the maintenance of an anti-inflammatory tumor microenvironment (TME) characterized by a myeloid-enriched phenotype.⁶ In addition, VISTA has been observed to regulate the chemotaxis of macrophages and MDSCs into the TME and regulate effective antigen presentation.^{6,10} Suppressing VISTA activity in these models has shown a variety of beneficial outcomes including promoting tumor-specific effector T cell activation; reducing Treg induction and function; and enhancing myeloid mediated inflammatory responses.^{6,11} The first data to report VISTA in human tumors demonstrated increased expression of VISTA on myeloid cells as a resistance mechanism to ICT (anti-CTLA-4).¹² Substantial evidence has also shown high levels of VISTA on MDSCs in patient samples across a wide range of cancers,¹³ and immunosuppression by MDSCs and upregulation of VISTA has been associated with acquired resistance to anti-CTLA-4 and anti-programmed cell death protein-1 (PD-1)/PD-L1 therapies in multiple malignancies such as melanoma and prostate cancer^{12,14} as well as in acute myeloid leukemia.¹⁵ Together, these observations suggest an independent and potentially synergistic role of VISTA with the PD-1/PD-L1 pathway.^{10,13}

The physiologically relevant binding partners of VISTA are yet to be conclusively determined, but two independent *in vitro* studies have demonstrated V-Set and Immunoglobulin domain containing 3 (VSIG3, or IGSF11:Immunoglobulin Superfamily Member 11) as a partner.^{11,16} VSIG3 is expressed on cancer cells with elevated expression reported in multiple malignancies including colorectal, hepatocellular, and intestinal-type gastric cancers.¹¹ Additionally, the VISTA-VSIG3 interaction has been shown to inhibit T cell proliferation, as well as proinflammatory cytokine and chemokine release.¹¹ VISTA has also been reported to bind to itself,¹⁷ leucine-rich repeats and immunoglobulin-like domains 1 (LRIG1) (WO2019165233, WO2021047104), and P-selectin glycoprotein-1 (PSGL-1) at an acidic pH.^{18,19} However, neither the physiological significance of these interactions nor their association with antitumor effector functions have been established.

Despite the lack of consensus around the most physiologically relevant VISTA binding partner, VISTA antagonists, including antibodies and small molecules, are being explored for the treatment of patients with cancer who do not respond to current therapies or

acquire resistance to PD-1/PD-L1 and CTLA-4 therapies. Development of effective antibody therapeutics has been hampered by the lack of control that conventional methods of antibody discovery provide for targeting specific functional regions.²⁰ As a result, isolated antibodies often do not possess the functional and developability characteristics necessary to become therapeutics. To date, no antibodies against VISTA have been reported that demonstrate comparable cross-species affinity and that do not require Fc-mediated effector functions (such as antibody dependent cell cytotoxicity (ADCC), antibody dependent cell phagocytosis (ADCP), complement dependent cytotoxicity (CDC), induction of cytokines/chemokines and endocytosis of opsonized targets)²¹ to antagonize VISTA activity. Only two antibodies have reached the clinic. Clone VSTB112 (now being developed as CI-8993) is an anti-human VISTA antibody leveraging a cell-depleting IgG1 backbone previously developed by Janssen/ImmuNext and currently pursued by Curis (NCT04475523). The Fc-dependent activity of the IgG1 isotype was shown to be critical for VSTB112 antitumor effects. VSTB112 was also observed to trigger substantial cytokine release leading to neurotoxicity even at subtherapeutic doses (Curis corporate presentation, January 2021). A second clone IGN175A (now renamed as W0180), also a cell depleting IgG1 isotype VISTA antibody, is currently being developed by Pierre Fabre, but no data has thus far emerged.

Here we report a novel neutralizing anti-VISTA antibody, HMBD-002, developed using an AI-directed rational antibody discovery approach, which uniquely targets a specific functional epitope on the unique C-C' loop of VISTA that is conserved in human, monkey, rat, and murine orthologs. The C-C' loop, is a 21 residue exposed motif, which has been reported to play a role in protein-protein interactions.¹⁶ Leveraging an IgG4 backbone, HMBD-002 is the first VISTA-targeting antibody that has been shown to block the inhibitory function of VISTA and induce an antitumor response, without requiring Fc-dependent IgG1 isotype activity. We demonstrate that HMBD-002 inhibits interactions of VISTA with potential binding partners, including VSIG3, where release of VISTA-VSIG3 suppression of T cell activity potentiated a distinct shift in inflammatory milieu to a proinflammatory phenotype and potent inhibition of tumor growth in *in vivo* preclinical syngenic and humanized murine models of colorectal, lung and breast cancer. Collectively, these data suggest that HMBD-002 may be an effective therapeutic option for addressing VISTA-mediated immunosuppression across a broad range of tumors.

METHODS

Antibody isolation and production

For isolation and production of all antibodies, see online supplemental files 1

ELISA binding assay

384-well plates were coated with 1 µg/mL of target antigen diluted in phosphate buffered saline (PBS) for 16 hours at 4°C. After blocking for 1 hour with 1% bovine serum albumin (BSA) in PBS at room temperature, HMBD-002 or human IgG4 isotype control (Biolegend #403702) were serially diluted using 1% BSA made with 1 × PBS at neutral pH 7 and added to the plate. For testing the binding of test article at different pH, 1% BSA was made using 1 × PBS at pH of 7.5, 7.0, 6.5, 6, 5.5 or 5. Post 1 hour incubation at room temperature, plates were washed three times with TBS containing 0.05% Tween 20 (TBS-T) and incubated with 1:7000 of goat anti-human IgG Fc-HRP (Abcam #ab97225) for 1 hour at room temperature. After washing, plates were developed with colorimetric detection substrate 3,3',5,5'-tetramethylbenzidine (Turbo-TMB; Thermo Fisher # 34022) for 10 min. The reaction was stopped with 2M H₂SO₄, and OD was measured at 450 nm on a BioTek Synergy HT.

Flow cytometry and analysis

HMBD-002 binding to cell surface expressed VISTA on either peripheral blood mononuclear cells (PBMC), or HEK293T cells engineered to express VISTA, was measured by flow cytometry. Wild type HEK293T cells were transiently transfected with VISTA complementary DNA expression plasmids encoding human, cynomolgus monkey, rat, and mouse VISTA (Sinobiological) using lipofectamine 2000 (Thermo Fisher Scientific #11668019) following the manufacturer's protocol. PBMCs from human, cynomolgus monkey, rat and mouse were procured from commercial vendor (Accegen) and blocked with Fc block (Human TruStain FcX, Biolegend #422302, Mouse TruStain FcX, Biolegend #101320, Anti-Rat CD32, BD Pharmingen #550270 and Rhesus FcR Binding Inhibitor, Thermo Fisher #14-9165-42) prior to staining. HMBD-002 or isotype control antibodies were conjugated with APC (Abcam # ab201807) as per manufacturer's protocol. For fluorescence activated cell sorting (FACS), cells were incubated with different concentration of APC tagged HMBD-002 or isotype control as indicated in the figure for 40 min at 4°C. To identify myeloid cells, PBMCs were further incubated with CD45 FITC and CD11b PE. Cells were washed again and resuspended in 200 µL of FACS flow buffer (PBS + 0.5% BSA + 2 mM EDTA) for flow cytometric analysis using MACSQuant 10 (Miltenyi). After acquisition, all raw data were analyzed using FlowLogic software. Cells were gated using forward and side scatter, and the percentage of positive cells was determined.

Immunohistochemistry

Tissue microarrays (TMA) of patients with triple negative breast cancer (TNBC), non-small cell lung cancer (NSCLC), mesothelioma and liver cancer (USBiomax, #BR1301, #LC1401, #MS481d, #LV8013a) comprising formalin-fixed paraffin-embedded (FFPE) tissues were stained for VISTA (HMBD-002-mIgG2a; dilution 1:800)

and VSIG3 (LS Biosciences #LS-C338858; dilution 1:300) and normal TMA (USBiomax #FDA999q) was also stained for VISTA (HMBD-002-mIgG2a). Slides were dried in a desiccator for 15 min–1 hour and placed in EnVision FLEX Target Retrieval Solution, low pH (Dako #K8005/DM829) for 20 min at 97°C for antigen retrieval. Slides were placed in Envision Flex buffer (1×) for 10 min prior to transferring to the Omnis instrument for staining. Slides were stained and counterstained on the Dako Link Omnis with the Envision Flex+ detection system (kit K800) using the kit-based protocol, followed by rinsing, dehydrating and coverslipping. The TMAs were semi-quantitatively scored by light microscopy to determine the relative intensity of staining (0–3+ intensity scale), distribution and localization of VISTA and VSIG3 protein expression in normal and tumor tissues.

VISTA-VSIG3 inhibition assay

VISTA-VSIG3 binding was confirmed using recombinant human VISTA-Fc protein (R&D #7126-B7) or irrelevant antigen (Human recombinant CD47 protein, Sinobiological #112283-HCCH) with standard ELISA method. For the inhibition assay, 384-well plates were coated with 2 µg/mL of human VISTA-Fc recombinant protein (R&D #7126-B7) diluted in PBS for 24 hours at 4°C. After blocking for 2 hours with 1% BSA at room temperature, plates were incubated with either HMBD-002 or isotype control for 30 min at room temperature. After 30 min, biotinylated recombinant human VSIG3-Fc (Recombinant Human VSIG3. Fc was biotinylated using Invitrogen kit #21455) at 24 nM (EC₅₀ of VISTA-VSIG3 binding) was added for 2 hours. Post incubation, plates were washed three times with TBS-T and incubated with streptavidin HRP (R&D #DY998) antibody for 1 hour at room temperature followed by three further washes. Colorimetric reactions were developed using standard protocol as described for ELISA above.

Cytokine release post HMBD-002 blocking of VISTA-VSIG3

PBMCs were cultured in plates coated with αCD3 monoclonal antibody (eBioscience #16-0037) and VSIG3-Fc (R&D #9229-VS) at ratios of either 1:0 (2 µg/mL αCD3 alone) and 1:2 (2 µg/mL αCD3: 4 µg/mL of VSIG3-Fc). Cells were then treated with either HMBD-002, VSTB112 or IgG4 isotype control (Biolegend #403702) at the indicated concentration and plate was incubated at 37°C. Supernatant was harvested after 24 hours and interferon (IFN)-γ levels was measured using Human IFN-γ Uncoated ELISA kit (Invitrogen #88-7316).

MDSC-T cell co-culture

Monocytes were isolated from fresh human PBMCs via negative enrichment using Classical Monocyte Isolation Kit (Miltenyi, #130-117-337). Subsequently, monocytes were differentiated to MDSCs for 7 days in the presence of granulocyte-macrophage colony-stimulating factor (GM-CSF) (10 ng/mL) (PeproTech #300-03) and interleukin (IL)-6 (10 ng/mL) (PeproTech #200-06). MDSCs were

harvested and cultured with freshly isolated autologous PBMCs at 2:1 ratio in the presence of human anti-CD3 antibody (OKT3, 1 µg/mL) (Biolegend, #317326) and in the presence or absence of test articles as indicated. Supernatant was harvested after 96 hours and IFN-γ levels were determined via ELISA (Thermo Fisher, USA, #88-7316-88). Data are presented as fold change with respect to the isotype for each antibody concentration.

Neutrophil chemotaxis assay

Neutrophils were isolated from whole blood using MACSxpress Whole Blood Neutrophil Isolation Kit (Miltenyi #130-104-434) and incubated with either HMBD-002, VSTB112 or isotype control, at the indicated concentration, for 60 min at 37°C. Post incubation, neutrophils were seeded in the upper chamber (300 µl/well) of 24 well transwell plate (Thermo Fisher #1406287) and media, with or without C5a at 50 ng/mL (Acro Biosystem #C5A-H5116), was added to the lower chamber (600 µl). Cells were incubated in the transwell for 1 hour at 37°C, after which adenosine triphosphate (ATP) levels of the migrated neutrophils in the lower chamber was measured using CellTiter-Glo (Promega #G7571) and luminescence was measured by Victor Nivo (PerkinElmer).

Human allogeneic mixed lymphocytic reaction

Fresh PBMCs were isolated from human whole blood (five donors in total) using lymphoprep (Stemcell Technologies, #07861), following manufacture's protocol and resuspended with CellGenix GMP dendritic cell (DC) medium at 5×10^6 cells/mL. 50 µl of DC medium was added into each well of 96-well round bottom plate followed by 50 µl of PBMCs from two donors at 1:1 ratio in the presence of either 50 µl of HMBD-002 or isotype control hIgG4 (InvivoGen #bgal-mab114) at 30, 10 and 1 µg/mL. A total of 10 donor pairs were used. Cells were incubated at 37°C for 96 hours. Supernatants were collected at 96 hours and the supernatant cytokine levels were detected by Luminex (R&D #LXSAHM-04/07). Data are presented as fold change from the relevant isotype for each antibody concentration.

Animal experiments

Balb/c mice were purchased from InVivos or Jackson Labs and CD34 engrafted humanized HiMice mice were purchased from Invivocue. All animals were housed under specific pathogen-free conditions in a facility accredited by Association for Assessment and Accreditation of Laboratory Animal Care, International and treated in strict compliance with the Institutional Animal Care and Use Committee guidelines.

In vivo tumor growth assays

Mice were subcutaneously implanted with tumor cells (10^5 for CT26, 10^6 for HCT15 and 5×10^6 for A549) in the right flank or for orthotopic breast model, tumor cells were implanted into the mammary fat pad (2×10^4

4T1 cells). Mice were treated two times per week with the indicated dose and interval of the test articles 3–6 days post implantation. Treatment was administered intraperitoneally for all subcutaneous models, and intratumorally for the orthotopic model. Tumor volume was measured using calipers as described previously.²²

Statistical analysis

Statistical analysis was performed using GraphPad Prism. Data acquired with two variables (dose titrations) was analyzed with two-way analysis of variances followed by Tukey's multiple comparisons test. For comparisons between two groups, an unpaired t-test was performed. Values of * $p \leq 0.05$, ** $p \leq 0.01$, *** $p \leq 0.001$, **** $p \leq 0.0001$, were considered significant.

RESULTS

VISTA is predominantly expressed on myeloid-derived cells in healthy tissues

As an important immune modulator, the distribution of VISTA expression was studied in healthy tissues to evaluate the optimal strategy for a VISTA antagonist. We first analyzed a single cell RNA-sequencing (RNA-seq) data set from 10X Genomics comprising 68,000 PBMCs, as described in the supplementary methods.²³ This revealed the presence of 14 major cell clusters (figure 1A). Although low levels of VISTA transcripts were identified in many cell populations, high expression was confined to myeloid-derived monocytes and dendritic cells in healthy human donors, with limited expression in T cells (figure 1B,C). VISTA protein expression in healthy human tissues was further characterized using immunohistochemistry (IHC) on FFPE TMA sections (figure 1D). The highest VISTA levels were detected in lymphoid organs (eg, spleen and bone marrow) and tissues with significant infiltration by leukocytes (eg, breast and lung). The distribution of VISTA across healthy tissues and diverse immune cells strongly supports the need to antagonize VISTA without depleting VISTA expressing cells for optimal therapeutic benefit and tolerable safety.

Solid tumors including TNBC and NSCLC show significant expression of VISTA and VSIG3

Previous studies have reported VISTA expression across a range of cancers.²⁴ We assessed the expression of VISTA in FFPE TMA sections of four solid cancers via IHC, including TNBC, NSCLC, hepatocellular carcinoma and mesothelioma. Patients with TNBC and NSCLC showed the highest VISTA expression, with 89% and 85%, of the cores showing moderate-high staining intensity, respectively (figure 1E). There have also been reports of expression of the VISTA binding partner VSIG3 in solid cancers¹¹ and we further evaluated the expression of VSIG3 in our TMAs. VSIG3 showed moderate-to-high staining in mesothelioma

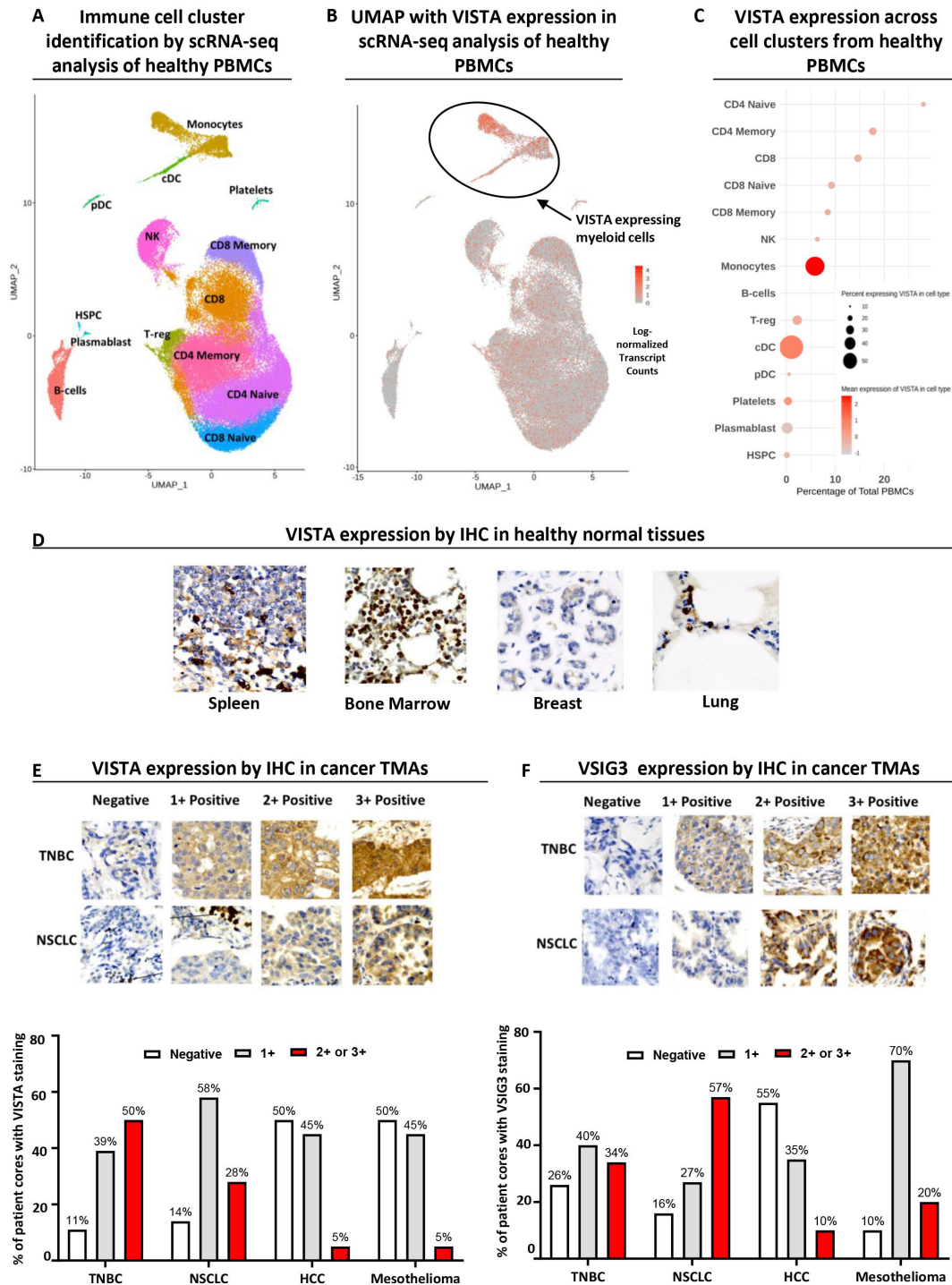


Figure 1 VISTA is predominantly expressed on myeloid-derived cells in healthy tissues and several solid tumors, including TNBC and NSCLC, show significant expression of VISTA and its binding partner VSIG3. (A) Immune cell cluster identification by RNA single-cell analysis of 10X Genomics data comprising 68,000 healthy PBMCs. (B and C) Uniform Manifold Approximation and Projection (UMAP) and summary plot of single-cell RNA-seq data for VISTA expression in different cell clusters, where cDC refers to classical dendritic cells, pDC to plasmacytoid dendritic cells and HSPC to hematopoietic stem and progenitor cells. (D) Representative immunohistochemical staining for healthy spleen, bone marrow, breast and lung TMA samples (n=99) stained with HMBD-002-mIgG2a at 0.02 mg/mL; magnification 200 \times . (E) Representative immunohistochemical staining for VISTA in TNBC (n=126) and NSCLC TMA samples (n=140) stained with HMBD-002-mIgG2a at 0.02 mg/mL; magnification 200 \times (top) and % of patients with negative (0), low (1), moderate (2) or high (3) staining intensity (bottom). (F) Representative immunohistochemical staining for VSIG3 in TNBC (n=126) and NSCLC TMA samples (n=140) stained with anti-VSIG3 at 0.003 mg/mL, magnification 200 \times (top) and % of patients with negative (0), low (1), moderate (2) or high (3) staining intensity (bottom). HCC, hepatocellular carcinoma; IHC, immunohistochemistry; NSCLC, non-small cell lung cancer; scRNA-seq, single-cell RNA sequencing; TMA, tissue microarrays; TNBC, triple negative breast cancer; VISTA, V-domain Ig suppressor of T cell activation; VSIG3, V-Set and Immunoglobulin domain containing 3.

(90%), NSCLC (84%), and TNBC (74%) (figure 1F). The observed high expression of both VISTA and VSIG3 in TNBC and NSCLC, is consistent with reports that the co-inhibitory function of VISTA may be mediated through VISTA-VSIG3 interactions suppressing T cell function¹¹ and further suggests that these could be priority indications to investigate the benefits of VISTA antagonism.

HMBD-002 is a unique IgG4 isotype anti-VISTA antibody immunoengineered to bind a rationally predicted species-conserved functional epitope on VISTA

Given the expression pattern of VISTA on healthy cells, we chose to develop an IgG4 isotype anti-VISTA antibody that would inhibit VISTA function by blocking interactions with its binding partners without depleting VISTA expressing cells through Fc-mediated effector functions.

VISTA is a B7 family receptor, and we hypothesized that the interaction surface for VISTA and its binding partners would be conserved across other B7 receptors, including PD1/PD-L1 (figure 2A). As such, the PD1/PD-L1 complex (PDB: 5IUS) was used as a template for structural alignment and the VISTA structure (PDB: 6OIL) was mapped onto the complex. This input structural model of VISTA was integrated with the available sequence data in humans and model species to predict solvent accessibility, post-translational modifications and other features of VISTA that would be important for the ability of an antibody to bind. We also applied machine learning algorithms, such as PRISM, to identify²⁵ low energy template interfaces overlapping with the PD1-PDL1 interface (online supplemental table S1). This approach highlighted antibody-available regions along the F, D, C, C' β -sheets and the C-C' loop predicted to be involved in mediating the interaction with VISTA's cognate receptor/ligand (figure 2B), and prioritized target regions in the C-C' loop that are unique to VISTA within the human proteome and highly conserved across model species (figure 2C,D, online supplemental figure S1A). The functional nature of this region is supported by the known interaction residues for VSIG3^{11,16} that are located within this C-C' loop region (figure 2E). Further, the proposed residues for VISTA-LRIG1 interaction also fall within this region, while those for VISTA-PSGL-1 interactions are more distant¹⁸ (online supplemental figure S1B).

This rationally predicted region was then used as input for an immunization approach which utilized computationally designed immunogens to bias the B cell response to the target functional region on VISTA. Monoclonal antibodies targeting this surface were isolated by immunization of mice with proprietary mixtures of these immunogens and customized adjuvants, before subsequent isolation of hybridoma clones. Clone V4P, was selected for further development based on preliminary binding affinity and specificity within the B7 family and

its ability to show Fc-independent in vivo efficacy as both a competent mIgG2a isotype (equivalent to human IgG1-Fc) and a mutant mIgG2a-LALAPG where Fc γ R binding is abolished (online supplemental figure S2). V4P was subsequently humanized, and affinity matured (online supplemental methods). The final VISTA targeting antibody, HMBD-002, was selected from among the optimized variants based on its in vitro physicochemical and functional properties (WO2019185879). An IgG4 isotype (with a S228P stabilizing mutation) was chosen as this Fc isotype is known to lack affinity to most activating Fc γ Rs as well as C1q, precluding the activation of ADCC and CDC depletion of antigen expressing cells. This was confirmed by the lack of binding of HMBD-002 to the activating Fc γ RIII and C1q proteins by ELISA (online supplemental figure S3A,B).

To confirm the HMBD-002 binding region, epitope mapping analysis by hydrogen–deuterium exchange mass spectrometry was conducted for the VISTA-HMBD-002 complex. Comparison of the deuterium exchange between HMBD-002 bound VISTA and free VISTA showed that significant decrease in deuterium uptake was observed at two loci spanning residues 69–85 and 85–97 (figure 2F), indicating that these regions were protected against deuterium exchange via protein–protein interaction. Furthermore, the reduced deuterium exchange at early time points observed for peptide 85–97 suggested that this is the primary epitope of HMBD-002. Reduction of deuterium exchange at later time points observed for peptide 69–85 may represent a secondary binding event subsequent to binding of the primary epitope. Mapping of these identified peptides to the VISTA structure confirmed that these sites overlapped with the predicted target region (figure 2D) and include three critical amino acid residues for VSIG3 binding (R86, F94 and Q95, figure 2E).¹⁶

We then compared the binding site of HMBD-002 to other published VISTA antibodies by epitope binning with the human VISTA-specific VSTB112 and IGN175A antibodies, and mouse VISTA ortholog specific 13F3 and MH5A antibodies.²⁶ Lack of interference in binding indicated that HMBD-002 and IGN175A have topologically distant epitopes on human VISTA (online supplemental figure S4A). Similarly, 13F3, MH5A and HMBD-002 are largely non-competing (online supplemental figure S4B). The partial interference of binding observed between VSTB112 and HMBD-002 suggests that the epitope of VSTB112 is distinct but closer than IGN175A to the epitope of HMBD-002. In conclusion, HMBD-002 binds to a unique epitope on human and mouse VISTA orthologs.

HMBD-002 shows specific, species-conserved, high affinity binding to VISTA, at a range of physiological pH

To support the therapeutic development of HMBD-002, its biophysical properties were evaluated to ensure they were appropriate for a therapeutic antibody. First, highly specific binding of HMBD-002 to VISTA among the other related members of the B7 family (B7H1/PDL-1, B7H3,

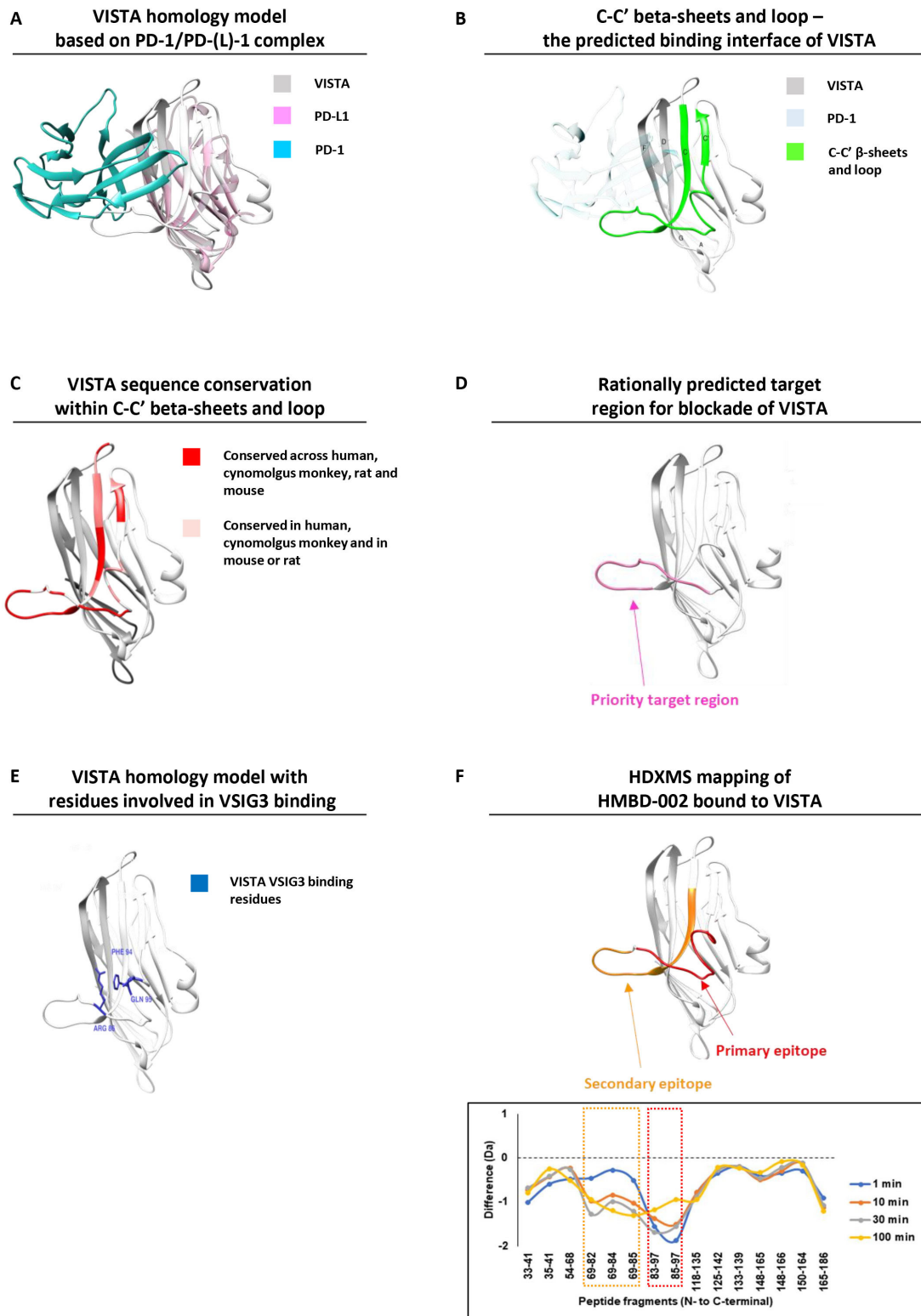


Figure 2 HMBD-002 is a unique anti-VISTA antibody, immunoengineered to bind to a rationally predicted functional epitope that is species-conserved and overlaps with key residues for VISTA interaction with VSIG3. (A) VISTA homology model (gray) superimposed with the complex of PD-L1 (purple) bound to its ligand PD-1 (cyan) from PDB:5IUS. (B) Front C-C' β sheets and loop of VISTA protein constituting the predicted binding interface for physiologically relevant binding partners (highlighted in green). (C) Three-dimensional (3D) overlay model of VISTA protein from mouse, rats, cynomolgus monkey and humans showing sequence conservation of the C-C' β sheets and loop. (D) 3D model of the computationally predicted target region for antibody blockade of VISTA. (E) Predicted VISTA homology model with residues implicated in VSIG3 binding. (F) Epitope mapping analysis of HMBD-002 bound to VISTA using hydrogen–deuterium exchange mass spectrometry. PD-1, programmed cell death protein-1; PD-L1, programmed death-ligand 1; VISTA, V-domain Ig suppressor of T cell activation; VSIG3, V-Set and Immunoglobulin domain containing 3.

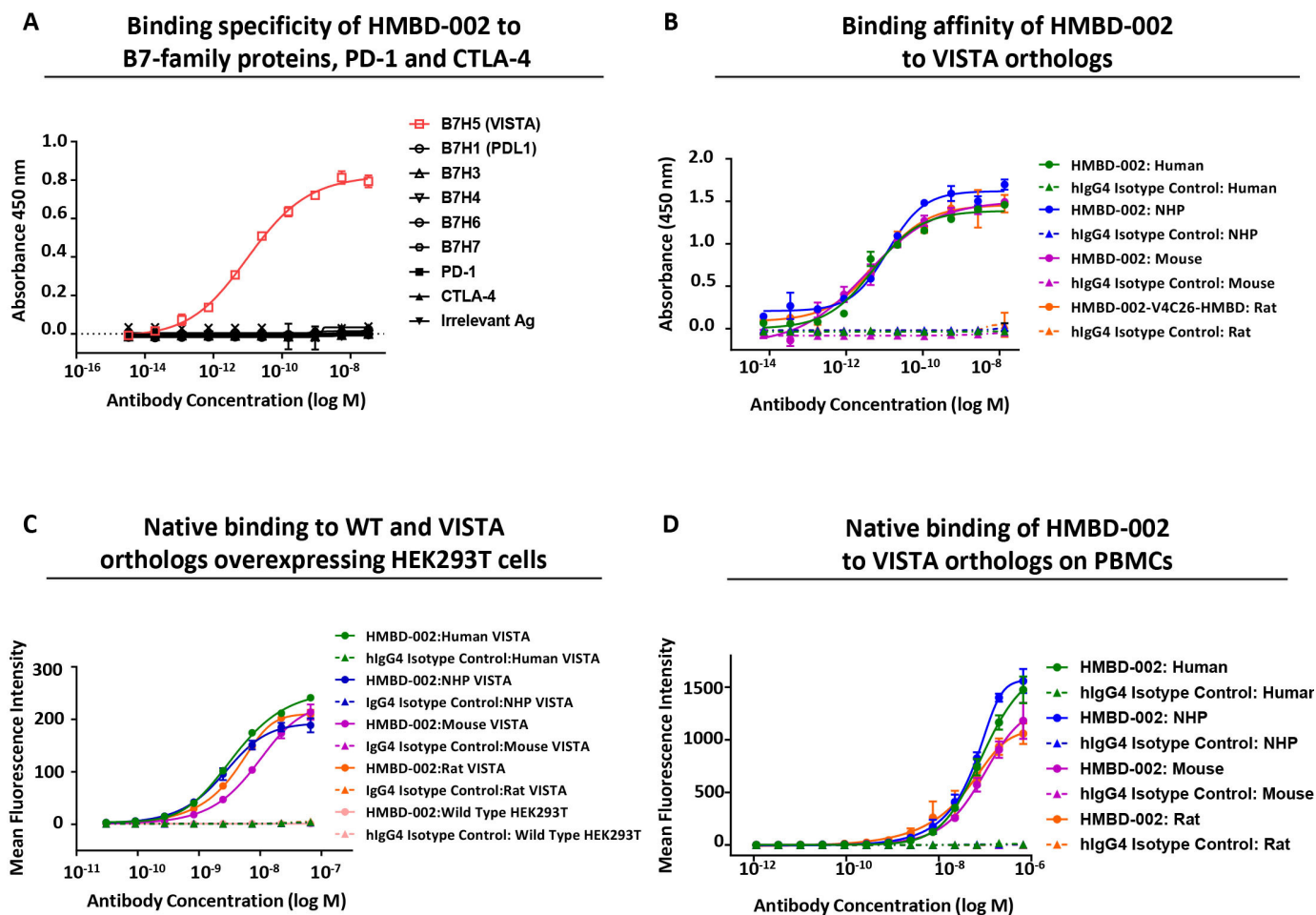


Figure 3 HMBD-002 binds with high affinity and specificity to a species-conserved epitope on recombinant and cell surface expressed VISTA orthologs. (A) Binding specificity of HMBD-002 by ELISA using human B7 family antigens as indicated. Data shown are mean $n=2$ measurements and error bars are SEM. (B) ELISA binding of HMBD-002 to VISTA orthologs; human, NHP, rat or mouse VISTA. Data shown are mean of $n=3$ measurements and error bars are SEM. (C and D) Binding specificity of HMBD-002 to cell surface expressed VISTA by flow cytometry on overexpressing HEK293T cells or wild type HEK293T (C) and CD11b+ myeloid cells isolated from human, NHP, rat or mouse PBMCs (D) Data shown are mean of $n=3$ measurements and error bars are SEM. NHP, non-human primate; PD-1, programmed cell death protein-1; PD-L1, programmed death-ligand 1; VISTA, V-domain Ig suppressor of T cell activation; WT, wild type.

B7H4, B7H6, B7H7), as well as PD-1 and CTLA-4, was confirmed by ELISA (figure 3A). Second, to support the use of rodent and non-human primate (NHP) species for efficacy, safety and PK models, the ability of HMBD-002 to bind to VISTA orthologs was assessed using ELISA and SPR (Biacore). HMBD-002 showed dose-dependent binding to human, NHP, rat and mouse VISTA-HIS protein by ELISA with an EC_{50} of 5.117 pM, 12.15 pM, 6.689 pM, and 3.549 pM, respectively (figure 3B). Further, HMBD-002 was observed to bind to human, NHP, rat and mouse VISTA orthologs with similar picomolar affinities (Kd) of 407 pM, 367 pM, 382 pM, and 549 pM, respectively (online supplemental figure S4C–F).

Cell surface binding of HMBD-002 to HEK293T cells expressing recombinant VISTA orthologs, as well as to myeloid cells within PBMC of relevant preclinical species, was further confirmed by FACS. HMBD-002 showed dose-dependent binding to VISTA orthologs of all species tested, with comparable EC_{50} values of

3.738 nM, 2.571 nM, 4.133 nM and 8.94 nM for human, NHP, rat, and mouse VISTA expressing HEK293T cells, respectively (figure 3C). There was no non-specific binding observed to wild type HEK293T cells, which do not express VISTA. HMBD-002 also showed comparable dose-dependent binding to endogenous VISTA expressed on the myeloid cells of all preclinical species tested, with EC_{50} of 108 nM, 67.6 nM, 48.6 nM and 111 nM for human, NHP, rat, and mouse VISTA, respectively (figure 3D).

Some tumor environments have been reported to be hypoxic, characterized by relatively low pH.²⁷ As VISTA contains many exposed histidine residues that are susceptible to protonation that may affect antibody binding, we evaluated the effect of pH on HMBD-002 binding. HMBD-002 was observed to bind VISTA with comparable affinity at pH 5.5–7.5, as assessed by ELISA (online supplemental figure S4G), confirming that HMBD-002 binds to VISTA across the range of

physiologically relevant pH and that the binding site is distinct from the histidine-rich regions.

HMBD-002 blocks VISTA-VSIG3 interactions and attenuates VSIG3-mediated suppression of IFN- γ release from activated T cells

Given the binding of HMBD-002 to the C-C' loop region, hypothesized to be a common functional region for VISTA to bind to multiple partners, we next determined the ability for HMBD-002 to inhibit these interactions. For this purpose, ELISA-based recombinant protein binding assays were developed that modeled the binding between VISTA and its binding partners, VSIG3 (online supplemental figure S5A) and LRIG1 (online supplemental figure S5B). HMBD-002 was observed to antagonize VISTA-VSIG3 interaction in a dose-dependent manner with an IC₅₀ of 673 pM (figure 4A). Similarly, HMBD-002 also showed a dose-dependent inhibition of VISTA-LRIG1 binding with a IC₅₀ value of 3.4 nM (online supplemental S5C). Conversely, the residues reported to be involved in the interaction of VISTA with PSGL-1 are outside of the C-C' loop and distal from the HMBD-002 epitope, and HMBD-002 was not observed to inhibit the VISTA-PSGL-1 interaction (online supplemental figure S5D,E).

To evaluate the functional effect of inhibiting VISTA-VSIG3 interaction with HMBD-002, we performed a surrogate assay for tumoricidal T cell activity.²⁸ In this assay, an anti-CD3 antibody mimics T cell receptor ligation, resulting in IFN- γ secretion that can be quantified in the supernatant by ELISA. As expected, incubating human PBMCs with VSIG3 significantly suppressed the release of IFN- γ (figure 4B). Notably, this suppression could be effectively released in a dose-dependent manner with the addition of HMBD-002, but not VSTB112, to the media (figure 4C). These data support the hypothesis that HMBD-002 functionally blocks interactions of VISTA with key protein partners, such as VSIG3, and further suggest a potential mechanism of action of HMBD-002 - blockade of VISTA-VSIG3 mediated suppression of proinflammatory IFN- γ secretion from activated T cells.

HMBD-002 neutralizes VISTA, reducing MDSC-mediated T cell suppression and inhibiting neutrophil chemotaxis

Previous studies have reported a key role for VISTA in the modulation of myeloid function.²⁹ To investigate the effect of VISTA blockade on myeloid cells that express the highest levels of VISTA, we evaluated the effect of HMBD-002 treatment in several in vitro models of myeloid function.

We first evaluated VISTA blockade by HMBD-002 on the function of human monocytic MDSCs. Previous studies have reported that MDSCs contribute significantly to suppression of T cell function in the TME.¹⁵ Monocytes differentiated to MDSCs for 7 days with GM-CSF and IL-6, were co-cultured with autologous PBMCs. T cells were then stimulated with an anti-CD3 antibody and IFN- γ levels in the culture supernatant were measured by ELISA. Addition of HMBD-002, but not VSTB112,

successfully reversed MDSC-mediated T cell suppression in response to anti-CD3 stimulation as indicated by the enhanced levels of IFN- γ (figure 4D).

Granulocytes such as neutrophils are an integral part of the innate immune response but can adversely effect cancer progression. Although it is challenging to model the function of granulocytic (g)-MDSCs in vitro, it is known that g-MDSCs can arise from neutrophils that have infiltrated the TME.³⁰ We therefore explored the effect of HMBD-002-mediated VISTA blockade on neutrophil chemotaxis using a transwell assay. In this assay, neutrophils migrate between chambers towards a physiologically relevant chemoattractant, C5a, and the percent of cells that have migrated to the lower chamber is then quantified via a luminescence readout. We observed that HMBD-002 potently inhibited neutrophil migration in a dose-dependent manner. VSTB112, in contrast, could only suppress neutrophil migration at much higher concentrations (figure 4E).

Collectively these results demonstrate that HMBD-002 potently neutralizes VISTA on myeloid cells leading to the increased secretion of proinflammatory cytokines and decreased migration of neutrophils.

HMBD-002 polarizes the immune cell milieu toward a proinflammatory Th1 immune response during an allogenic mixed lymphocyte reaction

To investigate the functional effect of VISTA blockade by HMBD-002 in more complex in vitro models of immune activation, we utilized an allogenic mixed lymphocyte reaction (MLR) assay. Briefly, PBMCs from five independent healthy human donors were mixed pairwise to model a self/anti-self immune response and were then cultured for up to 96 hours in the presence or absence of HMBD-002 before supernatants were analyzed for cytokine levels. The transcriptome of the cells was also analyzed using bulk RNA-seq. Cytokine levels in the supernatant were quantified by Luminex assay and showed that HMBD-002 induced a significant dose dependent increase in the levels of the Th1 cytokines IFN- γ and tumor necrosis factor (TNF)- α at 96 hours, comparable to the effect seen with PD-1/PD-L1 blockade by an anti-PD-1 antibody, pembrolizumab. Other changes in the levels of IL-4, IL-10 and IL-13 (Th2 cytokines) or IL-6, IL-17 or IL-23, although less apparent, were further indicative of the induction of a proinflammatory Th1/Th17 response by VISTA blockade, in agreement with previous reports (figure 5A, online supplemental figure S6A).^{31 32} This was further supported by bulk RNA-seq that highlighted an enrichment of transcript levels in genes associated with TLR, TNF- α , IL-1, JAK-STAT and IL-17 signaling pathways along with an increase in transcript levels of Th1 associated genes such as IFN- γ , TNF- α and IL-12A and a decrease in transcript levels of Th2 associated genes IL-4, IL-10, IL-13 and IL-9 (figure 5B, online supplemental figure S6B,C). Collectively, these results show that HMBD-002 blockade of VISTA can polarize the immune

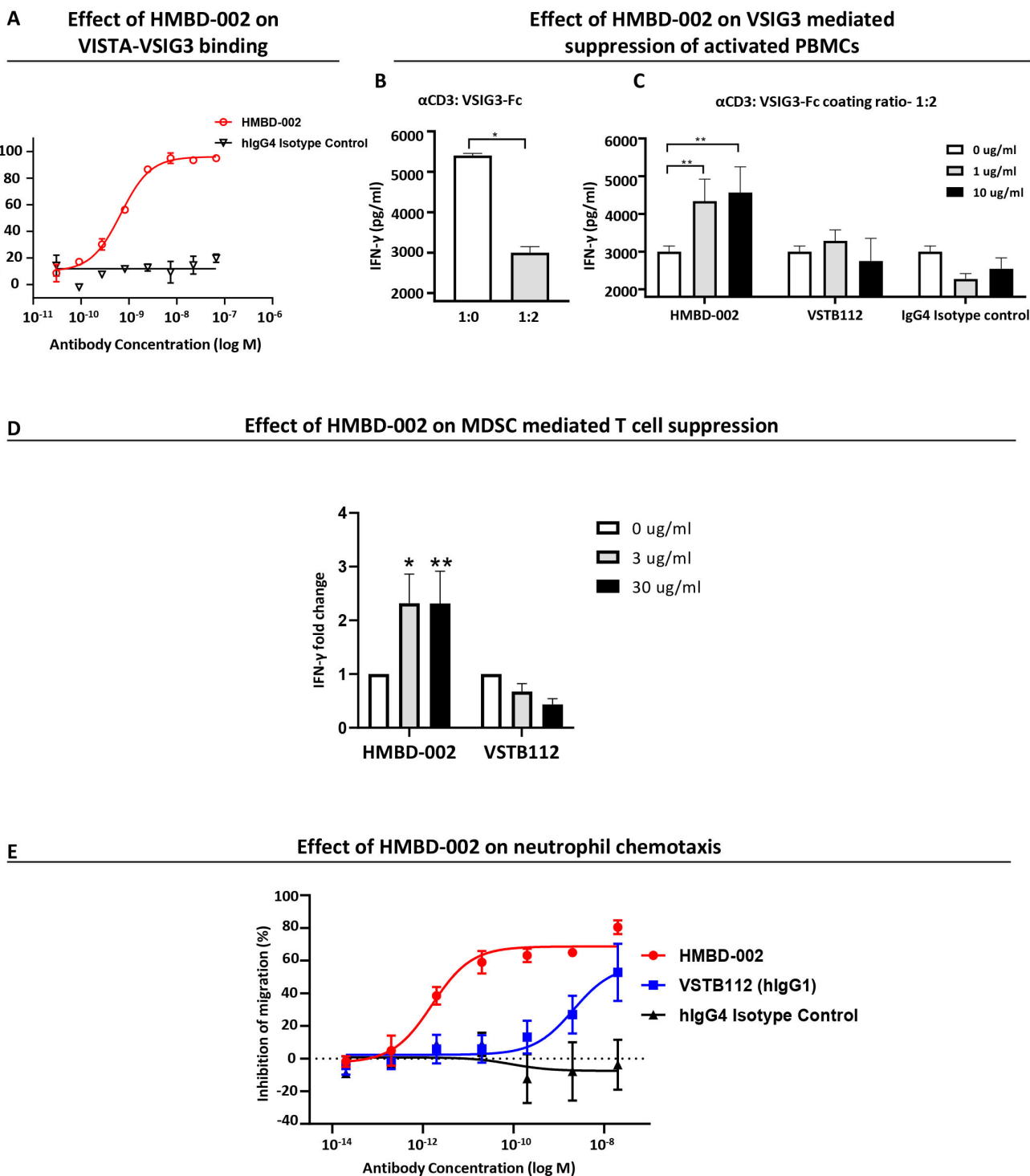


Figure 4 HMBD-002 neutralizes VISTA activity by inhibiting VISTA-VSIG3 binding, attenuating VSIG3-mediated suppression of IFN- γ release from activated T cells, reducing MDSC-mediated T cell suppression and inhibiting neutrophil chemotaxis. (A) Inhibition of VISTA:VSIG3 binding, analyzed by competition ELISA. Data shown are mean of n=3 measurements and error bars are SEM. (B and C) VSIG3 suppression of IFN- γ levels, measured by ELISA at 24 hours, from PBMC cultured in plates coated with α CD3 monoclonal antibody (OKT3) and VSIG3-Fc at ratios of 1:2, in presence and absence of test articles as indicated. Data shown are mean of n=3 measurements; error bars are SEM and p value was obtained by (B) paired t-test, *p<0.05 and (C) one-way analysis of variance (Tukey's multiple comparison test), **p<0.01. (D) Anti-CD3-induced IFN- γ secretion from MDSC co-cultured with autologous PBMCs after 96 hours, in presence or absence of indicated test articles as measured by ELISA. Data were normalized to isotype control. Data shown are mean of n=6 measurements and error bars are SEM and p value was obtained by unpaired t-test. *p<0.05, **p<0.01 (E) Inhibition of neutrophil migration to the bottom chambers of transwell coated with C5a and measured using CellTiter-Glo. Data shown are mean of n=3 measurements and error bars are SEM. IFN, interferon; MDSC, myeloid-derived suppressor cells; VISTA, V-domain Ig suppressor of T cell activation; VSIG3, V-Set and Immunoglobulin domain containing 3.

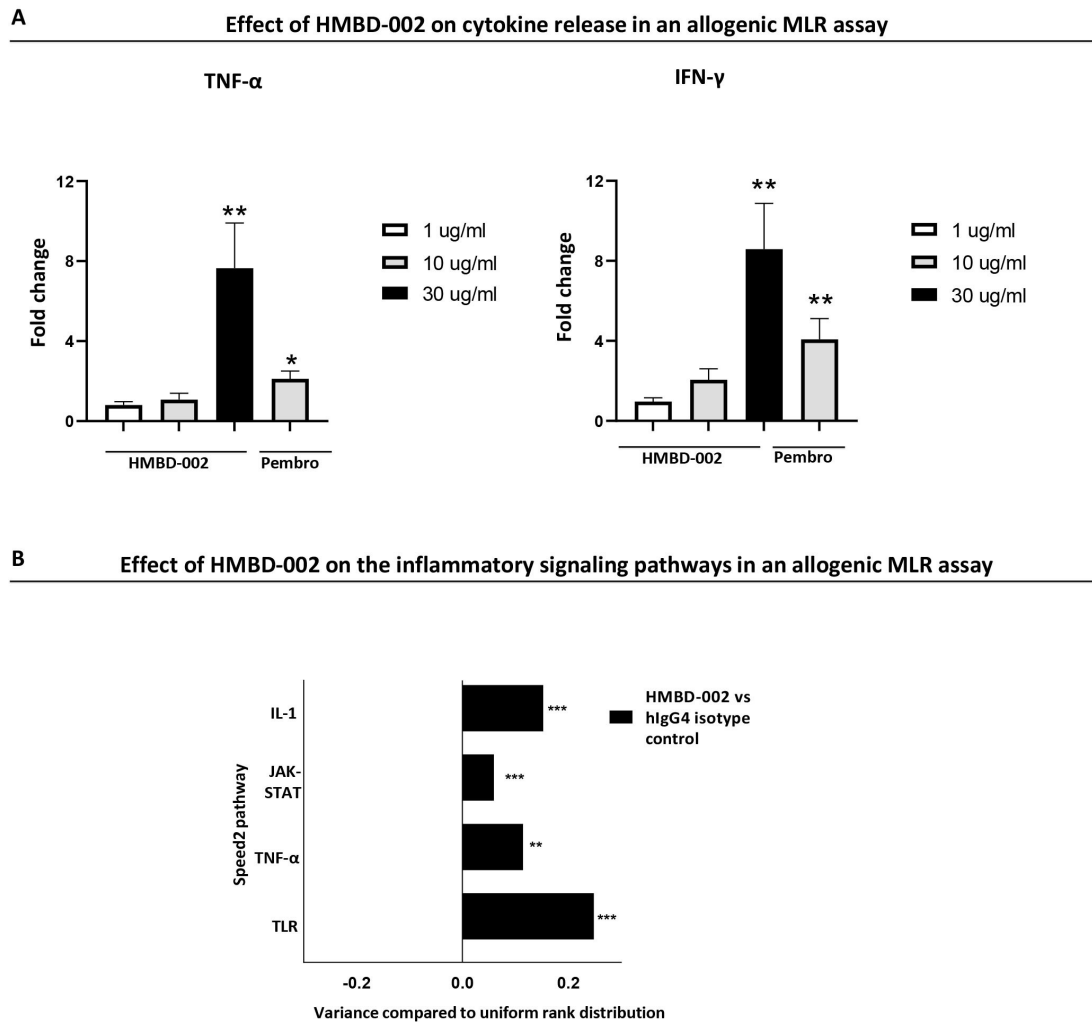


Figure 5 HMBD-002 remodels the immune milieu toward a proinflammatory Th1 immune response in an allogenic mixed lymphocyte reaction (MLR). (A) Cytokine levels measured at 96 hours by Luminex, from the supernatant of an allogenic mixed lymphocyte reaction. All concentrations of HMBD-002 and anti PD-1 antibody, pembrolizumab (annotated as pembro) in $\mu\text{g}/\text{ml}$. Data were normalized to isotype control. Data shown are mean of $n=10$ and error bars are SEM. P values were obtained by unpaired t-test, * $p<0.05$, ** $p<0.01$. (B) Speed2 pathway analysis from bulk RNA-sequencing of MLR samples ($n=10$). Data were normalized to isotype control, represented as mean \pm SD and the p adjusted values were obtained from bulk RNA sequencing analysis, ** $p<0.01$, *** $p<0.001$. IFN, interferon; IL, interleukin; PD-1, programmed cell death protein-1; TNF, tumor necrosis factor.

milieu toward an enhanced Th1/Th17 proinflammatory immune response.

HMBD-002 treatment induces strong antitumor responses in multiple immune competent syngenic and humanised cell-derived xenograft models of solid tumors

To explore the proinflammatory and antitumorigenic effects of HMBD-002 in vivo, tumor growth inhibition studies were conducted in multiple solid tumor models that included a syngenic murine cell-derived xenograft (CDX) subcutaneous model of colon cancer (CT26), a checkpoint inhibitor-resistant orthotopic CDX model of VISTA expressing breast cancer (4T1) and CD34 engrafted humanized models of human lung cancer (A549) and colorectal cancer (HCT15).

First, Balb/c mice were subcutaneously implanted (right flank) with CT26 tumors and treated biweekly with

500 μg (~25 mg/kg), of HMBD-002 (intraperitoneal) from 3 days post implantation (figure 6A), a dosing regimen routinely used for evaluating in vivo efficacy of antibodies against IO targets in mouse models.^{26 33 34} HMBD-002 demonstrated significant single agent efficacy with 84% inhibition of tumor growth compared with vehicle.

Second, a murine orthotopic model of breast cancer was established by implanting 4T1 cells overexpressing VISTA in the mammary fat pads of Balb/c mice. Mice were treated intratumorally with 50 μg of either HMBD-002 or the anti-mouse VISTA antibody 13F3 on days 7, 9, 12, 14, 16 post implantation. The 13F3 is frequently used as a mouse surrogate for studying the in vivo efficacy of anti-VISTA antibodies.^{2 6} HMBD-002 again showed significant tumor growth inhibition (TGI) (53%), which was comparable to that of 13F3 suggesting the two

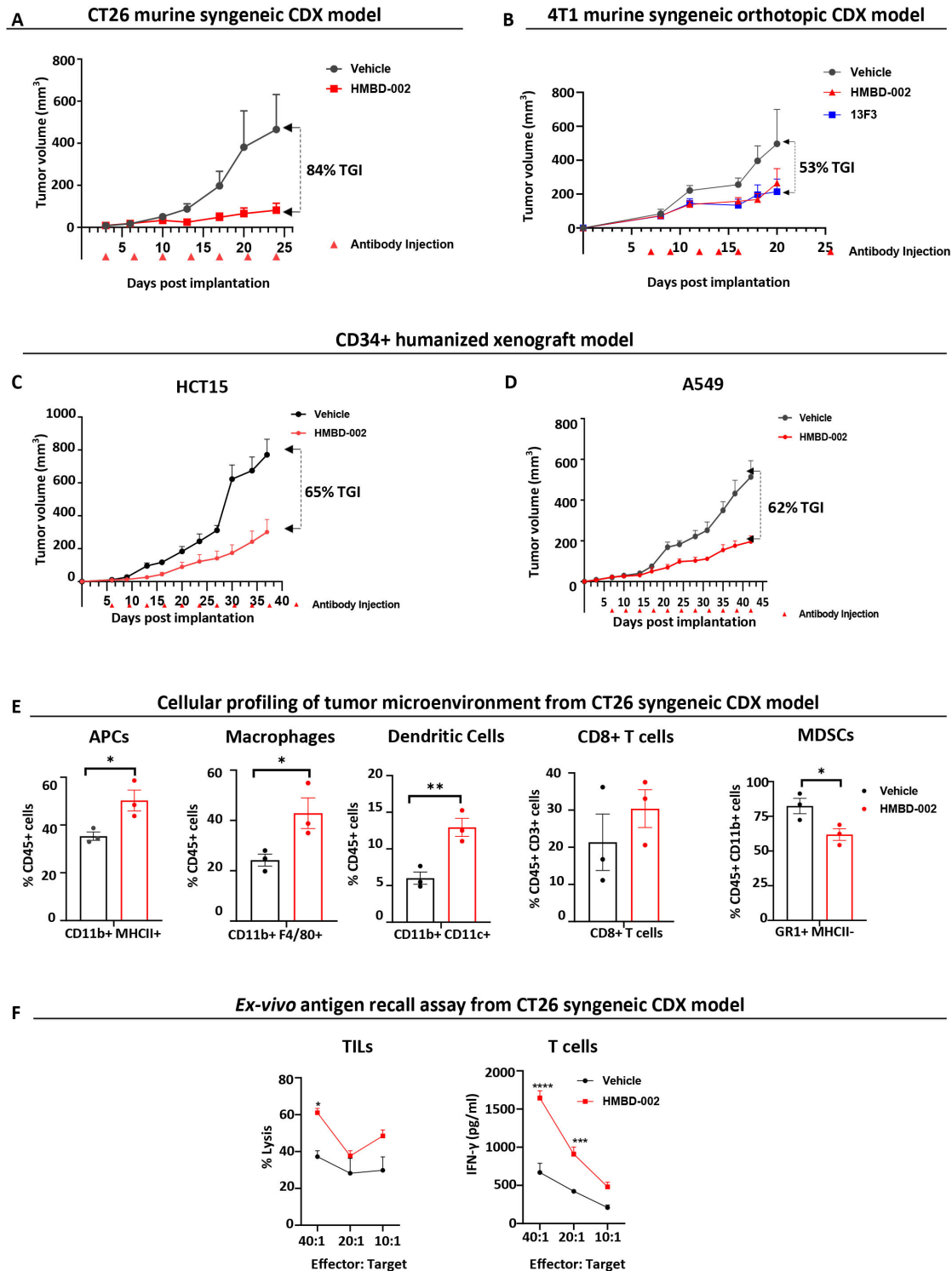


Figure 6 HMBD-002 demonstrates strong antitumor responses as a single agent in multiple CDX models of tumors and remodels the TME to an antitumorigenic, proinflammatory phenotype. (A–D) CDX models used in the study included female BALB/c mice, subcutaneously implanted with CT26 (A); Female Balb/c mice orthotopically implanted with VISTA O/E 4T1 cells (B) and CD34 engrafted humanized female HiMice, subcutaneously implanted with either A549 (C) or HCT15 (D) cells. Mice were randomized and dosed with concentrations of test articles at indicated time points. Tumor volumes were measured two times a week. Each data point represents the mean tumor volume \pm SEM from $n=10$ mice. (E) Tumor-infiltrating leukocyte (TIL) populations in the TME of CT26 syngeneic CDX model profiled by FACS. Data shown are mean of $n=3$ and error bars are SEM. (F) CT26 Antigen recall assay measured by ex vivo culture of TILs (CD45+) with CT26 cells to measure lysis or culture of tumor enriched T cells (CD4+/CD8+) with CT26 cells to measure T cell activation via IFN- γ secretion using ELISA. Data shown are mean of $n=3$ and error bars are SEM. All p values were obtained by unpaired t -tests, * $p<0.05$, ** $p<0.01$. Each data point represents a mouse. CDX, cell-derived xenograft; IFN, interferon; MDSCs, myeloid-derived suppressor cells; TME, tumor microenvironment; VISTA, V-domain Ig suppressor of T cell activation.

antibodies may share a common mechanism of action (figure 6B).

Finally, to confirm these effects were not limited to murine cancers, the *in vivo* efficacy of HMBD-002 was tested with human cell lines in humanized mice engrafted with CD34+ cord blood hematopoietic stem cells. After reconstitution for 3–4 months, these humanized mice received a GM-CSF/IL3 boost that stably reconstituted multiple human cell lineages such as T, B and myeloid cells in organs and blood, (online supplemental table S2). Two days post the boost, mice were subcutaneously implanted with either human HCT15 colorectal cancer cells or human A549 lung cancer cells and treated biweekly (intraperitoneal) with 500 µg (~25 mg/kg) of either HMBD-002 or vehicle control starting at 5 days post implantation. As observed in the syngenic models, HMBD-002 showed significant single agent antitumor efficacy of 65% and 62% TGI in these HCT15 colorectal and A549 lung humanized CDX models, respectively (figure 6C,D). The similar tumor inhibition observed after HMBD-002 treatment of both fully immune-competent murine tumor models and murine tumor models recapitulating the human immune compartment, suggests a conserved, and potentially translatable, mechanism of action shared between mouse and human antitumor immune responses.

HMBD-002 treatment remodels the TME of murine CDX models, increasing activated effector immune cells and decreasing suppressive cells

To understand the mechanism of the antitumor efficacy observed for HMBD-002 in murine models, tumors from the syngenic CT26 colon cancer models were further profiled using FACS. HMBD-002 treatment was observed to significantly increase the percentage of CD11b+ MHCII+ (antigen presenting cells), CD11b+ F4/80+ (macrophages) and CD11C+ (DCs) in the TME (figure 6E). An increase in CD8 +T cells was also observed, although this was not statistically significant. In contrast, the frequency of total MDSCs (CD11b+ GR1+ MHCII-) was significantly lower in the tumors of treated mice compared with vehicle control. To further assess the mechanism by which these changes in immune cell numbers were associated with the functional state of TILs, we performed an antigen recall assay by co-culturing CT26 cells and isolated TILs from the CDX models *in vitro*. Seventy-two hours after co-culture, TILs isolated from tumors treated with HMBD-002 showed significantly higher lysis of CT26 cells (figure 6F). This increased activity was further confirmed with an *in vivo* co-culture assay of infiltrating T cells with CT26 cells, where T cells from treated mice showed significantly higher IFN-γ levels, as measured by ELISA, compared with untreated mice (figure 6F).

These results suggest that VISTA blockade by HMBD-002 increases the levels of inflammatory effector cells with concomitant decrease of immunosuppressive MDSCs in the TME and enhances the antigen specific cytotoxic activity of TILs, likely contributing to the antitumor efficacy of HMBD-002.

HMBD-002 exhibits acceptable pharmacokinetic profiles in multiple species

Therapeutic antibodies should possess half-lives in plasma compatible with appropriate dosing regimens. Previous anti-VISTA antibodies have demonstrated poor PK characterized by rapid serum clearance,¹⁸ which may be explained by Fc-effector functions such as ADCC, especially of neutrophils, leading to rapid cell turnover of VISTA expressing cells and causing a significant antibody sink. The pharmacokinetic profile of HMBD-002 was therefore evaluated in healthy and tumor-bearing mice, and healthy rats and NHP.

In mice, a representative pharmacokinetic profile was determined for tumor-bearing and non-tumor bearing Balb/c mice that had been dosed intraperitoneally with increasing doses of HMBD-002 (5–20 mg/kg, online supplemental figure S7A). Non-tumor bearing mice demonstrated linear PK, however, profiles in tumor bearing mice were non-linear, likely due to the higher levels of the target and increased target mediated drug disposition. HMBD-002 serum half-life in the tumor bearing mice was calculated as 26.9–57.2 hours across doses, while in the non-tumor bearing mice serum half-life was 61.1–80.8 hours.

In Sprague-Dawley rats and cynomolgus monkeys, the PK profile was determined from measurements in both male and female animals. HMBD-002 was administered at single doses of 1 mg/kg, 10 mg/kg, and 100 mg/kg, as an intravenous bolus injection into the tail vein in rats. For cynomolgus monkeys, HMBD-002 was administered either once at doses of 1 mg/kg, 10 mg/kg, and 100 mg/kg or twice 1 week apart (days 1 and 8) at a dose of 10 mg/kg/week as an intravenous bolus injection into the peripheral vein. In both species, the PK profiles of HMBD-002 did not differ significantly between the genders and dose proportional increases in exposure were observed for C_{max} values across all doses. HMBD-002 serum half-life in the rats was calculated to be between 6.2 and 68.1 hours across doses (online supplemental figure S7B), and in the cynomolgus monkey serum half-life was calculated to be between 8.0 and 70.0 hours (online supplemental figure S7C).

Together, these results demonstrate that HMBD-002 appears to show reduced clearance relative to other anti-VISTA antibodies with a depleting IgG1 Fc domain.¹⁸

HMBD-002 is well tolerated in preclinical toxicology studies with no abnormal cytokine release

Optimal therapeutic antibodies should demonstrate minimal toxicity to normal tissues. As HMBD-002 shows species-conserved binding of VISTA orthologs, animals from the above PK studies were also monitored for adverse effects of HMBD-002 dosing, as part of concurrent tolerability studies. After intravenous injection in Sprague-Dawley rats and cynomolgus monkey, both species showed no treatment related morbidity/mortality or clinical signs, and no treatment related changes in body weight, food consumption, clinical chemistry, or

hematology parameters that continued for the duration of the 28-day observation period (online supplemental tables S3 and S4).

Additionally, *ex vivo* cytokine release assays were conducted with human whole blood and isolated PBMCs from healthy donors, to assess the potential immunotoxicity of HMBD-002 by evaluating the levels of IL-2, IL-4, IL-6, IL-10, TNF- α and IFN- γ in culture supernatants using a cytometric bead array approach. Cytokine levels were measured after stimulation for 24 hours with either HMBD-002, a positive control (anti-CD3 or staphylococcal enterotoxin B), or a negative isotype control in soluble stimulation format. HMBD-002 did not elicit any significant cytokine release in blood or in purified PBMCs (online supplemental figure S7D–G).

Together these results demonstrate that HMBD-002 is well tolerated in rats and cynomolgus monkeys and further suggests a low risk for potential immunotoxicity caused by cytokine release.

DISCUSSION

There is a growing interest in the negative checkpoint regulator VISTA as a therapeutic target to treat patients with cancer who do not respond to current therapies, or acquire resistance to other ICTs, due to its potent role in suppressing immune responses, its non-overlapping function with PD-L1 or CTLA-4, and its high expression on myeloid cells. Although numerous approaches are being adopted to develop VISTA inhibitors, previous attempts using conventional antibody discovery approaches have not yielded optimal immune modulating anti-VISTA antibodies with the characteristics appropriate for an effective therapeutic candidate, including functional blockade of VISTA inhibition and appropriate safety and PK profiles.

HMBD-002 was rationally developed as an IgG4 isotype anti-VISTA neutralizing antibody using Hummingbird Bioscience's AI-directed Rational Antibody Discovery platform. To focus development on a functional blocking antibody, we modeled the binding of VISTA to protein partners by hypothesizing that the B7 receptor family would utilize conserved interaction surfaces and then leveraged existing PD1/PD-L1 structural data as a template. A machine-learning based prediction algorithm prioritized a target region centered on the C-C' loop of VISTA, which also coincided with key residues that have been reported for the interaction of VISTA with VSIG3 and LRIG1, two of the proposed binding partners for VISTA. This region was then used to inform an epitope-directed immunization strategy that biased B cell responses to the target region using computationally-designed immunogens and custom adjuvants.

The resulting humanized antibody, HMBD-002, uniquely binds with picomolar affinity to a species-conserved epitope within the predicted functional C-C' loop region of VISTA. The HMBD-002 epitope was also confirmed to be distinct from the two clinical stage anti-VISTA antibodies, IGN175A and VSTB112. A recent

report using mutational screening further supports the uniqueness of the HMBD-002 epitope, locating the VSTB112 epitope further away from the C-C' loop and sharing several residues with the epitopes of two other recently reported preclinical anti-VISTA antibodies, BMS767 and SG7.²⁶ The conservation of the HMBD-002 epitope across species is suggestive of the evolutionary pressure that has maintained this critical region for protein–protein interactions. Comparable high affinity binding to murine orthologs also facilitated the development of HMBD-002 towards clinical evaluation, leveraging murine efficacy and toxicity data without requiring the use of murine surrogate antibodies. The only other murine cross-reactive anti-VISTA antibody, SG7, currently in early development, binds to a different region and shows much lower affinity to murine VISTA compared with human VISTA.²⁶ Furthermore, *in vitro* pharmacology studies demonstrated that the binding of HMBD-002 is highly selective and maintained even in low pH conditions that may represent those in the TME.

HMBD-002 is also distinct from previous anti-VISTA antibodies as it is the first antibody to demonstrate neutralization of VISTA activity in an Fc-independent manner. The Fc isotype of immune checkpoint antibodies has been known to affect their function and *in vivo* efficacy.²¹ Indeed, the efficacy of previous anti-VISTA antibodies was shown to be dependent on an IgG1 isotype that is able to bind to immune activating Fc receptors.³⁵ However, this binding often leads to ADCC or CDC mediated depletion of target cells. Due to the broad expression of VISTA that we and others have observed on normal healthy hematopoietic cells,^{36,37} HMBD-002 was developed as an IgG4 isotype antibody that circumvents the possibility of detrimental depletion of VISTA expressing cells. The importance of this strategy may explain previous observations. The only anti-VISTA antibody for which clinical observations are known is an IgG1 isotype and reported dose-limiting toxicity at subtherapeutic dose levels during phase 1 trials (low-grade CRS at 0.15 mg/kg and grade 3 neurotoxicity at 0.3 mg/kg),²⁶ (Curis Corporate Presentation, January 2021) perhaps explained by ADCC driven cytotoxicity of myeloid cells, which are major producers of CRS-related cytokines such as IL-6.³⁸ Additionally, cell depletion is also one explanation for the poor PK profile characterized by short serum half-life that has been observed for IgG1 anti-VISTA antibodies,¹⁸ as the fast turnover of VISTA expressing granulocytes could represent a significant sink that may quickly remove the antibody from circulation.

VSIG3 was selected as an exemplar VISTA binding partner as it is known to bind VISTA within the predicted functional C-C' loop region and has been independently validated as a binding partner by multiple groups.^{11,16} Further, the VISTA-VSIG3 interaction has demonstrable function through inhibition of T cell activation and inflammatory cytokine production.¹¹ The high co-expression of VISTA and VSIG3 that we observed in TNBC and NSCLC provides additional support to the relevance of the VISTA-VSIG3 axis in tumors. We therefore consider VISTA-VSIG3 a representative functional interaction.

Although future studies may reveal additional relevant VISTA binding partners, it is likely that binding will also use conserved C-C' loop interactions. Indeed, recent reports of LRIG1 binding to VISTA highlight interaction residues in the C-C' loop region (WO2019165233, WO2021047104). The binding epitope for HMBD-002 was confirmed to be within this predicted C-C' loop region, with an epitope that overlaps with key residues for both VSIG3 and LRIG1 binding, and HMBD-002 was able to block their interactions with VISTA. Furthermore, the inhibition of VISTA-VSIG3 interactions by HMBD-002 was confirmed to release VSIG3 mediated suppression of IFN- γ from anti-CD3 activated T cells. In contrast, residues reported to be involved in the interaction of VISTA with PSGL-1 are outside of the C-C' loop and distal from HMBD-002 epitope and, as expected, HMBD-002 was not observed to inhibit the VISTA-PSGL-1 interaction. It should be noted, however, that the physiological relevance of the low pH binding of VISTA to PSGL-1 is still uncertain, especially as the majority of functional assays that have elucidated the effects of VISTA inhibition, both in previous reports and those described for HMBD-002 here, have been performed at broadly neutral pH.

The functional blockade of VISTA by HMBD-002 showed broad effects on immune cells *in vitro*. Blockade of VISTA on MDSCs, co-cultured with anti-CD3 activated T cells, resulted in increased IFN- γ release, indicative of a reversal of the MDSC-mediated T cell suppression that is increasingly implicated in suppressing antitumor responses.³⁹ HMBD-002 also blocked the chemotaxis of granulocytic neutrophils, which are known to increase cancer cell invasion and have been associated with poor prognosis.⁴⁰ Notably, these immune stimulatory effects were not induced by other clinical candidate anti-VISTA antibodies in our experiments, even those that have been reported to inhibit VSIG-3 binding,¹⁶ again pointing to the potency of the mechanism of action of HMBD-002. Finally, in a mixed allogenic co-culture of PBMCs during a MLR assay, we noted a shift of the immune response towards a proinflammatory phenotype, with a significant upregulation of TNF- α , TLR, JAK-STAT, IL-17 signaling pathways, all of which are known to be associated with a Th1/Th17 cellular response.⁴¹ This is consistent with murine VISTA knockout models that lead to psoriasis and experimental autoimmune encephalomyelitis that have previously been reported to be characterized by a Th1/Th17 response.⁸

The favorable characteristics of HMBD-002 that support development into the clinic were again notable when evaluating *in vivo* models of efficacy, PK and tolerability. *In vivo* efficacy studies using HMBD-002 in murine syngenic models demonstrated that HMBD-002 treatment is effective as a single agent and significantly inhibits tumor growth in multiple tumor models. For the first time we also report the efficacy of an anti-VISTA antibody in humanized murine models of cancers. The remodeling of the TME towards a proinflammatory phenotype was clear when profiling tumors from the CT26 (colorectal) murine syngenic CDX model. This revealed a decrease

of broadly suppressive cell populations (GR1+ MHCII-MDSCs) and an increase in effector cell populations (CD11b+ MHCII+ antigen presenting cells, CD11C+ DC, F4/F80+ macrophages). Additionally, the TILs of treated mice from the CT26 model showed enhanced effector function, *ex vivo*. Deeper cell profiling of murine CDX models in future studies will be required to dissect the roles of subclasses of the immune cell compartment during responses to HMBD-002. These should also be confirmed using patient samples from clinical studies. Nevertheless, the remodeling of the TME by HMBD-002 towards a proinflammatory and antitumor phenotype that was observed in the current study is consistent with the primary mechanism of action being manipulation of the highly VISTA+ myeloid compartment.

Alongside *in vivo* efficacy, HMBD-002 demonstrated a pharmacokinetic profile in two pharmacologically relevant VISTA ortholog expressing species, rats and cynomolgus monkey, characterized by a serum half-life measured in days and in contrast to reports of previous IgG1 anti-VISTA antibodies which have suffered from faster serum clearance.¹⁸ Furthermore, despite reports of CRS at subtherapeutic doses for IgG1 isotype anti-VISTA depleting antibodies, we observed no concerning toxicities with respect to clinical observation, hematology or biochemistry in rodent and cynomolgus monkey models, generally considered good predictors of pharmacology in humans, nor in the *in vitro* human cytokine release assays. Although there remains the possibility of differences in human and model species pharmacology that can only be addressed in larger clinical trials, these data allow maximum flexibility in setting safe starting dose and scheduling for further evaluation of PK and tolerability of HMBD-002 in the clinic.

In conclusion, HMBD-002 represents a unique neutralizing and non-depleting IgG4 isotype anti-VISTA therapeutic antibody, the discovery of which was enabled by an AI-directed rational antibody discovery approach that identified and targeted a key functional region on VISTA to block its interaction with protein partners and potently release VISTA suppression of an antitumor immune response. The potent efficacy of HMBD-002 was also associated with a safety and pharmacokinetic profile that supports the rapid translation of the program into the clinic. Hummingbird Bioscience anticipates commencing First-in-Human trials of HMBD-002 in 2021.

Author affiliations

¹Hummingbird Bioscience, Singapore

²Department of Biological Sciences and Department of Biochemistry, National University of Singapore, Singapore

³Stanford University School of Medicine, Stanford, California, USA

⁴Hummingbird Bioscience, Houston, Texas, USA

Correction notice This article has been corrected since it was first published online. The author affiliations were incorrectly listed.

Acknowledgements The authors would like to thank all members of the Hummingbird Bioscience team for their assistance during the development of the molecule and data acquisition for this study. The authors would also like to thank

Singapore National Laboratory for Mass Spectrometry (SingMass), funded by National Research Foundation, Singapore, for assistance with hydrogen–deuterium exchange mass spectrometry experiments.

Contributors Conception and design: DT, JGG, LD, KHP, PJI, JB-K. Development of methodology: DT, PJI, JB-K. Acquisition of data (provided animals, acquired and managed patients, provided facilities, etc): DT, SG, LL, BD, SP, JGG, NKT. Analysis and interpretation of data (eg, statistical analysis, biostatistics, computational analysis): DT, SG, LL, BD, SP, JGG, NKT, SK, KHP, PJI, JB-K. Writing, review, and/or revision of the manuscript: SK, BD, DT, LD, KHP, JB-K. Administrative, technical, or material support (ie, reporting or organizing data, constructing databases): DT, LD, KHP, JB-K. Study supervision: DT, LD, PJI, JB-K. JB-K is the guarantor of the study.

Funding This work was supported by a grant from the Cancer Prevention and Research Institute of Texas (DP190027).

Competing interests All authors, except JGG and NKT are employees of Hummingbird Bioscience. DT is the principal scientist (Head of Pharmacology) at, and has ownership interest (including patents) in, Hummingbird Bioscience. SG is the Head of Production at, and has ownership interest (including patents) in, Hummingbird Bioscience. LD is the HMBD-002 Program Lead at, and has ownership interest in, Hummingbird Bioscience. KHP is the Chief Technology Officer at, and has ownership interest (including patents) in, Hummingbird Bioscience. PJI is the CEO at, and has ownership interest (including patents) in, Hummingbird Bioscience. JB-K is the Chief Scientific Officer at, and has ownership interest (including patents) in, Hummingbird Bioscience. No potential conflicts of interest were disclosed by the other authors.

Patient consent for publication Not applicable.

Provenance and peer review Not commissioned; externally peer reviewed.

Data availability statement All data relevant to the study are included in the article or uploaded as supplementary information.

Supplemental material This content has been supplied by the author(s). It has not been vetted by BMJ Publishing Group Limited (BMJ) and may not have been peer-reviewed. Any opinions or recommendations discussed are solely those of the author(s) and are not endorsed by BMJ. BMJ disclaims all liability and responsibility arising from any reliance placed on the content. Where the content includes any translated material, BMJ does not warrant the accuracy and reliability of the translations (including but not limited to local regulations, clinical guidelines, terminology, drug names and drug dosages), and is not responsible for any error and/or omissions arising from translation and adaptation or otherwise.

Open access This is an open access article distributed in accordance with the Creative Commons Attribution Non Commercial (CC BY-NC 4.0) license, which permits others to distribute, remix, adapt, build upon this work non-commercially, and license their derivative works on different terms, provided the original work is properly cited, appropriate credit is given, any changes made indicated, and the use is non-commercial. See <http://creativecommons.org/licenses/by-nc/4.0/>.

ORCID iD

Jerome D Boyd-Kirkup <http://orcid.org/0000-0002-6033-2619>

REFERENCES

- Sharma P, Hu-Lieskovan S, Wargo JA, *et al*. Primary, adaptive, and acquired resistance to cancer immunotherapy. *Cell* 2017;168:707–23.
- Wang L, Rubinstein R, Lines JL, *et al*. VISTA, a novel mouse Ig superfamily ligand that negatively regulates T cell responses. *J Exp Med* 2011;208:577–92.
- Lines JL, Pantazi E, Mak J, *et al*. VISTA is an immune checkpoint molecule for human T cells. *Cancer Res* 2014;74:1924–32.
- EITanbouly MA, Schaafsma E, Noelle RJ, *et al*. VISTA: coming of age as a multi-lineage immune checkpoint. *Clin Exp Immunol* 2020;200:120–30.
- Wang G, Tai R, Wu Y, *et al*. The expression and immunoregulation of immune checkpoint molecule VISTA in autoimmune diseases and cancers. *Cytokine Growth Factor Rev* 2020;52:1–14.
- Le Mercier I, Chen W, Lines JL, *et al*. VISTA regulates the development of protective antitumor immunity. *Cancer Res* 2014;74:1933–44.
- EITanbouly MA, Zhao Y, Nowak E, *et al*. VISTA is a checkpoint regulator for naive T cell quiescence and peripheral tolerance. *Science* 2020;367:eaay0524.
- Li N, Xu W, Yuan Y, *et al*. Immune-checkpoint protein VISTA critically regulates the IL-23/IL-17 inflammatory axis. *Sci Rep* 2017;7:1485.
- Han X, Vesely MD, Yang W, *et al*. PD-1H (VISTA)-mediated suppression of autoimmunity in systemic and cutaneous lupus erythematosus. *Sci Transl Med* 2019;11:eaax1159.
- Liu J, Yuan Y, Chen W, *et al*. Immune-checkpoint proteins VISTA and PD-1 nonredundantly regulate murine T-cell responses. *Proc Natl Acad Sci U S A* 2015;112:6682–7.
- Wang J, Wu G, Manick B, *et al*. VSIG-3 as a ligand of VISTA inhibits human T-cell function. *Immunology* 2019;156:74–85.
- Gao J, Ward JF, Pettaway CA, *et al*. VISTA is an inhibitory immune checkpoint that is increased after ipilimumab therapy in patients with prostate cancer. *Nat Med* 2017;23:551–5.
- Blando J, Sharma A, Higa MG, *et al*. Comparison of immune infiltrates in melanoma and pancreatic cancer highlights VISTA as a potential target in pancreatic cancer. *Proc Natl Acad Sci U S A* 2019;116:201811067.
- Kakavand H, Jackett LA, Menzies AM, *et al*. Negative immune checkpoint regulation by VISTA: a mechanism of acquired resistance to anti-PD-1 therapy in metastatic melanoma patients. *Mod Pathol* 2017;30:1666–76.
- Wang L, Jia B, Claxton DF, *et al*. VISTA is highly expressed on MDSCs and mediates an inhibition of T cell response in patients with AML. *Oncoimmunology* 2018;7:e1469594.
- Mehta N, Maddineni S, Mathews II, *et al*. Structure and functional binding epitope of V-domain Ig suppressor of T cell activation. *Cell Rep* 2019;28:2509–16.
- Yoon KW, Byun S, Kwon E, *et al*. Control of signaling-mediated clearance of apoptotic cells by the tumor suppressor p53. *Science* 2015;349:1261669.
- Johnston RJ, Su LJ, Pinckney J, *et al*. VISTA is an acidic pH-selective ligand for PSGL-1. *Nature* 2019;574:565–70.
- Mahoney KM, Freeman GJ. Acidity changes immunology: a new VISTA pathway. *Nat Immunol* 2020;21:13–16.
- Chames P, Van Regenmortel M, Weiss E, *et al*. Therapeutic antibodies: successes, limitations and hopes for the future. *Br J Pharmacol* 2009;157:220–33.
- Chen X, Song X, Li K, *et al*. FcγR-binding is an important functional attribute for immune checkpoint antibodies in cancer immunotherapy. *Front Immunol* 2019;10:292.
- Thakkar D, Sancenon V, Taguaim MM, *et al*. 10D1F, an Anti-HER3 antibody that uniquely blocks the receptor heterodimerization interface, potently inhibits tumor growth across a broad panel of tumor models. *Mol Cancer Ther* 2020;19:490–501.
- Stuart T, Butler A, Hoffman P, *et al*. Comprehensive integration of single-cell data. *Cell* 2019;177:1888–902.
- Mulati K, Hamanishi J, Matsumura N, *et al*. VISTA expressed in tumour cells regulates T cell function. *Br J Cancer* 2019;120:115–27.
- Tuncbag N, Gursoy A, Nussinov R, *et al*. Predicting protein-protein interactions on a proteome scale by matching evolutionary and structural similarities at interfaces using PRISM. *Nat Protoc* 2011;6:1341–54.
- Mehta N, Maddineni S, Kelly RL, *et al*. An engineered antibody binds a distinct epitope and is a potent inhibitor of murine and human VISTA. *Sci Rep* 2020;10:15171.
- Kato Y, Ozawa S, Miyamoto C, *et al*. Acidic extracellular microenvironment and cancer. *Cancer Cell Int* 2013;13:89.
- Terhune J, Berk E, Czerniecki BJ. Dendritic cell-induced Th1 and Th17 cell differentiation for cancer therapy. *Vaccines* 2013;1:527–49.
- Broughton TWK, EITanbouly MA, Schaafsma E, *et al*. Defining the signature of vista on myeloid cell chemokine responsiveness. *Front Immunol* 2019;10:2641.
- Zilio S, Serafini P, Neutrophils SP. Neutrophils and granulocytic MDSC: the Janus God of cancer immunotherapy. *Vaccines* 2016;4:31.
- Kaiko GE, Horvat JC, Beagley KW, *et al*. Immunological decision-making: how does the immune system decide to mount a helper T-cell response? *Immunology* 2008;123:326–38.
- Dulos J, Carven GJ, van Boxtel SJ, *et al*. Pd-1 blockade augments Th1 and Th17 and suppresses Th2 responses in peripheral blood from patients with prostate and advanced melanoma cancer. *J Immunother* 2012;35:169–78.
- Capasso A, Lang J, Pitts TM, *et al*. Characterization of immune responses to anti-PD-1 mono and combination immunotherapy in hematopoietic humanized mice implanted with tumor xenografts. *J Immunother Cancer* 2019;7:37.
- Burova E, Hermann A, Dai J, *et al*. Preclinical development of the anti-LAG-3 antibody REGN3767: characterization and activity in combination with the anti-PD-1 antibody cemiplimab in human PD-1xLAG-3-knockin mice. *Mol Cancer Ther* 2019;18.
- Mostböck S, Wu H, Fenn T. Abstract 3266: distinct immune stimulatory functions of anti-human VISTA antibodies are determined by the antibody isotype. *Immunology* 2019:3266.

- 36 Zong L, Mo S, Yu S, *et al.* Expression of the immune checkpoint VISTA in breast cancer. *Cancer Immunol Immunother* 2020;69:1437–46.
- 37 Villarreal-Espindola F, Yu X, Datar I, *et al.* Spatially resolved and quantitative analysis of VISTA/PD-1H as a novel immunotherapy target in human non-small cell lung cancer. *Clin Cancer Res* 2018;24:1562–73.
- 38 Tanaka T, Narazaki M, Kishimoto T. Immunotherapeutic implications of IL-6 blockade for cytokine storm. *Immunotherapy* 2016;8:959–70.
- 39 Movahedi K, Guillems M, Van den Bossche J, *et al.* Identification of discrete tumor-induced myeloid-derived suppressor cell subpopulations with distinct T cell-suppressive activity. *Blood* 2008;111:4233–44.
- 40 Gentles AJ, Newman AM, Liu CL, *et al.* The prognostic landscape of genes and infiltrating immune cells across human cancers. *Nat Med* 2015;21:938–45.
- 41 Hid Cadena R, Reitsem RD, Huitema MG, *et al.* Decreased expression of negative immune checkpoint VISTA by CD4+ T cells facilitates T helper 1, T helper 17, and T follicular helper lineage differentiation in GCA. *Front Immunol* 2019;10:1638.

Correction: *Rationally targeted anti-VISTA antibody that blockades the C-C' loop region can reverse VISTA immune suppression and remodel the immune microenvironment to potently inhibit tumor growth in an Fc independent manner*

Thakkar D, Paliwal S, Dharmadhikari B, *et al.* Rationally targeted anti-VISTA antibody that blockades the C-C' loop region can reverse VISTA immune suppression and remodel the immune microenvironment to potently inhibit tumor growth in an Fc independent manner. *J Immunother Cancer*. 2022;10:e003382. doi:10.1136/jitc-2021-003382

In this article the author affiliations were incorrectly listed. The author affiliations should be listed as follows:

Dipti Thakkar¹, Shalini Paliwal¹, Bhushan Dharmadhikari¹, Siyu Guan¹, Lillian Liu¹, Shreya Kar¹, Nikhil K. Tulsian², Joshua J. Gruber³, Leah DiMascio⁴, Konrad H. Paszkiewicz¹, Piers J. Ingram⁴, and Jerome D. Boyd-Kirkup^{4*}

Affiliations:

¹Hummingbird Bioscience, Singapore. ²Department of Biological Sciences and Department of Biochemistry, National University of Singapore, Singapore. ³Stanford University School of Medicine, Stanford, California, USA. ⁴Hummingbird Bioscience, Houston, Texas, USA.

Open access This is an open access article distributed in accordance with the Creative Commons Attribution Non Commercial (CC BY-NC 4.0) license, which permits others to distribute, remix, adapt, build upon this work non-commercially, and license their derivative works on different terms, provided the original work is properly cited, appropriate credit is given, any changes made indicated, and the use is non-commercial. See <http://creativecommons.org/licenses/by-nc/4.0/>.

© Author(s) (or their employer(s)) 2022. Re-use permitted under CC BY-NC. No commercial re-use. See rights and permissions. Published by BMJ.

J Immunother Cancer 2022;10:e003382corr1. doi:10.1136/jitc-2021-003382corr1



SUPPLEMENTARY FILES

SUPPLEMENTARY FIGURE LEGENDS

S1. VISTA sequence homology and reported interaction residues with binding partners (VSIG3, LRIG1 and PSGL-1).

A. VISTA sequence alignment between mouse, rats, cynomolgus monkey and humans from MultAlign and visualized via ESPript. B. VISTA homology model showing VSIG3, PSGL-1 and LRIG1 epitope residues, reported to be involved in binding human VISTA.

S2. Murine anti-VISTA antibody, V4P, binds to VISTA with high affinity and specificity and demonstrates Fc-independent inhibition of tumor growth in vivo

A. Binding specificity of V4P by ELISA using human B7 family antigens as indicated. Data shown are mean n=2 measurements and error bars are SEM. **(B-C)** Cell derived xenograft models of C54BL/6 mice subcutaneously implanted with EL4 (B) and BALB/c mice, subcutaneously implanted with CT26 (C). Mice were randomized and dosed with concentrations of test articles at indicated time-points. Tumor volumes were measured twice a week. Each data point represents the mean tumor volume +/- SEM of n=6 mice.

S3. HMBD-002, an IgG4 monoclonal antibody, does not bind to FcγRIII or C1q that are required for Fc-mediated ADCC and CDC activity.

A. Binding of HMBD-002 to FcγRIII and B.C1q proteins as assessed by ELISA. Data shown are mean of n=3 measurements and error bars are SEM.

S4. HMBD-002 binds to a unique epitope on VISTA with very high binding affinity across a range of physiological pH.

A. HMBD-002 epitope binning, using examples of human VISTA antibodies (VSTB112, IGN175A) and B. mouse anti-VISTA antibodies (13F3, MH5A) in-tandem method was used to

test competitive binding of antibody pairs to VISTA by biolayer interferometry and signals were aligned to baseline. C-F. Surface plasma resonance (Biacore) binding kinetics of HMBD-002 to VISTA orthologs; human, mouse, rat and cyno VISTA. G. Binding affinity of HMBD-002 across pH range 5.5-7.5. Data shown are mean of n=3 measurements and error bars are SEM.

Figure S5. VISTA interacts with VSIG3, LRIG1, PSGL-1 and HMBD-002 inhibits the VISTA-LRIG1 interaction but does not inhibit the VISTA-PSGL-1 interaction.

A and B. Binding of VISTA with its binding partner VSIG3 (A) and LRIG1 (B) by ELISA. Data shown are mean of n=3 measurements and error bars are SEM. C. Inhibition of VISTA:LRIG1 binding, analyzed by competition ELISA. Data shown are mean of n=3 measurements and error bars are SEM. D. Binding of VISTA to its putative binding partner PSGL-1 at pH6 and pH7 by ELISA. Data shown are mean of n=3 measurements and error bars are SEM. E. Inhibition of VISTA:PSG-L-1 binding at pH6, analyzed by competition ELISA. Data shown are mean of n=3 measurements and error bars are SEM.

S6. HMBD-002 remodels the immune milieu toward an enhanced pro-inflammatory Th1/Th17 immune response in an allogenic Mixed Lymphocyte Reaction. A. Cytokine levels measured at 96 hrs by Luminex, from the supernatant of an allogenic mixed lymphocyte reaction. All concentrations of HMBD-002 and anti PD-1 antibody, Pembrolizumab (annotated as Pembro) in $\mu\text{g/ml}$. Data was normalized to isotype control. Data shown are mean of n=10 and error bars are SEM. B. KEGG pathway analysis using WebGestalt from bulk RNA-sequencing of MLR samples (n=10). Data was normalized to IgG4 isotype control. C. Enrichment of transcript levels in genes associated with type-I and Type-II interferon genes from bulk RNA-sequencing of MLR samples (n=10). Data represented as mean \pm SD.

S7. HMBD-002 exhibited acceptable pharmacokinetic and safety profiles in multiple pre-clinical toxicology species.

Serum concentration of HMBD-002 in **(A)** Balb/c tumor-bearing and non-tumor bearing mice (n=3), **(B)** Sprague Dawley rats (n=6) and **(C)** cynomolgus monkey (n=2). HMBD-002 was administered at the indicated concentration via intraperitoneal injection in mice, IV bolus injection into the tail vein in rats, and IV bolus injection into the peripheral vein in monkeys **(D-G)** Cytokine release assay showing representative cytokine levels of IL-2 and IL-6 using whole blood (D and E) and PBMC (F and G) treated with indicated test articles and concentrations. HMBD-002 is referred to in the figure as V4C26.hIgG4 in D-G. Data shown are mean of n=10 measurements and each point represents an independent donor.

SUPPLEMENTARY METHODS

Antibody isolation

Six- to eight-week-old female BALB/c mice were repeatedly immunized with custom immunogens. Twenty-four hours after the final immunization, total splenocytes were isolated and fused with the myeloma cell line P3X63.Ag8.653 (ATCC) using ClonaCell-HY Hybridoma Cloning Kit, in accordance with the manufacturer's instructions (Stemcell Technologies). After 7 to 10 days, single hybridoma clones were isolated and antibody-producing hybridomas were selected by screening supernatants for antigen binding using ELISA and flow cytometry. Variable regions of selected clones were amplified (SMARTer RACE 5'/3' Kit, Clontech), sequenced and cloned into expression vector and expressed in mammalian cells for in vitro functional testing. One clone, V4P, was selected for development and subsequently humanized and further affinity matured into the final antibody HMBD-002.

Hybridoma production

Approximately 6-week-old female BALB/c mice were obtained from InVivos (Singapore). Animals were housed under specific pathogen-free conditions and were treated in compliance with the Institutional Animal Care and Use Committee (IACUC) guidelines. Using our proprietary immunization protocol (mAbHits), mice were immunized with proprietary mixtures of custom immunogens. Total splenocytes were isolated and fused with the myeloma cell line P3X63.Ag8.653 (ATCC, USA) using polyethylene glycol (PEG) and ClonaCell-HY Hybridoma Cloning Kit (Stemcell Technologies, Canada), according to manufacturer's instructions. Monoclonal hybridomas were selected and supernatants from

the resulting clones were screened by enzyme linked immunosorbent assay (ELISA) and fluorescent activated cell sorting (FACS).

Antibody variable region cloning and sequencing

Total RNA was extracted from hybridoma cells using TRIzol reagent (Life Technologies, Inc., USA) according to the manufacturer's instructions. Double-stranded cDNA was synthesized using SMARTer RACE 5'/3' Kit (Clontech). The race-ready cDNAs were amplified using SeqAmp DNA Polymerase (Clontech™) and primer mixes. The resulting variable heavy (VH) and light (VL) amplicons were cloned into pJET1.2/blunt vector using CloneJET PCR Cloning Kit (Thermo Scientific) and purified PCR amplicons were sequenced through AITBiotech Pte. Ltd. (Singapore). The sequencing data was analysed using the international IMGT (ImMunoGeneTics) information system[1] to characterize the individual complementarity-determining regions (CDRs) and framework sequences.

Humanization and affinity maturation of mouse antibody

Humanization of the variable regions of the mouse sequence was performed by CDR grafting into human framework sequences and backmutation of residues in canonical positions to preserve antigen binding. The humanised antibody was further affinity matured against mouse VISTA to increase the cross-species affinity by random mutagenesis using yeast scFv surface display. Briefly, ScFv bearing the parental VH and VL in a single chain was amplified by mutagenesis PCR (Agilent Technologies GeneMorph II Random Mutagenesis Kit) for library creation, the resulting library was further amplified and cloned into yeast expression vector pCTcon2 (Addgene) for yeast surface expression by electroporation. The transfected cells were screened by mouse VISTA binding using FACS and high binder cell was sorted by BD FACS Aria II cell sorter. Selected high binder clones were enriched by 2 additional rounds

of sorting. Cells were plated in SDCAA to isolate single clones followed by DNA extraction and sequencing. The final sequence of HMBD-002 was selected from among the optimized variants based on its developability characteristics as well as in vitro physicochemical and functional properties.

Cell lines

All cell lines were purchased from ATCC and cultured as recommended. Cells were maintained in culture medium supplemented with 10% FBS and 1% Pen/Strep (ThermoFisher) and cultured at 37°C, in 5% CO₂ incubators. Prior to use, fresh vials of cells were thawed and passaged 2-5 times. And Mycoplasma testing was performed by PCR using DreamTaq Green PCR master mix (ThermoFisher #K1081) according to manufacturer's instruction. Mycoplasma (*M. orale*) positive control template (Agilent Mycosensor assay kit) and the following primers were used:

Fwd. 5' GGGAGCAAACAGGATTAGATACCCT 3'

Rev. 5' TGCACCATCTGTCACTCTGTAAACCTC 3'

Stable cell line generation

CHO-k1 cells at an optimal density of 1*10⁶ cell/ml were electroporated with 5 µg of linearized IgG expression plasmid using 4D-Nucleofactor kit (Lonza) according to manufacturer's protocol. Electroporated cells were cultured in static cell incubator in a 6-well plate containing 2 ml growth medium for 24 hr. Subsequently, medium was exchanged to selection medium containing 250 nM Methotrexate (Sigma) and 200 µg/ml Zeocin (InvivoGen). Cells were spun down and re-suspended in fresh selection medium and

re-seeded to a density of 5×10^5 cell/ml once per week. Selection was completed when 95% viability was restored. Cells were transferred to shaker-incubator.

Antibody production and purification

Antibodies were produced by cultivation of stable cells in Fed-Batch mode in a shaker-incubator and subsequently purified from culture supernatants by affinity, size exclusion or mixed modal anion exchange followed by a final anion exchange chromatography. Antibody purity was assessed by size exclusion chromatography and SDS-PAGE.

VISTA sequence analysis and visualization

Multiple sequence alignments were performed with MultAlign[2] and visualized with EPScript[3]. 3D models were generated using UCSF Chimera[4].

sc-RNA-seq analysis of 68k PBMC dataset

To determine the cell types in which VISTA transcripts were most highly expressed, a publicly available 68k PBMC dataset was retrieved from the 10X Genomics website and processed using Seurat v3.2[5]. Cells with more than 6% mitochondrial transcripts, or less than 200 distinct transcripts were excluded. Data was normalized using default parameters and variable features identified using the VST method with 20,000 features. Data was subsequently scaled and then a PCA decomposition run with 15 principal components. A UMAP projection was carried out using default parameters and the FindClusters function run with a resolution of 0.8. To label the clusters the PBMC3k dataset[6] from the SeuratData package was used as a reference to map cell identities.

Epitope mapping by hydrogen-deuterium exchange mass spectrometry (HDXMS)

Epitope mapping by HDXMS was conducted using his-tagged human VISTA (residues 33-194, Sino Biological #13482-H08H) and HMBD-002 following procedures described previously[7]. Briefly, free VISTA was diluted in deuterated PBS with final deuterium oxide (D₂O) concentration at 90%. For VISTA/HMBD-002 complex, VISTA and HMBD-002 were mixed in 2:1 ratio and incubated for 15 mins at 25°C prior to deuterium labelling. Deuterium labelling reactions were carried out at 25°C for 1-, 10-, 30- and 100-min time points. Samples were then subjected to pepsin proteolytic cleavage followed by separation on an ACQUITY C18 column (1.0 x 100 mm) by nanoACQUITY UPLC (Waters) and detection by Synapt G2-Si mass spectrometer (Waters), operated in HDMS^E mode. Peptide identification and deuterium uptake monitoring were respectively performed using Protein Lynx Global Server 3.0.1 and DynamX 3.0 (Waters). Deuterium uptake for the peptides were calculated as differences in masses of the centroids of deuterated and undeuterated samples and reported as an average of triplicate measurements.

Epitope Binning

For epitope binning, human VISTA-His, or mouse VISTA-his recombinant protein (Sino Biological Inc.) in PBS was immobilized to Anti-Penta His sensor (HIS1K, Molecular Device) on an Octet QK384 (Molecular Device) instrument, for 5 mins. Sensors were briefly washed in PBS for 30s before loading 400 nM saturating antibody in PBS for 10 mins at a shake speed of 1,000 rpm. Subsequently, biosensors were washed for 2 min before immersing in 400 nM competing antibody in PBS for 7.5 mins at a shake speed of 1,000 rpm. Binding events which are correlated to change in wavelength (nm shift) reported from sensorgram, are monitored at the detector in real time.

Cross-species antibody binding affinity measurement

The affinity of HMBD-002 was determined by Surface Plasmon Resonance (SPR) using a Biacore. The assay was performed using a CM5 sensor chip (Cytiva #29104988). A Biacore HIS capture kit (GE Healthcare #28-9950-56) was employed to immobilize human, cynomolgus monkey, rat and mouse VISTA-HIS on-chip surface or left alone for background signal correction. Briefly, VISTA-HIS was captured for a contact time of 60 s at a flow rate of 5 μ l/min. HMBD-002 was flowed in two-fold serial dilutions from 50E-9 M to 390E-12 M for human, cynomolgus monkey and rat VISTA and from 12.5E-9 M to 390E-12 M for mouse VISTA, at a flow rate of 30 μ l/min for 90 sec association and 3000 sec dissociation at RT. The obtained sensograms were analyzed using Biacore T200 software and KD was calculated by fitting to a 1:1 binding kinetics model.

Antibody-dependent cellular cytotoxicity and complement-dependent cytotoxicity

96 well plates were coated with either 1 μ g/well of human C1q protein or 0.5 μ g/well of human CD16a in PBS at 4°C. Post overnight incubation, plates were washed thrice and blocked for 1 hr with blocking buffer at room temperature. Plates were incubated with HMBD-002 or isotype control for 1 hr at room temperature and incubated with 1:7000 dilution of HRP-conjugated anti-human Fc antibody for 1 hr at room temperature. Colorimetric reactions were developed using standard protocol as described for ELISA above.

VISTA-LRIG1 Inhibition Assay

VISTA-LRIG1 binding was confirmed using recombinant human VISTA-Fc protein (R&D #7126-B7) or irrelevant antigen (Human recombinant CD47 protein, Sinobiological #112283-HCCH) with standard ELISA method. For inhibition assay, 384-well plates were coated with 5 μ g/ml of human VISTA-Fc recombinant protein (R&D #7126-B7) diluted in PBS for 24 hrs at 4°C. After blocking for 2 hrs with 1% BSA at room temperature, plates were

incubated with either HMBD-002 or isotype control (Biolegend #403702) for 60 mins at room temperature. After 60 mins, recombinant human LRIG1.HIS at 1 µg/ml (EC_{50} of VISTA-LRIG1 binding) was added for 2 hrs. Post incubation, plates were washed three times with TBST and incubated with anti-HIS HRP (Abcam #ab1187) antibody for 1 hr at room temperature followed by three further washes. Colorimetric reactions were developed using standard protocol as described for ELISA above.

VISTA-PSGL-1 Inhibition Assay

VISTA-PSGL-1 binding was confirmed using recombinant human VISTA-HIS protein (Acro Biosystems #B75-H52H0) or irrelevant antigen (Rat recombinant HER3-HIS protein, Elabscience #PKSR030358) with standard ELISA method. For the inhibition assay, 384-well plates were coated with 5 µg/ml of human VISTA-HIS recombinant protein (Acro Biosystems #B75-H52H0) diluted in PBS for 24 hrs at 4°C. After blocking for 2 hrs with 1% BSA (pH6) at room temperature, plates were incubated with either HMBD-002 or isotype control for 60 mins at room temperature in 1% BSA (pH6). After 60 mins, biotinylated recombinant human PSGL-1-Fc (R&D #3345-PS) (Recombinant Human PSGL-1-Fc was biotinylated using Invitrogen kit #21455) at 9.5E-8 M (EC_{80} of VISTA-PSGL-1 binding) was added for 2 hrs. Post incubation, plates were washed three times with TBST (pH6) and incubated with streptavidin HRP (R&D #DY998) antibody for 1 hr at room temperature followed by three further washes. Colorimetric reactions were developed using standard protocol as described for ELISA above.

Bulk RNA-seq

10 samples per condition (V4C26, V9, anti-PD1, and IgG4) were taken from the MLR assay 96 hours after treatment. These were prepared for RNA-seq using the NEBNext Ultra II RNA library preparation kit (NEB #E7770S) and run on an Illumina NovaSeq S4 flowcell with v1.5

chemistry. Adaptor-trimmed and filtered data was evaluated using FASTQC and MultiQC[8] and reads aligned to the GRC37 human reference transcriptome using Kallisto v0.46[9]. Data was imported to R using TxImport. Normalized gene counts and gene-level differential expression was obtained using DESeq2[10]. Pathway activity was estimated using the SPEED2[11] package using default parameters.

CT26 tumor profiling

Single cell suspensions were generated by digestion of finely cut tumor tissue with 0.1 mg/ml of DNase I (Sigma #11284932001) and 1 mg/ml Collagenase (Sigma #1108866001) for 45 minutes at 37°C. Fc receptors were blocked with Human TruStain FcX (BioLegend #422302). Cells were stained with fluorophore conjugated antibodies for markers of immune cells (Table S5), washed and resuspended in buffer (1xPBS + 0.5% BSA + 1mM EDTA). Frequency of immune cell populations was determined via flow cytometry. Data was acquired on MACSQuant 10 (Milteny #130-096-343) and analyzed using FlowLogic software V7.

CT26 antigen recall assay

Single cell tumor suspensions were generated as described earlier. TILs (CD45+) or T cells (CD4+/CD8+) were enriched from the cell suspension using CD45 MicroBeads (Milteny #130-110-618) or CD4/CD8 MicroBeads (Milteny #130-116-480) as per manufacturer's protocol. CT26 cells (T: target cells), seeded 24 hrs prior, were co-cultured with enriched TILs or T cells (E: effector cells) from tumors for 72 hours at effector to target (E:T) cell ratios as indicated. All conditions were in triplicates. Cell viability was determined by CellTiter Glo (Promega#G7571). IFN- γ levels in supernatants were determined by ELISA (Invitrogen#BMS606). Lysis was calculated as: % Lysis = $((T - E:T)/T) * 100$.

Pharmacokinetics

Pharmacokinetic profile of HMBD-002 was evaluated in male and female Balb/c mice, Sprague Dawley rats and cynomolgus monkeys. HMBD-002 was administered in a single dose at the indicated concentration via IP injection in mice and IV bolus injection into the tail vein in rats. For cynomolgus monkeys, HMBD-002 was administered either once at doses of 1, 10, or 100 mg/kg or twice one week apart (Days 1 and 8) at a dose of 10 mg/kg/week by IV bolus injection into the peripheral vein. Blood was drawn at different timepoints post dosing and antibody concentration in the serum was quantified by ELISA. The parameters for the pharmacokinetic analysis were derived from a non-compartmental model: maximum concentration (C_{max}), AUC (0-336hr), AUC (0-infinity), half-life (t_{1/2}), clearance (CL) and volume of distribution at steady state (V_{ss}).

SUPPLEMENTARY TABLES

Table S1: Top low energy template interfaces predicted by PRISM, utilizing the VISTA and PD-L1 structures (PDB IDs 60IL, 3BIK respectively)

PRISM Pseudo energy Score	Template
-56.25	2dpfCD
-34.28	3b76AB

Table S2: Reconstitution composition for CD34+ humanized mice.

CDX Model	Mouse ID#	%hCD45	% Relative to hCD45				
			hB cells	hCD14 Monocyte	Total hT cells	hCD4T	hCD8T
HCT15	1532	13.4%	54.0%	0.4%	39.6%	26.8%	9.6%
	1533	13.9%	73.4%	1.6%	16.8%	13.5%	3.0%
	1534	16.1%	71.4%	2.0%	18.1%	13.6%	3.7%
	1535	14.1%	64.4%	0.9%	22.7%	16.6%	5.7%
	1536	17.6%	57.1%	1.9%	35.4%	27.6%	7.5%
	1537	15.4%	64.3%	2.9%	23.6%	17.6%	6.0%
	1538	11.3%	48.2%	1.8%	43.1%	25.9%	15.7%
	1539	14.6%	35.2%	3.3%	50.5%	41.8%	7.4%
	1540	12.0%	68.2%	2.4%	16.3%	11.9%	3.9%
	1541	26.2%	47.8%	0.7%	45.7%	34.1%	11.3%
A549	1544	23.9%	54.8%	2.3%	35.3%	29.7%	5.4%

	1545	23.9%	53.7%	4.1%	36.0%	26.8%	8.8%
	1546	18.7%	63.9%	1.1%	29.1%	21.3%	7.0%
	1547	15.2%	30.7%	6.8%	55.3%	40.5%	14.2%
	1548	31.6%	50.5%	1.6%	39.4%	29.0%	9.7%
	1549	42.8%	56.1%	3.9%	30.9%	22.1%	7.5%
	1550	44.2%	56.5%	2.9%	29.9%	22.2%	6.8%
	1551	19.6%	41.0%	3.2%	50.5%	41.6%	8.5%
	1552	23.8%	58.2%	1.4%	32.7%	24.8%	7.3%
	1553	17.9%	45.5%	3.3%	43.2%	32.7%	9.8%

Table S3: Clinical observations, food consumption, body weight, and clinical pathology findings during single dose intravenous tolerability study in Sprague-Dawley rats.

Endpoints Evaluated	Results
Clinical Observations	<ul style="list-style-type: none"> • No test article-related clinical signs observed
Food Consumption	<ul style="list-style-type: none"> • Variations observed in food consumption of animals were of minimal magnitude and lacked a dose-response relationship • No test article-related changes observed in food consumption of female rats • Decreased food consumption observed for male rats in 1 mg/kg/dose group, however, relationship to test article unlikely due to lack of dose-response relationship, and absence of similar observation in females
Body Weight	<ul style="list-style-type: none"> • Body weight variations observed in animals were of minimal magnitude and lacked a dose-response relationship • No test article-related changes observed in body weights of female rats • 15% change in body weight observed for male rats in 1 mg/kg/dose group, however, relationship to test article was unlikely due to lack of dose-response

	relationship, and absence of similar observation in females
<p>Hematology:</p> <p>Leukocyte counts, Erythrocyte count, Hemoglobin, Hematocrit, Mean corpuscular volume, Mean corpuscular hemoglobin concentration, Reticulocyte count, RBC distribution width, Platelet count, Mean platelet volume, absolute and percent WBC Differential (Neutrophils, Eosinophils, Basophils, Monocytes, Lymphocytes), absolute Large unstained cells, percent Large unstained cells and percent Reticulocyte count</p>	<ul style="list-style-type: none"> • No test article-related changes observed in hematology parameters • All differences observed were considered incidental due to lack of a dose-response relationship, minimal magnitude and/or the individual values were within the historical control data range
<p>Serum Chemistry:</p> <p>Alanine Aminotransferase, Aspartate Aminotransferase,</p>	<ul style="list-style-type: none"> • No test article-related changes observed in serum chemistry • All differences observed were considered incidental due to lack of a dose-response relationship, minimal

Total Protein, Albumin, Globulin, Albumin/Globulin Ratio, Alkaline Phosphatase, γ -glutamyltransferase, Glucose, Urea, Creatinine, Calcium, Phosphorus, Total Cholesterol, Triglycerides, Total Bilirubin, Sodium, Potassium, Chloride, Creatine Kinase and C-reactive protein	magnitude and/or the individual values were within the historical control data range
---	--

Table S4: Clinical observations, food consumption, body weight, and clinical pathology findings during single dose intravenous tolerability study in cynomolgus monkeys.

Endpoints Evaluated	Results
Clinical Observations	<ul style="list-style-type: none"> No test article-related clinical signs observed
Food Consumption	<ul style="list-style-type: none"> No test article-related changes observed in food consumption
Body Weight	<ul style="list-style-type: none"> No test article-related changes observed in body weights
Hematology: Leukocyte counts, Erythrocyte count, Hemoglobin, Hematocrit, Mean corpuscular volume, Mean corpuscular hemoglobin concentration, Reticulocyte count, RBC distribution width, Platelet count, Mean platelet volume, absolute and percent	<ul style="list-style-type: none"> No test article-related changes observed in hematology parameters All differences observed were considered incidental due to lack of a dose-response relationship, minimal magnitude and/or the individual values were within the historical control data range

<p>WBC Differential (Neutrophils, Eosinophils, Basophils, Monocytes, Lymphocytes), absolute Large unstained cells, percent Large unstained cells and percent Reticulocyte count</p>	
<p>Serum Chemistry:</p> <p>Alanine Aminotransferase, Aspartate Aminotransferase, Total Protein, Albumin, Globulin, Albumin/Globulin Ratio, Alkaline Phosphatase, γ-glutamyltransferase, Glucose, Urea, Creatinine, Calcium, Phosphorus, Total Cholesterol, Triglycerides, Total Bilirubin, Sodium, Potassium, Chloride, Creatine Kinase and C-reactive protein</p>	<ul style="list-style-type: none"> • No test article-related changes observed in serum chemistry • All differences observed were considered incidental due to lack of a dose-response relationship, minimal magnitude and/or the individual values were within the historical control data range

Table S5: List of antibodies.

Antibody	Company and Catlog
Anti-mouse MHCI	Invitrogen #48-5321-82
Anti-mouse Gr1	BioLegend #108437
Anti-mouse CD19	BioLegend #152408
Anti-mouse CD3	BioLegend #100219, BioLegend #100236
Anti-mouse CD11b	BioLegend #101211, BioLegend #101206, Milteny #130-113-243
Anti-mouse CD45	BioLegend #103154
Anti-mouse Ly-6C	BioLegend #128006
Anti-mouse Ly-6G	BioLegend #127618
Anti-mouse F4/80	BioLegend #123109
Anti-mouse CD11c	BioLegend #117310
Anti-mouse CD44	BioLegend #103020
Anti-mouse CD4	BioLegend #100406
Anti-mouse CD8	BioLegend #100708
Anti-mouse CD25	BioLegend #102061
Anti-mouse CD206	BioLegend #141720
Anti-mouse PD1	BioLegend #135241
Human CD45	Biologend # 304006
Mouse CD45	Biologend #103108
Rat CD45	Biologend # 202205
Anti NHP CD45	BD Pharmingen # 557803
Human/Rhesus CD11b	Biologend # 301306
Mouse CD11b	Biologend # 101208
Rat CD11b	Biologend # 201807

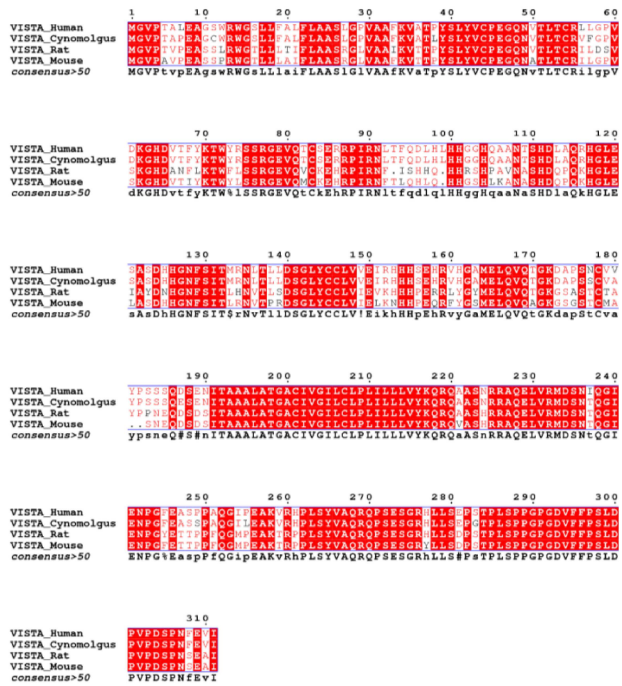
References

1. Lefranc M-P, Giudicelli V, Duroux P, et al. IMGT®, the international ImMuNoGeneTics information system® 25 years on. *Nucleic Acids Res* 2015;43:D413–22. doi:10.1093/nar/gku1056
2. Corpet F. Multiple sequence alignment with hierarchical clustering. *Nucleic Acids Res* 1988;16:10881–90. doi:10.1093/nar/16.22.10881
3. Robert X, Gouet P. Deciphering key features in protein structures with the new ENDscript server. *Nucleic Acids Res* 2014;42:W320–4. doi:10.1093/nar/gku316
4. Pettersen EF, Goddard TD, Huang CC, et al. UCSF Chimera—A visualization system for exploratory research and analysis. *J Comput Chem* 2004;25:1605–12. doi:10.1002/jcc.20084
5. Stuart T, Butler A, Hoffman P, et al. Comprehensive Integration of Single-Cell Data. *Cell* 2019;177:1888-1902.e21. doi:10.1016/j.cell.2019.05.031
6. Hafemeister C, Satija R. Normalization and variance stabilization of single-cell RNA-seq data using regularized negative binomial regression. *Biorxiv* 2019;:576827. doi:10.1101/576827

7. Wales TE, Fadgen KE, Gerhardt GC, et al. High-Speed and High-Resolution UPLC Separation at Zero Degrees Celsius. *Anal Chem* 2008;80:6815–20. doi:10.1021/ac8008862
8. Ewels P, Magnusson M, Lundin S, et al. MultiQC: summarize analysis results for multiple tools and samples in a single report. *Bioinformatics* 2016;32:3047–8. doi:10.1093/bioinformatics/btw354
9. Bray NL, Pimentel H, Melsted P, et al. Near-optimal probabilistic RNA-seq quantification. *Nat Biotechnol* 2016;34:525–7. doi:10.1038/nbt.3519
10. Love MI, Huber W, Anders S. Moderated estimation of fold change and dispersion for RNA-seq data with DESeq2. *Genome Biol* 2014;15:550. doi:10.1186/s13059-014-0550-8
11. Rydenfelt M, Klinger B, Klünemann M, et al. SPEED2: inferring upstream pathway activity from differential gene expression. *Nucleic Acids Res* 2020;48:W307–12. doi:10.1093/nar/gkaa236

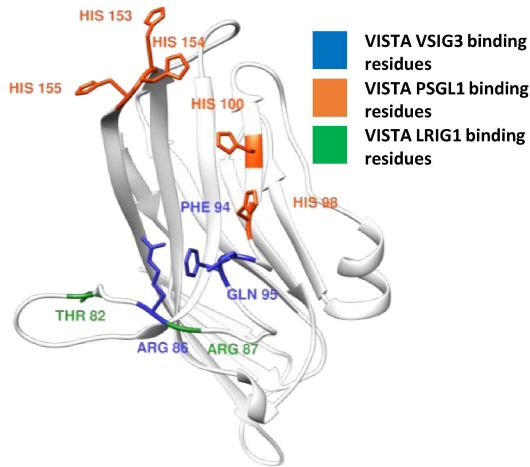
A

VISTA ortholog sequence alignment



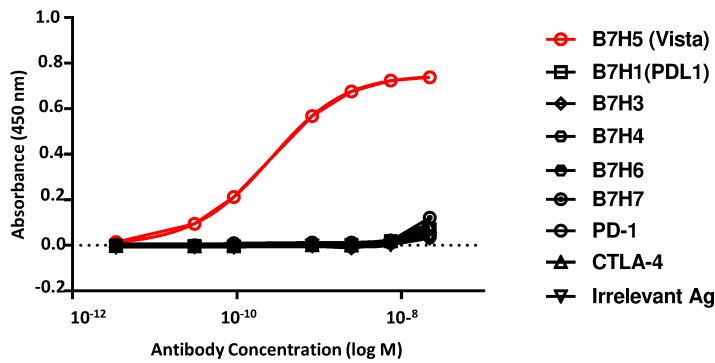
B

VISTA homology model with highlighted residues involved in binding with putative partners



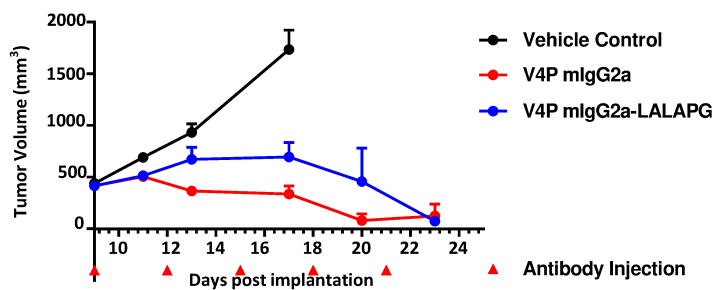
A

Binding of V4P to B7-family proteins, PD-1 and CTLA-4



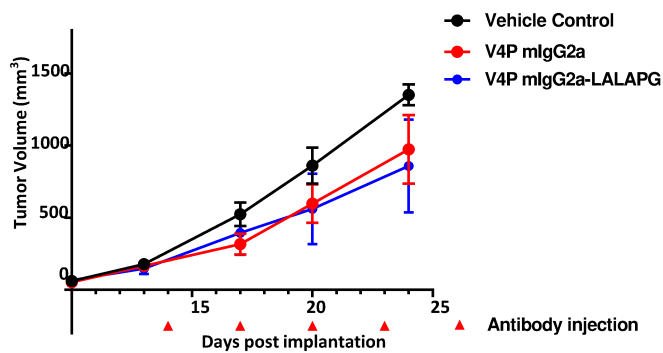
B

Efficacy of Fc-competent V4P-mIgG2a vs Fc-silent V4P-mIgG2a-LALAPG in EL4 murine syngeneic CDX model

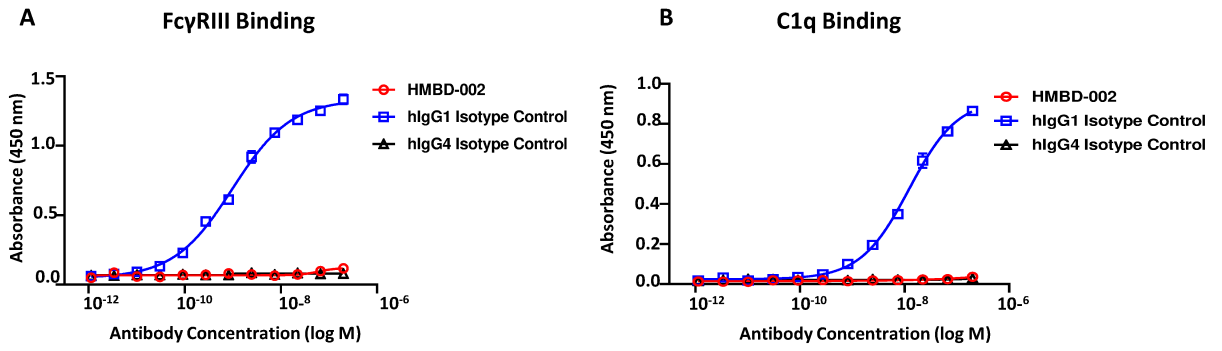


C

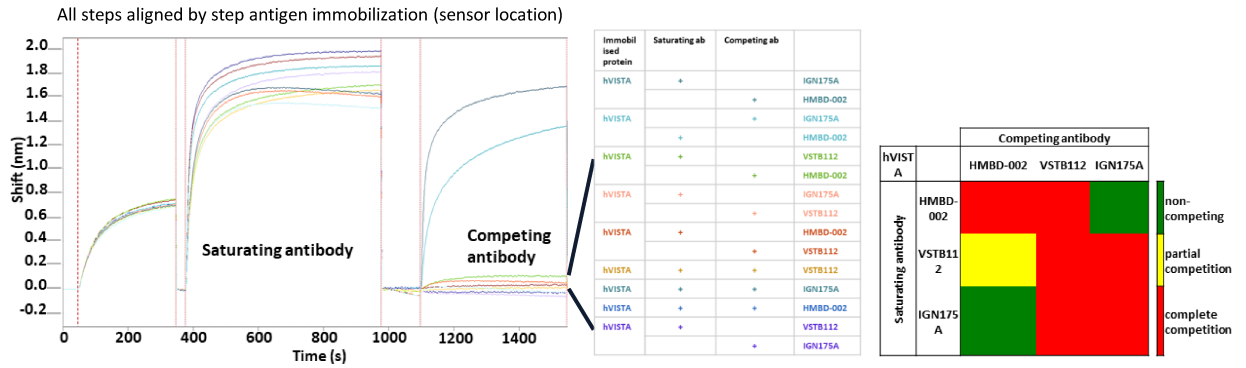
Efficacy of Fc-competent V4P-mIgG2a vs Fc-silent V4P-mIgG2a-LALAPG in CT26 murine syngeneic CDX model



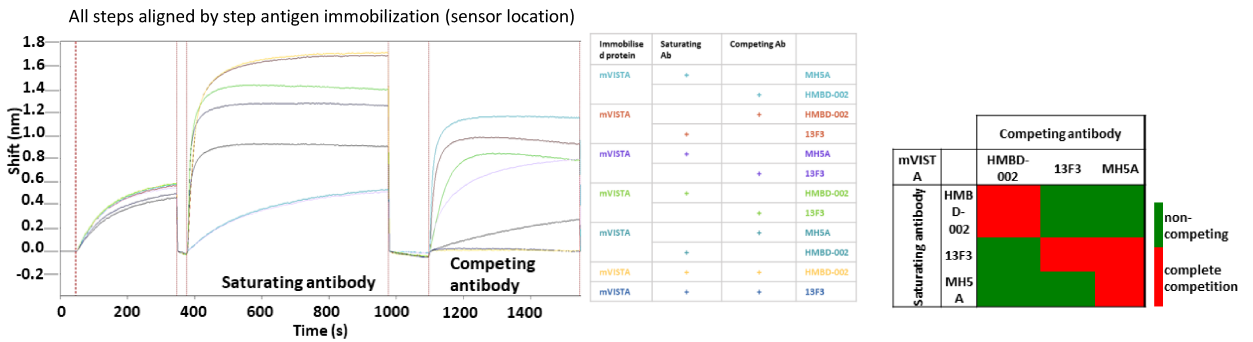
Binding of HMBD-002 to FcγRIII and C1q



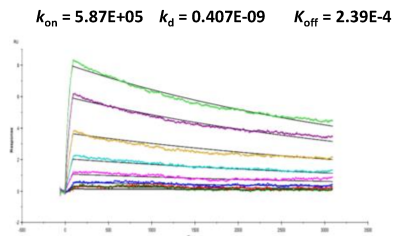
A Epitope Binning of HMBD-002 with other anti-human VISTA binding antibodies



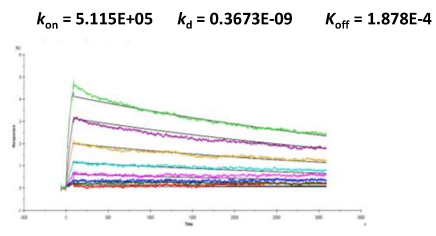
B Epitope Binning of HMBD-002 with other anti-mouse VISTA binding antibodies



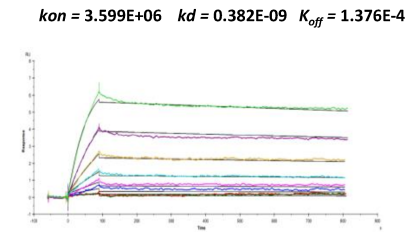
C Affinity - Human VISTA



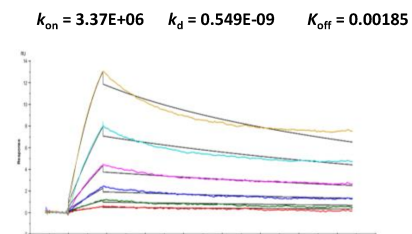
D Affinity - NHP VISTA



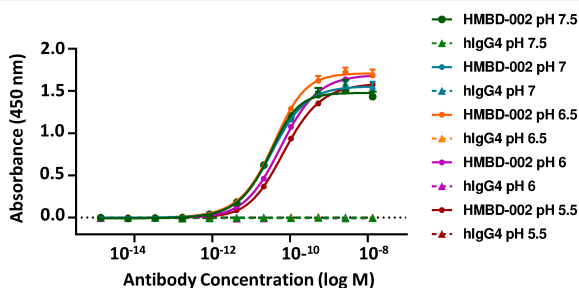
E Affinity - Rat VISTA



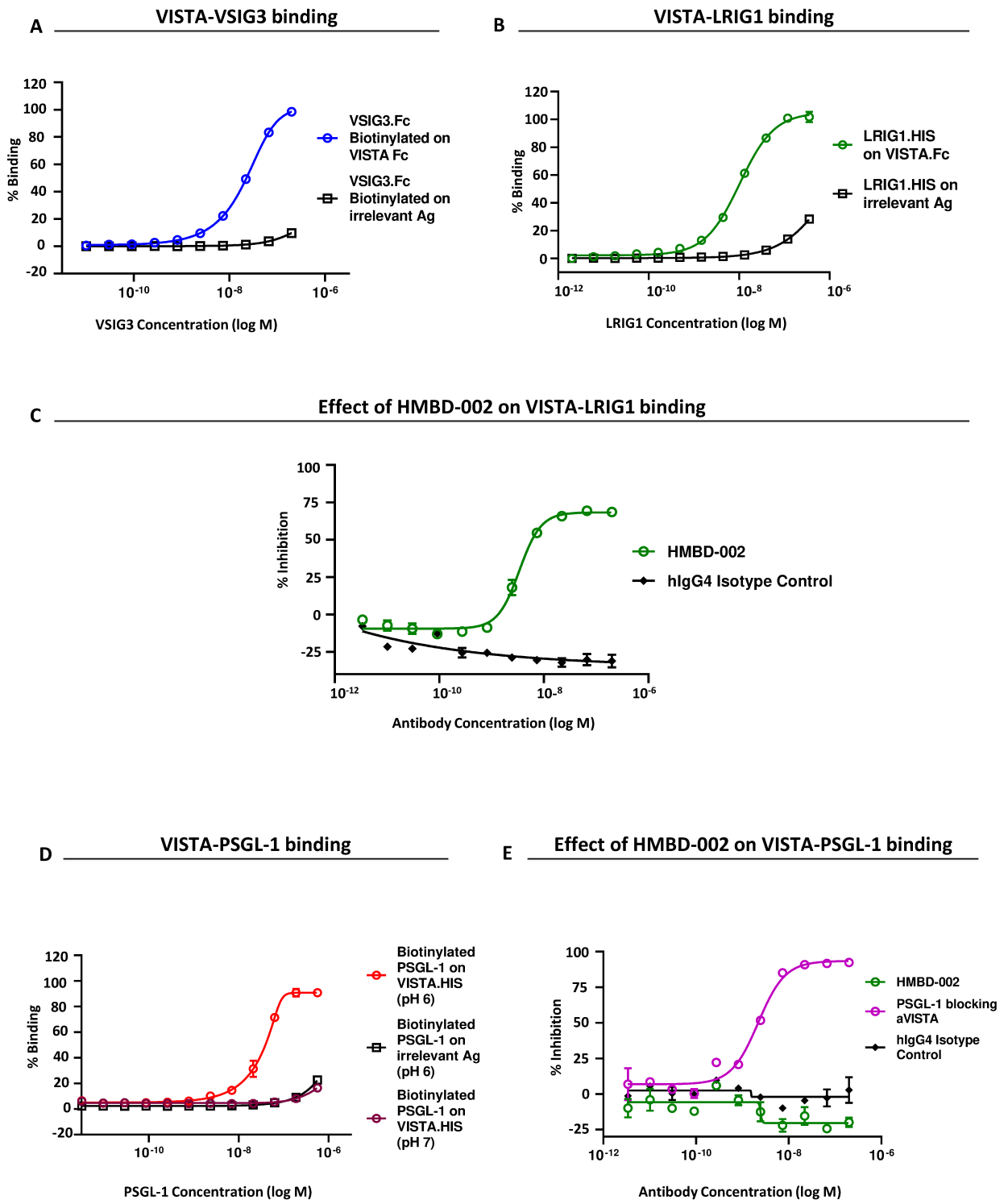
F Affinity - Mouse VISTA

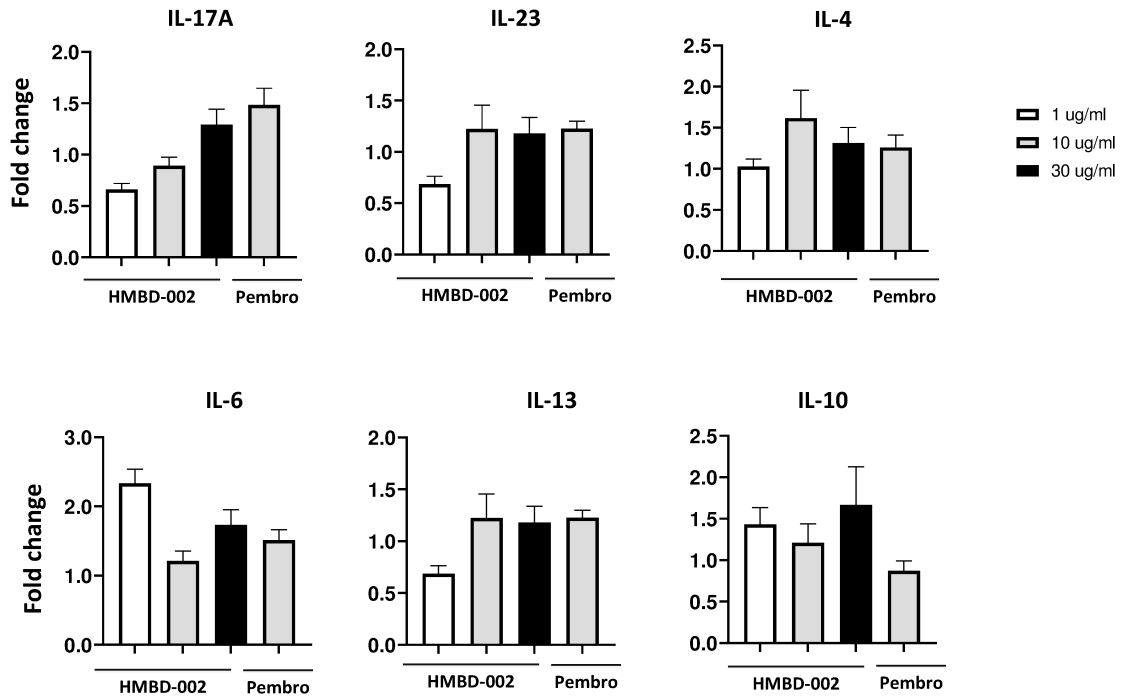
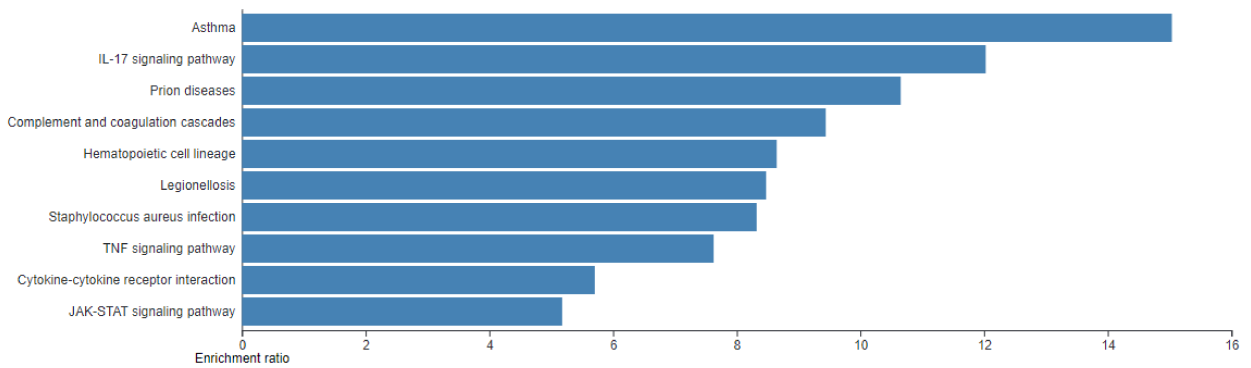
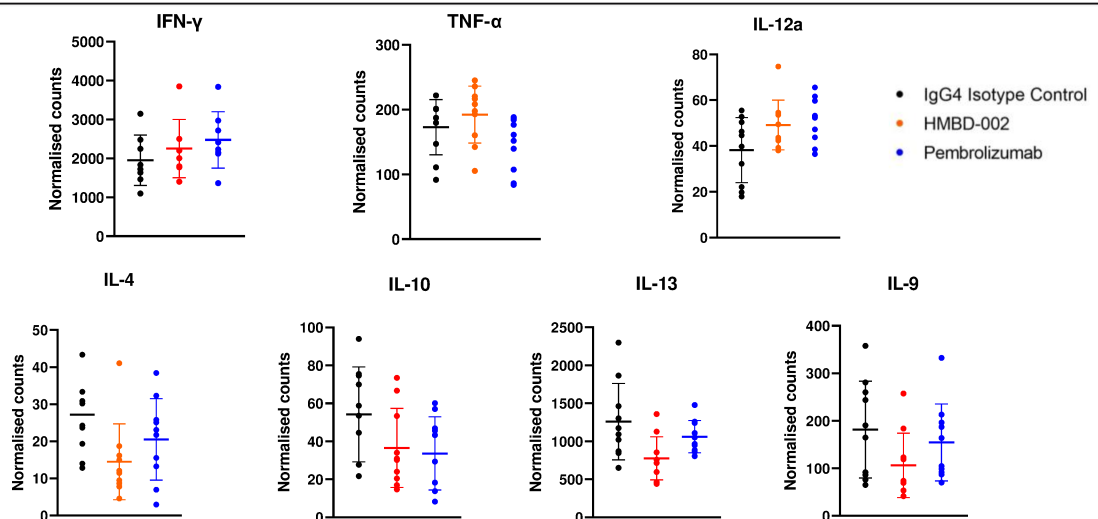


G Binding of HMBD-002 to VISTA across a pH range

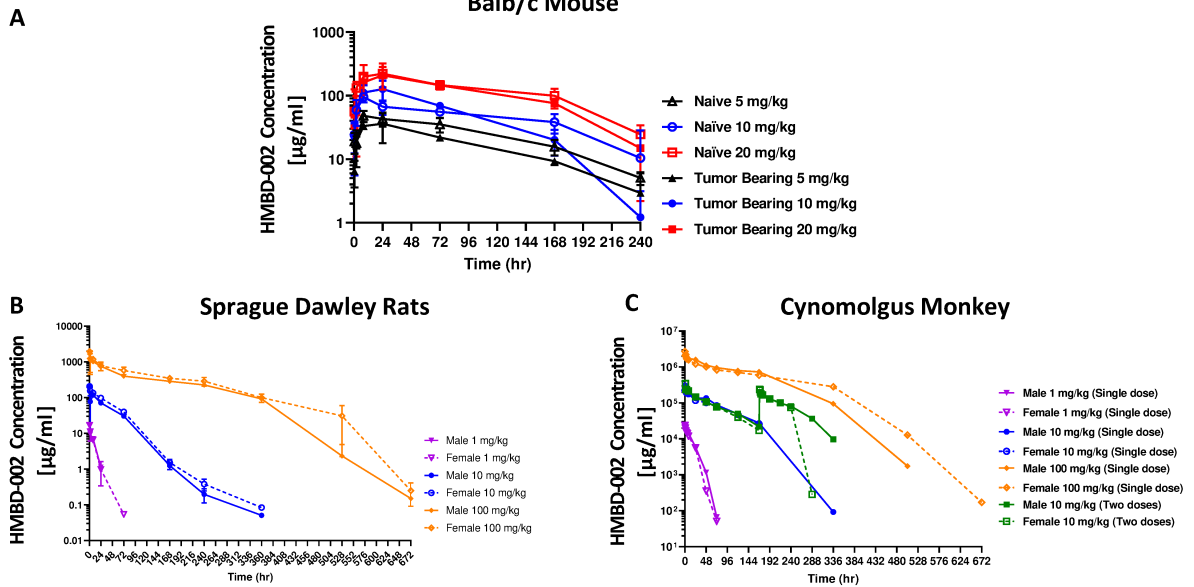


pH	EC ₅₀
7.5	2.871e-011
7	3.431e-011
6.5	3.630e-011
6	5.890e-011
5.5	7.308e-011

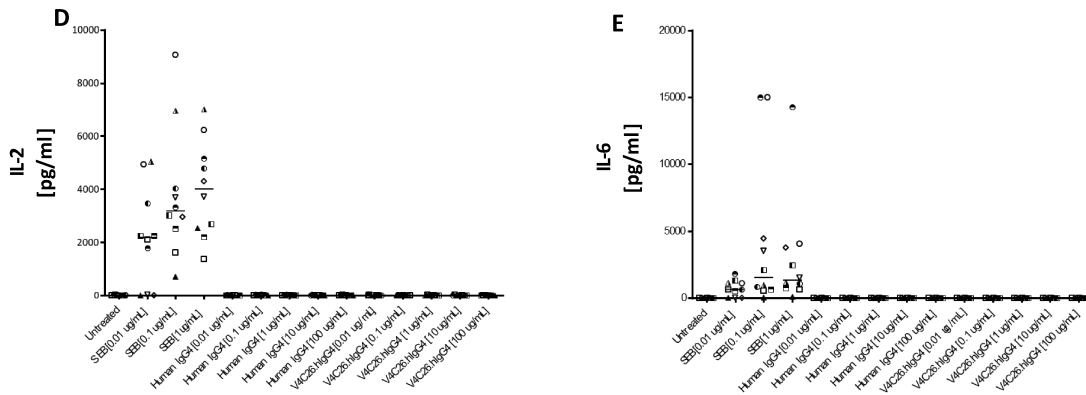


A Effect of HMBD-002 on cytokine release in an allogenic MLR assay**B** Effect of HMBD-002 on the inflammatory signaling pathways in an allogenic MLR assay**C** Effect of HMBD-002 on transcriptomic profile in an allogenic MLR assay

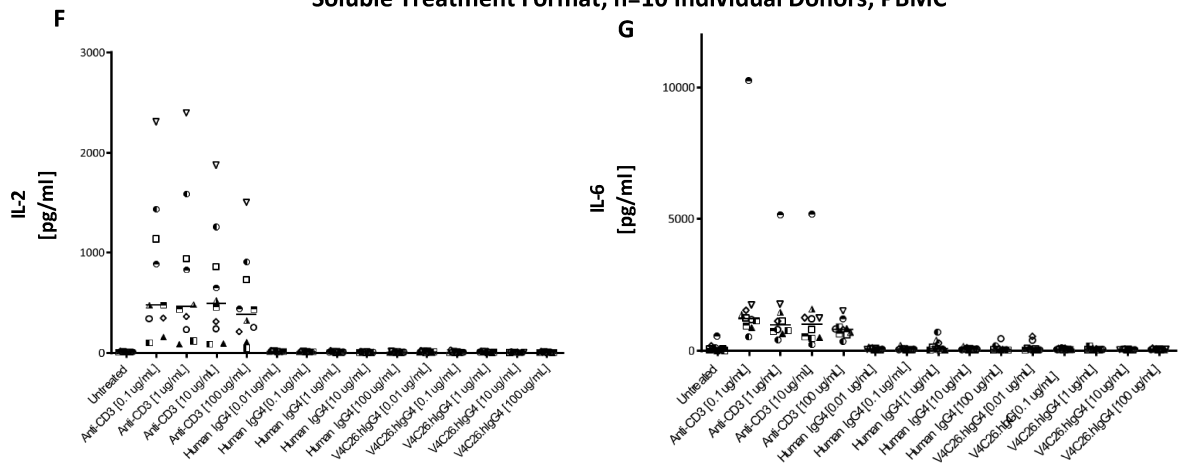
Pharmacokinetic profile of HMBD-002 in pre-clinical toxicology species

Effect of HMBD-002 on an *in vitro* cytokine release assay

Soluble Treatment Format; n=10 Individual Donors; Whole Blood



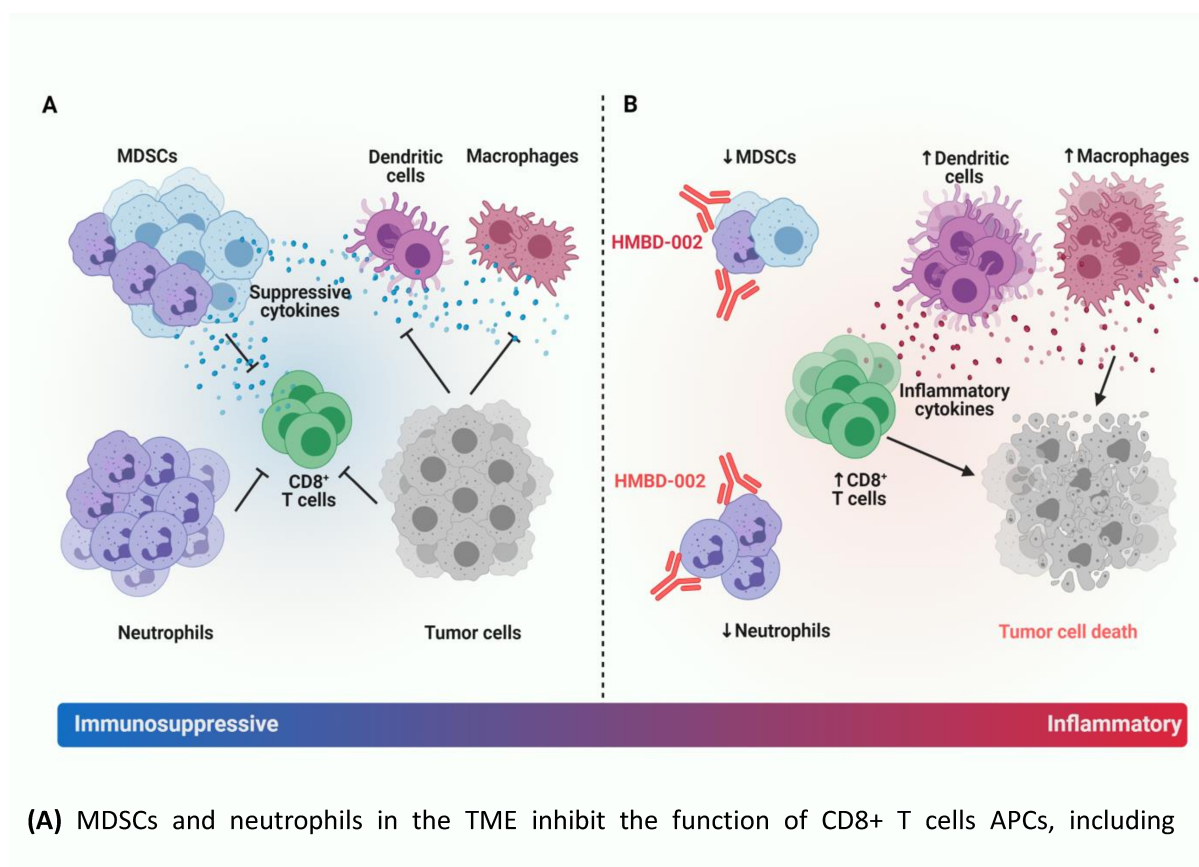
Soluble Treatment Format; n=10 Individual Donors; PBMC



Title: A rationally targeted anti-VISTA antibody that blockades the C-C' loop region can reverse VISTA immune suppression and remodel the immune microenvironment to potently inhibit tumor growth in an Fc independent manner

Authors:

Dipti Thakkar¹, Shalini Paliwal¹, Bhushan Dharmadhikari¹, Siyu Guan¹, Lillian Liu¹, Shreya Kar¹, Nikhil K. Tulsian², Joshua J. Gruber³, Leah DiMascio⁴, Konrad H. Paszkiewicz¹, Piers J. Ingram⁴, and Jerome D. Boyd-Kirkup^{4*}



(A) MDSCs and neutrophils in the TME inhibit the function of CD8+ T cells APCs, including macrophages and dendritic cells leading to an immunosuppressive TME permissive of tumor growth. **(B)** HMBD-002 binds to and blocks VISTA on neutrophils and MDSCs, releasing their immunosuppressive effects and shifting the TME to a pro-inflammatory anti-tumorigenic phenotype, characterised by increased inflammatory cytokine release and increased proliferation and activation of CD8+ T cells and APCs.

SUPPLEMENTARY FILES

SUPPLEMENTARY FIGURE LEGENDS

S1. VISTA sequence homology and reported interaction residues with binding partners (VSIG3, LRIG1 and PSGL-1).

A. VISTA sequence alignment between mouse, rats, cynomolgus monkey and humans from MultAlign and visualized via ESPript. B. VISTA homology model showing VSIG3, PSGL-1 and LRIG1 epitope residues, reported to be involved in binding human VISTA.

S2. Murine anti-VISTA antibody, V4P, binds to VISTA with high affinity and specificity and demonstrates Fc-independent inhibition of tumor growth in vivo

A. Binding specificity of V4P by ELISA using human B7 family antigens as indicated. Data shown are mean n=2 measurements and error bars are SEM. **(B-C)** Cell derived xenograft models of C54BL/6 mice subcutaneously implanted with EL4 (B) and BALB/c mice, subcutaneously implanted with CT26 (C). Mice were randomized and dosed with concentrations of test articles at indicated time-points. Tumor volumes were measured twice a week. Each data point represents the mean tumor volume +/- SEM of n=6 mice.

S3. HMBD-002, an IgG4 monoclonal antibody, does not bind to FcγRIII or C1q that are required for Fc-mediated ADCC and CDC activity.

A. Binding of HMBD-002 to FcγRIII and B.C1q proteins as assessed by ELISA. Data shown are mean of n=3 measurements and error bars are SEM.

S4. HMBD-002 binds to a unique epitope on VISTA with very high binding affinity across a range of physiological pH.

A. HMBD-002 epitope binning, using examples of human VISTA antibodies (VSTB112, IGN175A) and B. mouse anti-VISTA antibodies (13F3, MH5A) in-tandem method was used to

test competitive binding of antibody pairs to VISTA by biolayer interferometry and signals were aligned to baseline. C-F. Surface plasma resonance (Biacore) binding kinetics of HMBD-002 to VISTA orthologs; human, mouse, rat and cyno VISTA. G. Binding affinity of HMBD-002 across pH range 5.5-7.5. Data shown are mean of n=3 measurements and error bars are SEM.

Figure S5. VISTA interacts with VSIG3, LRIG1, PSGL-1 and HMBD-002 inhibits the VISTA-LRIG1 interaction but does not inhibit the VISTA-PSGL-1 interaction.

A and B. Binding of VISTA with its binding partner VSIG3 (A) and LRIG1 (B) by ELISA. Data shown are mean of n=3 measurements and error bars are SEM. C. Inhibition of VISTA:LRIG1 binding, analyzed by competition ELISA. Data shown are mean of n=3 measurements and error bars are SEM. D. Binding of VISTA to its putative binding partner PSGL-1 at pH6 and pH7 by ELISA. Data shown are mean of n=3 measurements and error bars are SEM. E. Inhibition of VISTA:PSG-L-1 binding at pH6, analyzed by competition ELISA. Data shown are mean of n=3 measurements and error bars are SEM.

S6. HMBD-002 remodels the immune milieu toward an enhanced pro-inflammatory Th1/Th17 immune response in an allogenic Mixed Lymphocyte Reaction. A. Cytokine levels measured at 96 hrs by Luminex, from the supernatant of an allogenic mixed lymphocyte reaction. All concentrations of HMBD-002 and anti PD-1 antibody, Pembrolizumab (annotated as Pembro) in $\mu\text{g/ml}$. Data was normalized to isotype control. Data shown are mean of n=10 and error bars are SEM. B. KEGG pathway analysis using WebGestalt from bulk RNA-sequencing of MLR samples (n=10). Data was normalized to IgG4 isotype control. C. Enrichment of transcript levels in genes associated with type-I and Type-II interferon genes from bulk RNA-sequencing of MLR samples (n=10). Data represented as mean \pm SD.

S7. HMBD-002 exhibited acceptable pharmacokinetic and safety profiles in multiple pre-clinical toxicology species.

Serum concentration of HMBD-002 in **(A)** Balb/c tumor-bearing and non-tumor bearing mice (n=3), **(B)** Sprague Dawley rats (n=6) and **(C)** cynomolgus monkey (n=2). HMBD-002 was administered at the indicated concentration via intraperitoneal injection in mice, IV bolus injection into the tail vein in rats, and IV bolus injection into the peripheral vein in monkeys **(D-G)** Cytokine release assay showing representative cytokine levels of IL-2 and IL-6 using whole blood (D and E) and PBMC (F and G) treated with indicated test articles and concentrations. HMBD-002 is referred to in the figure as V4C26.hIgG4 in D-G. Data shown are mean of n=10 measurements and each point represents an independent donor.

SUPPLEMENTARY METHODS

Antibody isolation

Six- to eight-week-old female BALB/c mice were repeatedly immunized with custom immunogens. Twenty-four hours after the final immunization, total splenocytes were isolated and fused with the myeloma cell line P3X63.Ag8.653 (ATCC) using ClonaCell-HY Hybridoma Cloning Kit, in accordance with the manufacturer's instructions (Stemcell Technologies). After 7 to 10 days, single hybridoma clones were isolated and antibody-producing hybridomas were selected by screening supernatants for antigen binding using ELISA and flow cytometry. Variable regions of selected clones were amplified (SMARTer RACE 5'/3' Kit, Clontech), sequenced and cloned into expression vector and expressed in mammalian cells for in vitro functional testing. One clone, V4P, was selected for development and subsequently humanized and further affinity matured into the final antibody HMBD-002.

Hybridoma production

Approximately 6-week-old female BALB/c mice were obtained from InVivos (Singapore). Animals were housed under specific pathogen-free conditions and were treated in compliance with the Institutional Animal Care and Use Committee (IACUC) guidelines. Using our proprietary immunization protocol (mAbHits), mice were immunized with proprietary mixtures of custom immunogens. Total splenocytes were isolated and fused with the myeloma cell line P3X63.Ag8.653 (ATCC, USA) using polyethylene glycol (PEG) and ClonaCell-HY Hybridoma Cloning Kit (Stemcell Technologies, Canada), according to manufacturer's instructions. Monoclonal hybridomas were selected and supernatants from

the resulting clones were screened by enzyme linked immunosorbent assay (ELISA) and fluorescent activated cell sorting (FACS).

Antibody variable region cloning and sequencing

Total RNA was extracted from hybridoma cells using TRIzol reagent (Life Technologies, Inc., USA) according to the manufacturer's instructions. Double-stranded cDNA was synthesized using SMARTer RACE 5'/3' Kit (Clontech). The race-ready cDNAs were amplified using SeqAmp DNA Polymerase (Clontech™) and primer mixes. The resulting variable heavy (VH) and light (VL) amplicons were cloned into pJET1.2/blunt vector using CloneJET PCR Cloning Kit (Thermo Scientific) and purified PCR amplicons were sequenced through AITBiotech Pte. Ltd. (Singapore). The sequencing data was analysed using the international IMGT (ImMunoGeneTics) information system[1] to characterize the individual complementarity-determining regions (CDRs) and framework sequences.

Humanization and affinity maturation of mouse antibody

Humanization of the variable regions of the mouse sequence was performed by CDR grafting into human framework sequences and backmutation of residues in canonical positions to preserve antigen binding. The humanised antibody was further affinity matured against mouse VISTA to increase the cross-species affinity by random mutagenesis using yeast scFv surface display. Briefly, ScFv bearing the parental VH and VL in a single chain was amplified by mutagenesis PCR (Agilent Technologies GeneMorph II Random Mutagenesis Kit) for library creation, the resulting library was further amplified and cloned into yeast expression vector pCTcon2 (Addgene) for yeast surface expression by electroporation. The transfected cells were screened by mouse VISTA binding using FACS and high binder cell was sorted by BD FACS Aria II cell sorter. Selected high binder clones were enriched by 2 additional rounds

of sorting. Cells were plated in SDCAA to isolate single clones followed by DNA extraction and sequencing. The final sequence of HMBD-002 was selected from among the optimized variants based on its developability characteristics as well as in vitro physicochemical and functional properties.

Cell lines

All cell lines were purchased from ATCC and cultured as recommended. Cells were maintained in culture medium supplemented with 10% FBS and 1% Pen/Strep (ThermoFisher) and cultured at 37°C, in 5% CO₂ incubators. Prior to use, fresh vials of cells were thawed and passaged 2-5 times. And Mycoplasma testing was performed by PCR using DreamTaq Green PCR master mix (ThermoFisher #K1081) according to manufacturer's instruction. Mycoplasma (*M. orale*) positive control template (Agilent Mycosensor assay kit) and the following primers were used:

Fwd. 5' GGGAGCAAACAGGATTAGATACCCT 3'

Rev. 5' TGCACCATCTGTCACTCTGTAAACCTC 3'

Stable cell line generation

CHO-k1 cells at an optimal density of 1*10⁶ cell/ml were electroporated with 5 µg of linearized IgG expression plasmid using 4D-Nucleofactor kit (Lonza) according to manufacturer's protocol. Electroporated cells were cultured in static cell incubator in a 6-well plate containing 2 ml growth medium for 24 hr. Subsequently, medium was exchanged to selection medium containing 250 nM Methotrexate (Sigma) and 200 µg/ml Zeocin (InvivoGen). Cells were spun down and re-suspended in fresh selection medium and

re-seeded to a density of 5×10^5 cell/ml once per week. Selection was completed when 95% viability was restored. Cells were transferred to shaker-incubator.

Antibody production and purification

Antibodies were produced by cultivation of stable cells in Fed-Batch mode in a shaker-incubator and subsequently purified from culture supernatants by affinity, size exclusion or mixed modal anion exchange followed by a final anion exchange chromatography. Antibody purity was assessed by size exclusion chromatography and SDS-PAGE.

VISTA sequence analysis and visualization

Multiple sequence alignments were performed with MultAlign[2] and visualized with EPScript[3]. 3D models were generated using UCSF Chimera[4].

sc-RNA-seq analysis of 68k PBMC dataset

To determine the cell types in which VISTA transcripts were most highly expressed, a publicly available 68k PBMC dataset was retrieved from the 10X Genomics website and processed using Seurat v3.2[5]. Cells with more than 6% mitochondrial transcripts, or less than 200 distinct transcripts were excluded. Data was normalized using default parameters and variable features identified using the VST method with 20,000 features. Data was subsequently scaled and then a PCA decomposition run with 15 principal components. A UMAP projection was carried out using default parameters and the FindClusters function run with a resolution of 0.8. To label the clusters the PBMC3k dataset[6] from the SeuratData package was used as a reference to map cell identities.

Epitope mapping by hydrogen-deuterium exchange mass spectrometry (HDXMS)

Epitope mapping by HDXMS was conducted using his-tagged human VISTA (residues 33-194, Sino Biological #13482-H08H) and HMBD-002 following procedures described previously[7]. Briefly, free VISTA was diluted in deuterated PBS with final deuterium oxide (D₂O) concentration at 90%. For VISTA/HMBD-002 complex, VISTA and HMBD-002 were mixed in 2:1 ratio and incubated for 15 mins at 25°C prior to deuterium labelling. Deuterium labelling reactions were carried out at 25°C for 1-, 10-, 30- and 100-min time points. Samples were then subjected to pepsin proteolytic cleavage followed by separation on an ACQUITY C18 column (1.0 x 100 mm) by nanoACQUITY UPLC (Waters) and detection by Synapt G2-Si mass spectrometer (Waters), operated in HDMS^E mode. Peptide identification and deuterium uptake monitoring were respectively performed using Protein Lynx Global Server 3.0.1 and DynamX 3.0 (Waters). Deuterium uptake for the peptides were calculated as differences in masses of the centroids of deuterated and undeuterated samples and reported as an average of triplicate measurements.

Epitope Binning

For epitope binning, human VISTA-His, or mouse VISTA-his recombinant protein (Sino Biological Inc.) in PBS was immobilized to Anti-Penta His sensor (HIS1K, Molecular Device) on an Octet QK384 (Molecular Device) instrument, for 5 mins. Sensors were briefly washed in PBS for 30s before loading 400 nM saturating antibody in PBS for 10 mins at a shake speed of 1,000 rpm. Subsequently, biosensors were washed for 2 min before immersing in 400 nM competing antibody in PBS for 7.5 mins at a shake speed of 1,000 rpm. Binding events which are correlated to change in wavelength (nm shift) reported from sensorgram, are monitored at the detector in real time.

Cross-species antibody binding affinity measurement

The affinity of HMBD-002 was determined by Surface Plasmon Resonance (SPR) using a Biacore. The assay was performed using a CM5 sensor chip (Cytiva #29104988). A Biacore HIS capture kit (GE Healthcare #28-9950-56) was employed to immobilize human, cynomolgus monkey, rat and mouse VISTA-HIS on-chip surface or left alone for background signal correction. Briefly, VISTA-HIS was captured for a contact time of 60 s at a flow rate of 5 μ l/min. HMBD-002 was flowed in two-fold serial dilutions from 50E-9 M to 390E-12 M for human, cynomolgus monkey and rat VISTA and from 12.5E-9 M to 390E-12 M for mouse VISTA, at a flow rate of 30 μ l/min for 90 sec association and 3000 sec dissociation at RT. The obtained sensograms were analyzed using Biacore T200 software and KD was calculated by fitting to a 1:1 binding kinetics model.

Antibody-dependent cellular cytotoxicity and complement-dependent cytotoxicity

96 well plates were coated with either 1 μ g/well of human C1q protein or 0.5 μ g/well of human CD16a in PBS at 4°C. Post overnight incubation, plates were washed thrice and blocked for 1 hr with blocking buffer at room temperature. Plates were incubated with HMBD-002 or isotype control for 1 hr at room temperature and incubated with 1:7000 dilution of HRP-conjugated anti-human Fc antibody for 1 hr at room temperature. Colorimetric reactions were developed using standard protocol as described for ELISA above.

VISTA-LRIG1 Inhibition Assay

VISTA-LRIG1 binding was confirmed using recombinant human VISTA-Fc protein (R&D #7126-B7) or irrelevant antigen (Human recombinant CD47 protein, Sinobiological #112283-HCCH) with standard ELISA method. For inhibition assay, 384-well plates were coated with 5 μ g/ml of human VISTA-Fc recombinant protein (R&D #7126-B7) diluted in PBS for 24 hrs at 4°C. After blocking for 2 hrs with 1% BSA at room temperature, plates were

incubated with either HMBD-002 or isotype control (Biolegend #403702) for 60 mins at room temperature. After 60 mins, recombinant human LRIG1.HIS at 1 µg/ml (EC_{50} of VISTA-LRIG1 binding) was added for 2 hrs. Post incubation, plates were washed three times with TBST and incubated with anti-HIS HRP (Abcam #ab1187) antibody for 1 hr at room temperature followed by three further washes. Colorimetric reactions were developed using standard protocol as described for ELISA above.

VISTA-PSGL-1 Inhibition Assay

VISTA-PSGL-1 binding was confirmed using recombinant human VISTA-HIS protein (Acro Biosystems #B75-H52H0) or irrelevant antigen (Rat recombinant HER3-HIS protein, Elabscience #PKSR030358) with standard ELISA method. For the inhibition assay, 384-well plates were coated with 5 µg/ml of human VISTA-HIS recombinant protein (Acro Biosystems #B75-H52H0) diluted in PBS for 24 hrs at 4°C. After blocking for 2 hrs with 1% BSA (pH6) at room temperature, plates were incubated with either HMBD-002 or isotype control for 60 mins at room temperature in 1% BSA (pH6). After 60 mins, biotinylated recombinant human PSGL-1-Fc (R&D #3345-PS) (Recombinant Human PSGL-1-Fc was biotinylated using Invitrogen kit #21455) at 9.5E-8 M (EC_{80} of VISTA-PSGL-1 binding) was added for 2 hrs. Post incubation, plates were washed three times with TBST (pH6) and incubated with streptavidin HRP (R&D #DY998) antibody for 1 hr at room temperature followed by three further washes. Colorimetric reactions were developed using standard protocol as described for ELISA above.

Bulk RNA-seq

10 samples per condition (V4C26, V9, anti-PD1, and IgG4) were taken from the MLR assay 96 hours after treatment. These were prepared for RNA-seq using the NEBNext Ultra II RNA library preparation kit (NEB #E7770S) and run on an Illumina NovaSeq S4 flowcell with v1.5

chemistry. Adaptor-trimmed and filtered data was evaluated using FASTQC and MultiQC[8] and reads aligned to the GRC37 human reference transcriptome using Kallisto v0.46[9]. Data was imported to R using TxImport. Normalized gene counts and gene-level differential expression was obtained using DESeq2[10]. Pathway activity was estimated using the SPEED2[11] package using default parameters.

CT26 tumor profiling

Single cell suspensions were generated by digestion of finely cut tumor tissue with 0.1 mg/ml of DNase I (Sigma #11284932001) and 1 mg/ml Collagenase (Sigma #1108866001) for 45 minutes at 37°C. Fc receptors were blocked with Human TruStain FcX (BioLegend #422302). Cells were stained with fluorophore conjugated antibodies for markers of immune cells (Table S5), washed and resuspended in buffer (1xPBS + 0.5% BSA + 1mM EDTA). Frequency of immune cell populations was determined via flow cytometry. Data was acquired on MACSQuant 10 (Milteny #130-096-343) and analyzed using FlowLogic software V7.

CT26 antigen recall assay

Single cell tumor suspensions were generated as described earlier. TILs (CD45+) or T cells (CD4+/CD8+) were enriched from the cell suspension using CD45 MicroBeads (Milteny #130-110-618) or CD4/CD8 MicroBeads (Milteny #130-116-480) as per manufacturer's protocol. CT26 cells (T: target cells), seeded 24 hrs prior, were co-cultured with enriched TILs or T cells (E: effector cells) from tumors for 72 hours at effector to target (E:T) cell ratios as indicated. All conditions were in triplicates. Cell viability was determined by CellTiter Glo (Promega#G7571). IFN- γ levels in supernatants were determined by ELISA (Invitrogen#BMS606). Lysis was calculated as: % Lysis = $((T - E:T)/T) * 100$.

Pharmacokinetics

Pharmacokinetic profile of HMBD-002 was evaluated in male and female Balb/c mice, Sprague Dawley rats and cynomolgus monkeys. HMBD-002 was administered in a single dose at the indicated concentration via IP injection in mice and IV bolus injection into the tail vein in rats. For cynomolgus monkeys, HMBD-002 was administered either once at doses of 1, 10, or 100 mg/kg or twice one week apart (Days 1 and 8) at a dose of 10 mg/kg/week by IV bolus injection into the peripheral vein. Blood was drawn at different timepoints post dosing and antibody concentration in the serum was quantified by ELISA. The parameters for the pharmacokinetic analysis were derived from a non-compartmental model: maximum concentration (C_{max}), AUC (0-336hr), AUC (0-infinity), half-life (t_{1/2}), clearance (CL) and volume of distribution at steady state (V_{ss}).

SUPPLEMENTARY TABLES

Table S1: Top low energy template interfaces predicted by PRISM, utilizing the VISTA and PD-L1 structures (PDB IDs 60IL, 3BIK respectively)

PRISM Pseudo energy Score	Template
-56.25	2dpfCD
-34.28	3b76AB

Table S2: Reconstitution composition for CD34+ humanized mice.

CDX Model	Mouse ID#	%hCD45	% Relative to hCD45				
			hB cells	hCD14 Monocyte	Total hT cells	hCD4T	hCD8T
HCT15	1532	13.4%	54.0%	0.4%	39.6%	26.8%	9.6%
	1533	13.9%	73.4%	1.6%	16.8%	13.5%	3.0%
	1534	16.1%	71.4%	2.0%	18.1%	13.6%	3.7%
	1535	14.1%	64.4%	0.9%	22.7%	16.6%	5.7%
	1536	17.6%	57.1%	1.9%	35.4%	27.6%	7.5%
	1537	15.4%	64.3%	2.9%	23.6%	17.6%	6.0%
	1538	11.3%	48.2%	1.8%	43.1%	25.9%	15.7%
	1539	14.6%	35.2%	3.3%	50.5%	41.8%	7.4%
	1540	12.0%	68.2%	2.4%	16.3%	11.9%	3.9%
	1541	26.2%	47.8%	0.7%	45.7%	34.1%	11.3%
A549	1544	23.9%	54.8%	2.3%	35.3%	29.7%	5.4%

	1545	23.9%	53.7%	4.1%	36.0%	26.8%	8.8%
	1546	18.7%	63.9%	1.1%	29.1%	21.3%	7.0%
	1547	15.2%	30.7%	6.8%	55.3%	40.5%	14.2%
	1548	31.6%	50.5%	1.6%	39.4%	29.0%	9.7%
	1549	42.8%	56.1%	3.9%	30.9%	22.1%	7.5%
	1550	44.2%	56.5%	2.9%	29.9%	22.2%	6.8%
	1551	19.6%	41.0%	3.2%	50.5%	41.6%	8.5%
	1552	23.8%	58.2%	1.4%	32.7%	24.8%	7.3%
	1553	17.9%	45.5%	3.3%	43.2%	32.7%	9.8%

Table S3: Clinical observations, food consumption, body weight, and clinical pathology findings during single dose intravenous tolerability study in Sprague-Dawley rats.

Endpoints Evaluated	Results
Clinical Observations	<ul style="list-style-type: none"> • No test article-related clinical signs observed
Food Consumption	<ul style="list-style-type: none"> • Variations observed in food consumption of animals were of minimal magnitude and lacked a dose-response relationship • No test article-related changes observed in food consumption of female rats • Decreased food consumption observed for male rats in 1 mg/kg/dose group, however, relationship to test article unlikely due to lack of dose-response relationship, and absence of similar observation in females
Body Weight	<ul style="list-style-type: none"> • Body weight variations observed in animals were of minimal magnitude and lacked a dose-response relationship • No test article-related changes observed in body weights of female rats • 15% change in body weight observed for male rats in 1 mg/kg/dose group, however, relationship to test article was unlikely due to lack of dose-response

	relationship, and absence of similar observation in females
<p>Hematology:</p> <p>Leukocyte counts, Erythrocyte count, Hemoglobin, Hematocrit, Mean corpuscular volume, Mean corpuscular hemoglobin concentration, Reticulocyte count, RBC distribution width, Platelet count, Mean platelet volume, absolute and percent WBC Differential (Neutrophils, Eosinophils, Basophils, Monocytes, Lymphocytes), absolute Large unstained cells, percent Large unstained cells and percent Reticulocyte count</p>	<ul style="list-style-type: none"> • No test article-related changes observed in hematology parameters • All differences observed were considered incidental due to lack of a dose-response relationship, minimal magnitude and/or the individual values were within the historical control data range
<p>Serum Chemistry:</p> <p>Alanine Aminotransferase, Aspartate Aminotransferase,</p>	<ul style="list-style-type: none"> • No test article-related changes observed in serum chemistry • All differences observed were considered incidental due to lack of a dose-response relationship, minimal

Total Protein, Albumin, Globulin, Albumin/Globulin Ratio, Alkaline Phosphatase, γ -glutamyltransferase, Glucose, Urea, Creatinine, Calcium, Phosphorus, Total Cholesterol, Triglycerides, Total Bilirubin, Sodium, Potassium, Chloride, Creatine Kinase and C-reactive protein	magnitude and/or the individual values were within the historical control data range
---	--

Table S4: Clinical observations, food consumption, body weight, and clinical pathology findings during single dose intravenous tolerability study in cynomolgus monkeys.

Endpoints Evaluated	Results
Clinical Observations	<ul style="list-style-type: none"> • No test article-related clinical signs observed
Food Consumption	<ul style="list-style-type: none"> • No test article-related changes observed in food consumption
Body Weight	<ul style="list-style-type: none"> • No test article-related changes observed in body weights
Hematology: Leukocyte counts, Erythrocyte count, Hemoglobin, Hematocrit, Mean corpuscular volume, Mean corpuscular hemoglobin concentration, Reticulocyte count, RBC distribution width, Platelet count, Mean platelet volume, absolute and percent	<ul style="list-style-type: none"> • No test article-related changes observed in hematology parameters • All differences observed were considered incidental due to lack of a dose-response relationship, minimal magnitude and/or the individual values were within the historical control data range

<p>WBC Differential (Neutrophils, Eosinophils, Basophils, Monocytes, Lymphocytes), absolute Large unstained cells, percent Large unstained cells and percent Reticulocyte count</p>	
<p>Serum Chemistry:</p> <p>Alanine Aminotransferase, Aspartate Aminotransferase, Total Protein, Albumin, Globulin, Albumin/Globulin Ratio, Alkaline Phosphatase, γ-glutamyltransferase, Glucose, Urea, Creatinine, Calcium, Phosphorus, Total Cholesterol, Triglycerides, Total Bilirubin, Sodium, Potassium, Chloride, Creatine Kinase and C-reactive protein</p>	<ul style="list-style-type: none"> ● No test article-related changes observed in serum chemistry ● All differences observed were considered incidental due to lack of a dose-response relationship, minimal magnitude and/or the individual values were within the historical control data range

Table S5: List of antibodies.

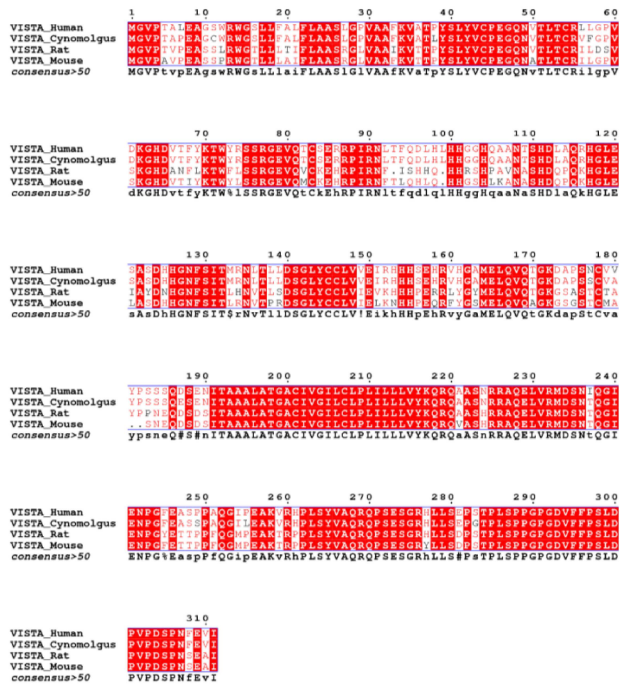
Antibody	Company and Catlog
Anti-mouse MHCI	Invitrogen #48-5321-82
Anti-mouse Gr1	BioLegend #108437
Anti-mouse CD19	BioLegend #152408
Anti-mouse CD3	BioLegend #100219, BioLegend #100236
Anti-mouse CD11b	BioLegend #101211, BioLegend #101206, Milteny #130-113-243
Anti-mouse CD45	BioLegend #103154
Anti-mouse Ly-6C	BioLegend #128006
Anti-mouse Ly-6G	BioLegend #127618
Anti-mouse F4/80	BioLegend #123109
Anti-mouse CD11c	BioLegend #117310
Anti-mouse CD44	BioLegend #103020
Anti-mouse CD4	BioLegend #100406
Anti-mouse CD8	BioLegend #100708
Anti-mouse CD25	BioLegend #102061
Anti-mouse CD206	BioLegend #141720
Anti-mouse PD1	BioLegend #135241
Human CD45	Biologend # 304006
Mouse CD45	Biologend #103108
Rat CD45	Biologend # 202205
Anti NHP CD45	BD Pharmingen # 557803
Human/Rhesus CD11b	Biologend # 301306
Mouse CD11b	Biologend # 101208
Rat CD11b	Biologend # 201807

References

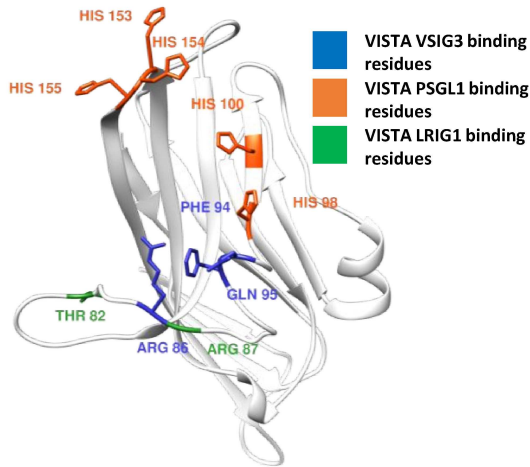
1. Lefranc M-P, Giudicelli V, Duroux P, et al. IMGT®, the international ImMuNoGeneTics information system® 25 years on. *Nucleic Acids Res* 2015;43:D413–22. doi:10.1093/nar/gku1056
2. Corpet F. Multiple sequence alignment with hierarchical clustering. *Nucleic Acids Res* 1988;16:10881–90. doi:10.1093/nar/16.22.10881
3. Robert X, Gouet P. Deciphering key features in protein structures with the new ENDscript server. *Nucleic Acids Res* 2014;42:W320–4. doi:10.1093/nar/gku316
4. Pettersen EF, Goddard TD, Huang CC, et al. UCSF Chimera—A visualization system for exploratory research and analysis. *J Comput Chem* 2004;25:1605–12. doi:10.1002/jcc.20084
5. Stuart T, Butler A, Hoffman P, et al. Comprehensive Integration of Single-Cell Data. *Cell* 2019;177:1888-1902.e21. doi:10.1016/j.cell.2019.05.031
6. Hafemeister C, Satija R. Normalization and variance stabilization of single-cell RNA-seq data using regularized negative binomial regression. *Biorxiv* 2019;:576827. doi:10.1101/576827

7. Wales TE, Fadgen KE, Gerhardt GC, et al. High-Speed and High-Resolution UPLC Separation at Zero Degrees Celsius. *Anal Chem* 2008;80:6815–20. doi:10.1021/ac8008862
8. Ewels P, Magnusson M, Lundin S, et al. MultiQC: summarize analysis results for multiple tools and samples in a single report. *Bioinformatics* 2016;32:3047–8. doi:10.1093/bioinformatics/btw354
9. Bray NL, Pimentel H, Melsted P, et al. Near-optimal probabilistic RNA-seq quantification. *Nat Biotechnol* 2016;34:525–7. doi:10.1038/nbt.3519
10. Love MI, Huber W, Anders S. Moderated estimation of fold change and dispersion for RNA-seq data with DESeq2. *Genome Biol* 2014;15:550. doi:10.1186/s13059-014-0550-8
11. Rydenfelt M, Klinger B, Klünemann M, et al. SPEED2: inferring upstream pathway activity from differential gene expression. *Nucleic Acids Res* 2020;48:W307–12. doi:10.1093/nar/gkaa236

A VISTA ortholog sequence alignment

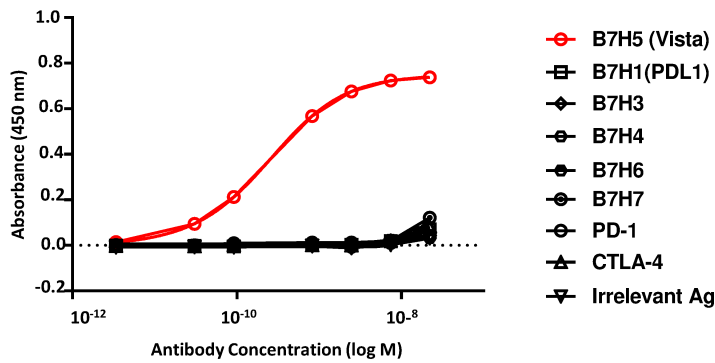


B VISTA homology model with highlighted residues involved in binding with putative partners



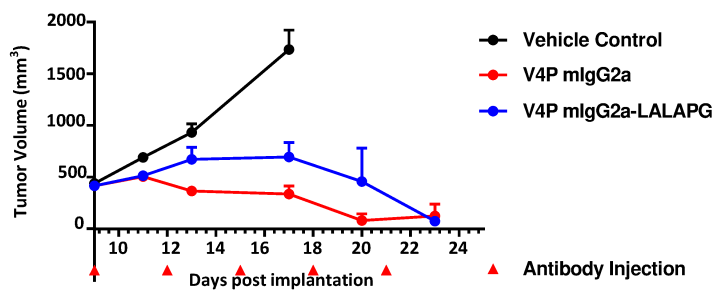
A

Binding of V4P to B7-family proteins, PD-1 and CTLA-4



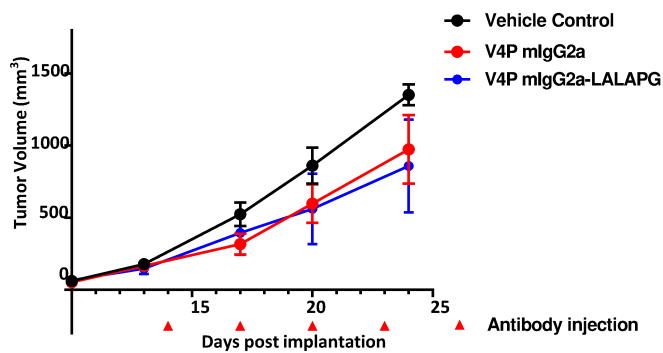
B

Efficacy of Fc-competent V4P-mIgG2a vs Fc-silent V4P-mIgG2a-LALAPG in EL4 murine syngeneic CDX model

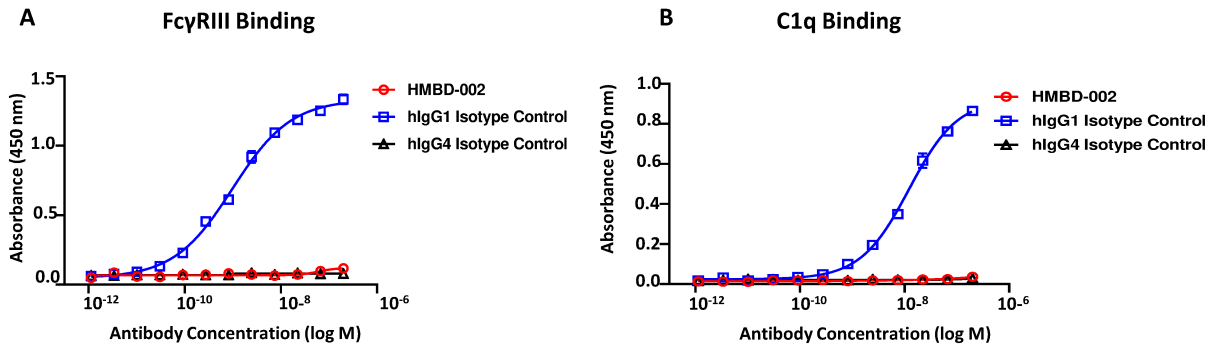


C

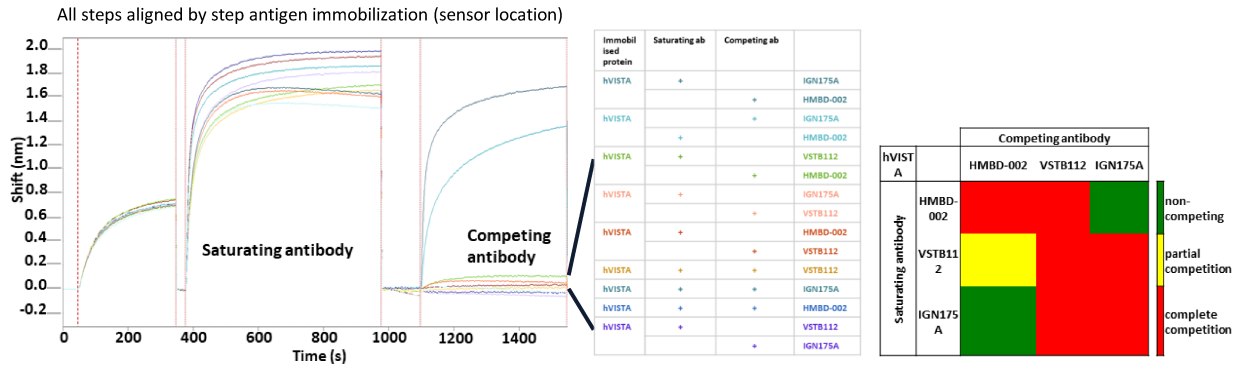
Efficacy of Fc-competent V4P-mIgG2a vs Fc-silent V4P-mIgG2a-LALAPG in CT26 murine syngeneic CDX model



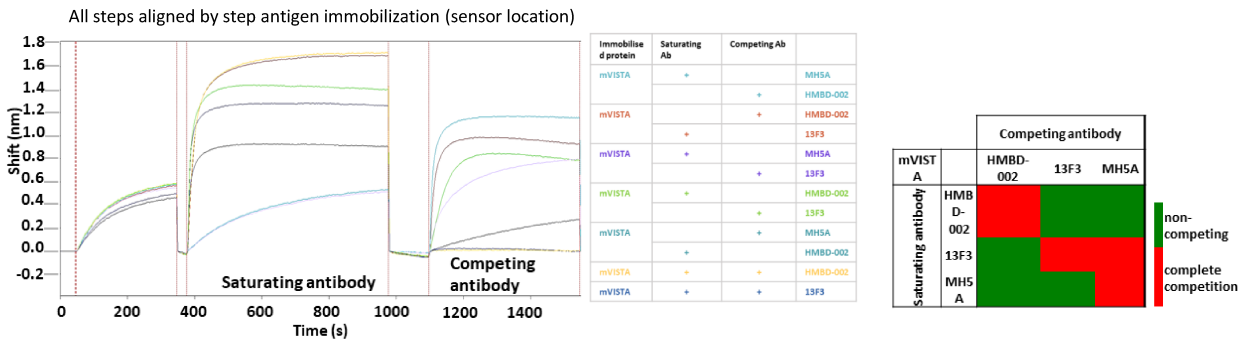
Binding of HMBD-002 to FcγRIII and C1q



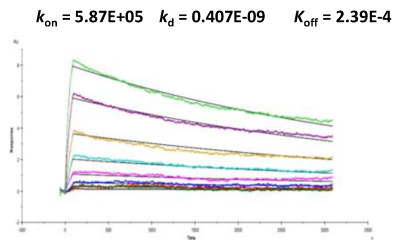
A Epitope Binning of HMBD-002 with other anti-human VISTA binding antibodies



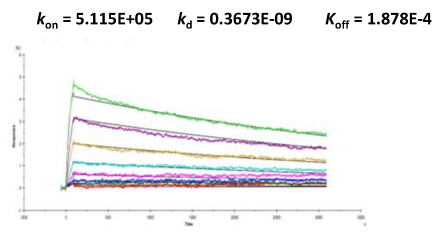
B Epitope Binning of HMBD-002 with other anti-mouse VISTA binding antibodies



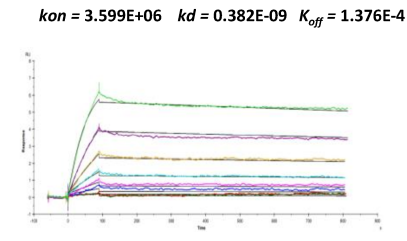
C Affinity - Human VISTA



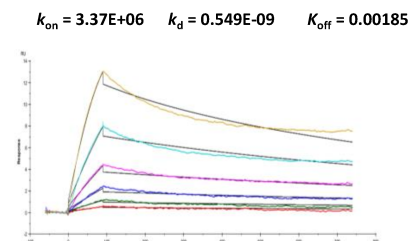
D Affinity - NHP VISTA



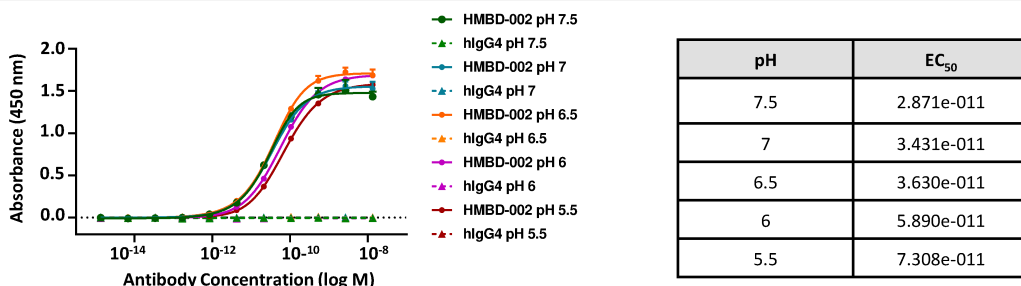
E Affinity - Rat VISTA

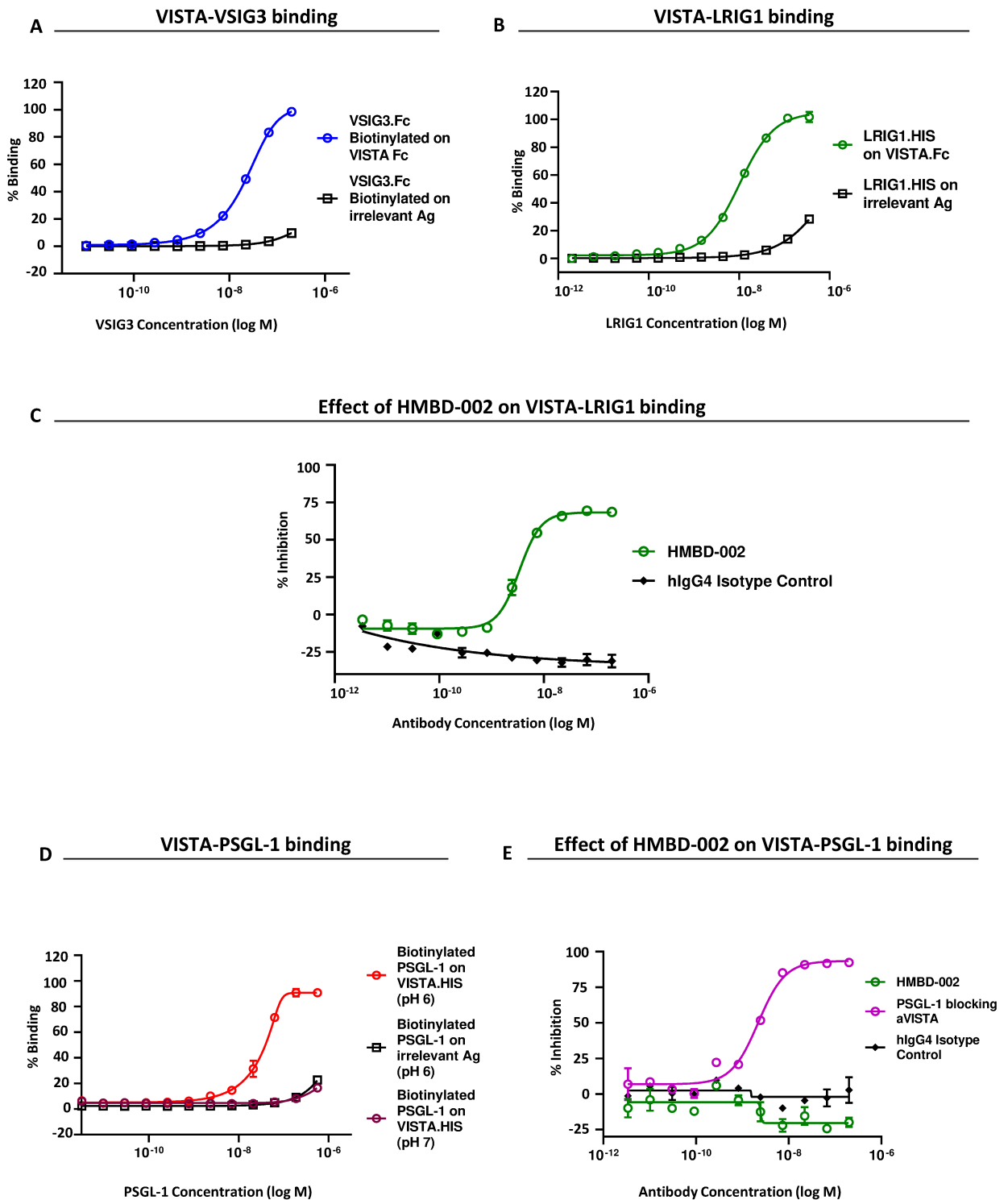


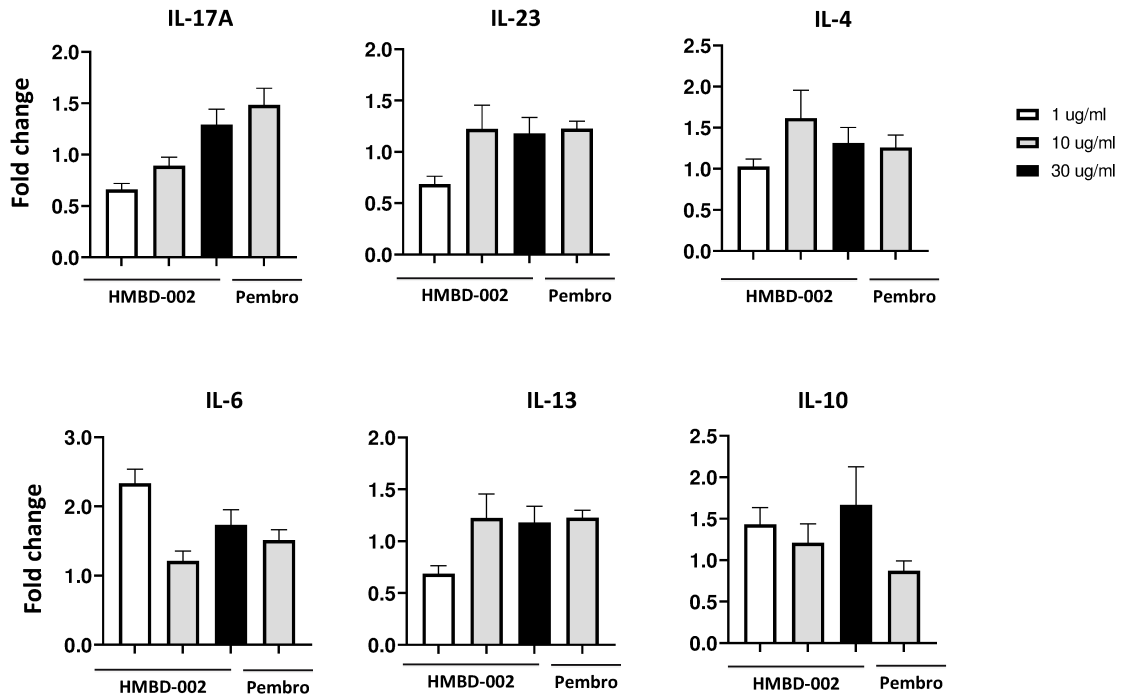
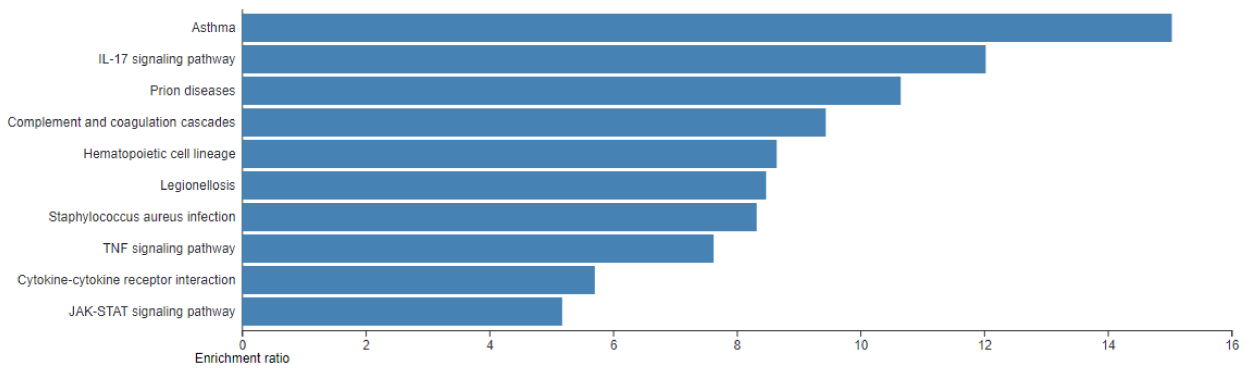
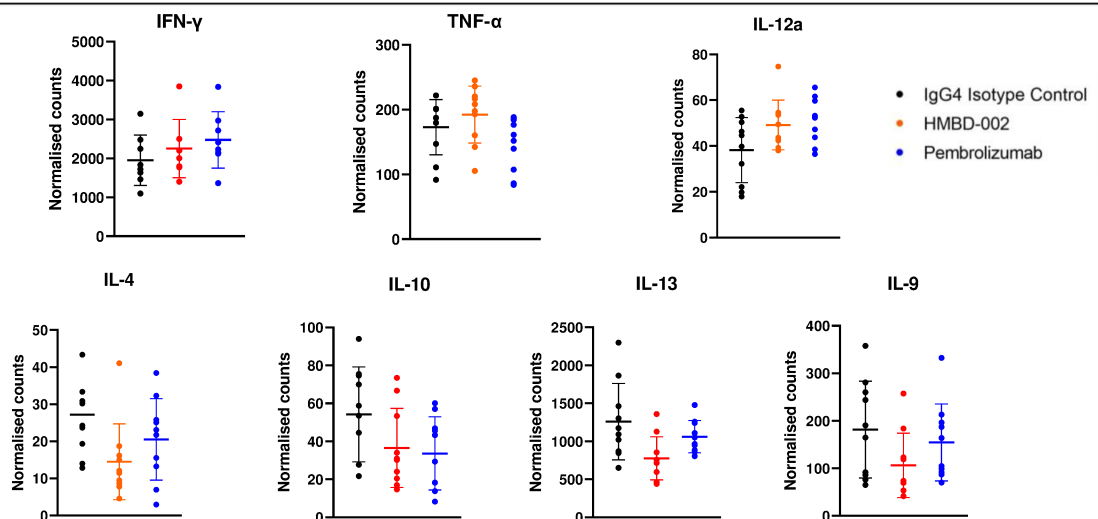
F Affinity - Mouse VISTA



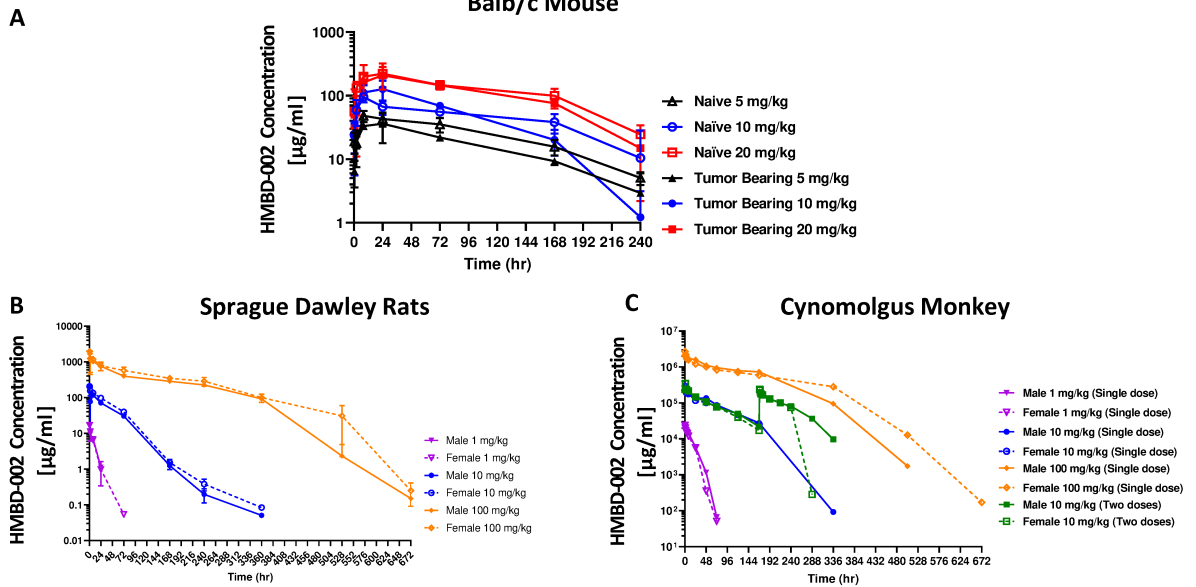
G Binding of HMBD-002 to VISTA across a pH range



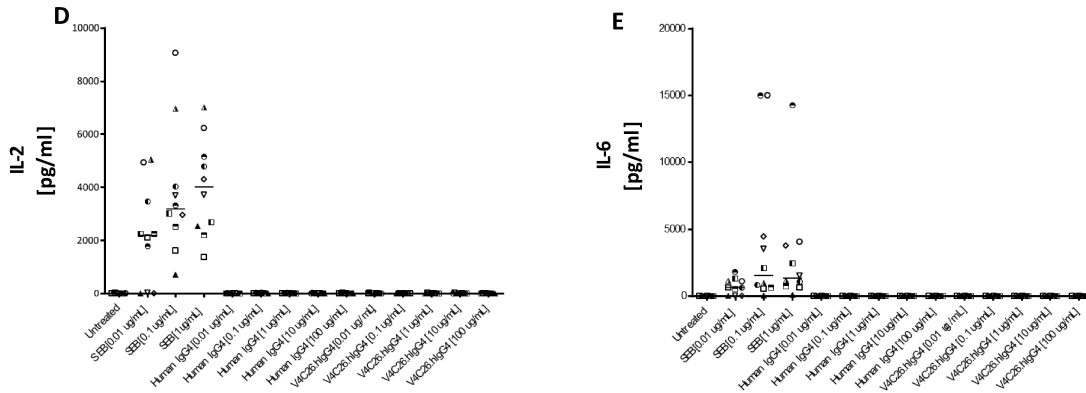


A Effect of HMBD-002 on cytokine release in an allogenic MLR assay**B** Effect of HMBD-002 on the inflammatory signaling pathways in an allogenic MLR assay**C** Effect of HMBD-002 on transcriptomic profile in an allogenic MLR assay

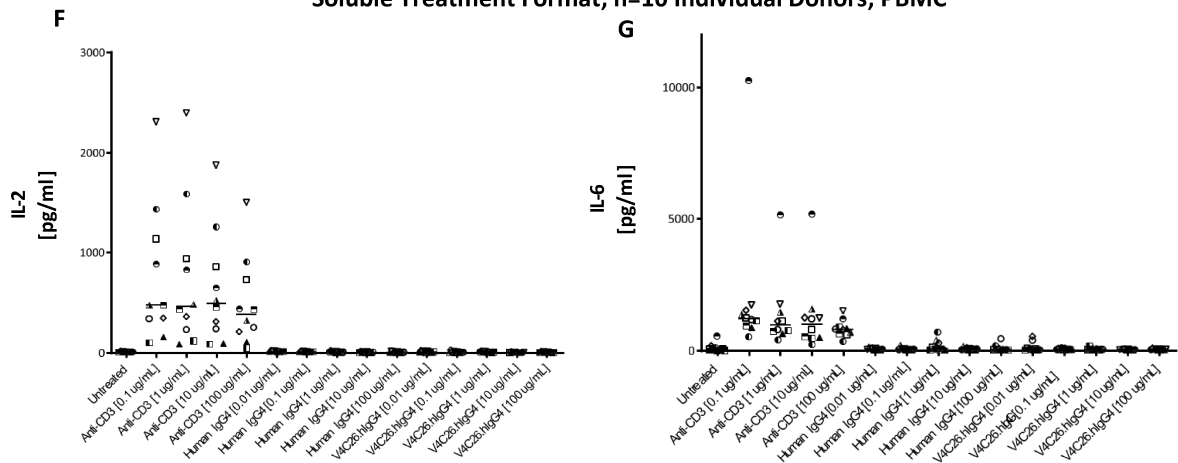
Pharmacokinetic profile of HMBD-002 in pre-clinical toxicology species

Effect of HMBD-002 on an *in vitro* cytokine release assay

Soluble Treatment Format; n=10 Individual Donors; Whole Blood



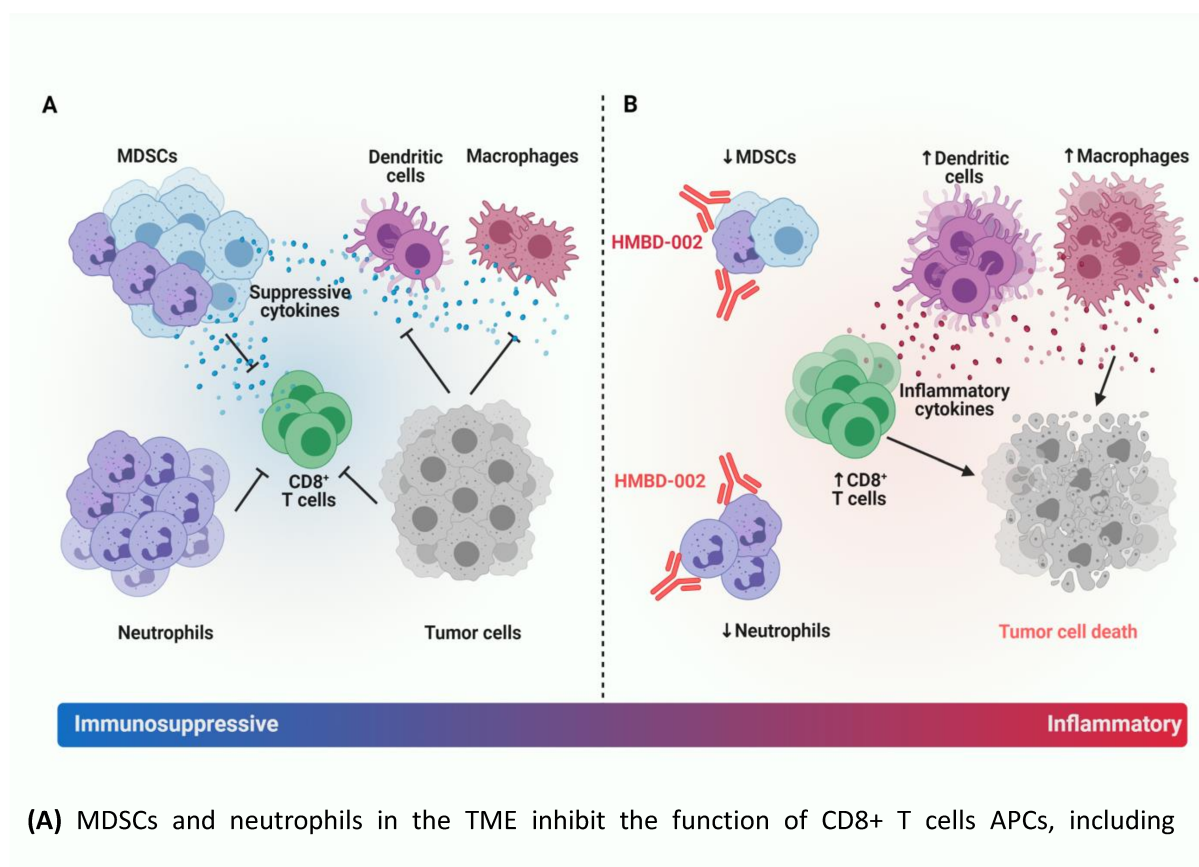
Soluble Treatment Format; n=10 Individual Donors; PBMC



Title: A rationally targeted anti-VISTA antibody that blockades the C-C' loop region can reverse VISTA immune suppression and remodel the immune microenvironment to potently inhibit tumor growth in an Fc independent manner

Authors:

Dipti Thakkar¹, Shalini Paliwal¹, Bhushan Dharmadhikari¹, Siyu Guan¹, Lillian Liu¹, Shreya Kar¹, Nikhil K. Tulsian², Joshua J. Gruber³, Leah DiMascio⁴, Konrad H. Paszkiewicz¹, Piers J. Ingram⁴, and Jerome D. Boyd-Kirkup^{4*}



(A) MDSCs and neutrophils in the TME inhibit the function of CD8⁺ T cells APCs, including macrophages and dendritic cells leading to an immunosuppressive TME permissive of tumor growth. **(B)** HMBD-002 binds to and blocks VISTA on neutrophils and MDSCs, releasing their immunosuppressive effects and shifting the TME to a pro-inflammatory anti-tumorigenic phenotype, characterised by increased inflammatory cytokine release and increased proliferation and activation of CD8⁺ T cells and APCs.